Aus dem Institut für Virologie
des Fachbereichs Veterinärmedizin
der Freien Universität Berlin

Marek's disease virus genome replication, telomere integration, and live-cell visualization

Inaugural-Dissertation
zur Erlangung des Grades eines
Doctor of Philosophy (PhD)
in Biomedical Sciences
an der Freien Universität Berlin

vorgelegt von
Tereza Vychodil, geb. Faflíková
aus Prag, Tschechische Republik

Berlin 2022
Journal-Nr.: 4365

Aus dem Institut für Virologie

des Fachbereichs Veterinärmedizin

der Freien Universität Berlin

Marek's disease virus genome replication, telomere integration, and live-cell visualization

Inaugural-Dissertation
zur Erlangung des Grades eines
Doctor of Philosophy (PhD)
in Biomedical Sciences
an der
Freien Universität Berlin

vorgelegt von

Tereza Vychodil, geb. Faflíková

aus Prag, Tschechische Republik

Berlin 2022

Journal-Nr.: 4365

Dekan: Univ.-Prof. Dr. Uwe Rösler

Erster Gutachter: Univ.-Prof. Benedikt B. Kaufer, PhD

Zweiter Gutachter: PD Dr. rer. nat. Michael Veit

Dritter Gutachter: Univ.-Prof. Dr. Andreas Herrmann

Deskriptoren (nach CAB-Thesaurus): Marek`s disease

gallid herpesvirus 2

genomes

replication

telomeres

fluorescence in situ hybridization

Tag der Promotion: 19.10.2022

This thesis is based on the following manuscripts:

Table of contents

List of figures

List of tables

List of abbreviations

Å	Ångström
AAV	Adeno-associated virus
AcMNPV	Autographa californica multiple nucleopolyhedrovirus
ANOVA	Analysis of variance
BAC	Bacterial artificial chromosome
bp	Base pairs
ca	Circa
CD	Cluster of differentiation
cDNA	Complementary DNA
CECs	Chicken embryo cells
chHDAC	Chicken histone deacetylase
CO_2	Carbon dioxide
CPE	Cytopathic effect
CRISPR	Clustered regularly interspaced short palindromic repeats
DAPI	4′,6-diamidino-2-phenylindole
DC	Dendritic cells
dCas9	Dead CRISPR-associated protein 9
DDR	DNA damage response
DEF	Duck embryo fibroblasts
DNA	Deoxyribonucleic acid
dpi	Days post infection
DSB	Double strand breaks
dsDNA	Double stranded DNA
E	Early
EBV	Epstein-Barr virus
EDTA	Ethylenediamine tetraacetic acid
eGFP	Enhanced green fluorescent protein
ESCDL-1	Embryonic stem cell derived line-1
eYFP	Enhanced yellow fluorescent protein
FACS	Fluorescence-activated cell sorting
FAM	6-carboxyfluorescein
FAO	Food and Agriculture Organization
FBS	Fetal bovine serum
FFE	Feather follicle epithelium
FISH	Fluorescence in situ hybridization
for	Forward primer
FP	Fluorescent protein
g	Gramm
GaHV	Gallid herpesvirus
GAPDH	Glyceraldehyde 3-phosphate dehydrogenase
GCN4	general control nonderepressible 4
GFP	Green fluorescent protein
H3K27me3	Trimethylation of lysine 27 of histone H3
H3K4me	Methylation of lysine 4 of histone H3
H3K4me3	Trimethylation of lysine 4 of histone H3
H3K9ac	Acetylation of lysine 9 of histone H3
H3K9me3	Trimethylation of lysine 9 of histone H3
HCMV	Human cytomegalovirus
HCV	Hepatitis C virus
HEPES	N-2-Hydroxyethylpiperazine-N'-2-Ethanesulfonic Acid
HHV	Human herpesvirus
HIV	Human immunodeficiency virus
hpi	Hours post infection
HR	Homologous recombination
HSV	Herpes simplex virus
HVT	Herpesvirus of turkeys

List of abbreviations

ICP	Infected cell protein
ICTV	International Committee on Taxonomy of Viruses
IE	Immediate early
IFN	Interferon
IgG	Immunoglobulin G
iNOS	Inducible nitric oxide synthase
IRES	Internal ribosomal entry site
IR_L	Internal repeat long
IR_{LS}	Internal repat long and short
$IR_{LS\text{-}HR}$	Internal repat long and short with sequences for homologous recombination
IR_S	Internal repeat short
JJHan	Human lymphoblastic leukemia T cells
kbp	Kilobase pairs
KSHV	Kaposi's sarcoma-associated herpesvirus
L	Late
LacI	Lactose repressor
LacO	Lactose operator
LATs	Latency associated transcripts
MAP kinase	Mitogen-activated protein kinase
MD	Marek's disease
MDV	Marek's disease virus
meq	MDV Eco Q-encoded protein
mini-F	Minimal fertility factor replicon
MIP	Maximum-intensity projection
miRNA	Micro RNA
ml	Milliliter
MOI	Multiplicity of infection
MRN	Mre11, Rad50, and Nbs1
mTMRs	Multiple telomeric repeats
MΦ	Macrophages
n	Sample size
NaCl	Sodium chloride
NaOH	Sodium hydroxide
NGS	Next-generation sequencing
NK cells	Natural killer cells
NLS	Nuclear localization signal
nm	Nanometer
OriS	Origin of replication
P2a	2A self-cleaving peptide
PBMC	Peripheral blood mononuclear cells
PBS	Phosphate-buffered saline
PFA	Paraformaldehyde
PFU	Plaque-forming unit
pH	Potential of hydrogen
POT1	Protection of Telomere 1
pp24	Phosphoprotein 24
pp38	Phosphoprotein 38
pTK	Thymidine kinase promoter
qPCR	quantitative polymerase chain reaction
RAP1	Repressor / Activator Protein 1
RC	Replication compartment
rev	Reverse primer
RFLP	Restriction fragment length polymorphism
RLORF	Repeat long open reading frame
RNA	Ribonucleic acid
RPMI	Roswell Park Memorial Institute Medium
RT-qPCR	Real-time quantitative polymerase chain reaction
scFv	Single-chain variable fragment
SD	Standard deviation

SDS	Sodium dodecyl sulphate
SDS-PAGE	Sodium dodecyl sulphate-polyacrylamide gel electrophoresis
sgRNA	Small guide RNA
SNPs	Single nucleotide polymorphism
SORF	Open reading frame in unique short region
ssDNA	Single stranded DNA
sTMRs	Short telomeric repeats
SV-40	Simian virus 40
TAMRA	Tetramethylrhodamine
TERT	Telomerase reverse transcriptase
tetO	Tetracycline operator
TetR	Tetracycline repressor
TIN2	TRF1- and TRF2-Interacting Nuclear Protein 2
TK	Thymidin kinase
TMRs	Telomeric repeats
TPP1	Telomere protection protein 1
TRF	Telomeric repeat-binding Factor
Tris-HCl	Tris (hydroxymethyl) aminomethane hydrochloride
TRL	Terminal repeat long
TRS	Terminal repeat short
U	Unit
U2OS	Human bone osteosarcoma epithelial cells
U_L	Unique long region
U_S	Unique short region
US	United states
VACV	Vaccinia virus
vCXCL	Viral CXC ligand
vDNA	Viral DNA
vIL-8	Viral interleukin-8
VP16	Virion protein 16
VRC	Viral replication compartment
vTR	Viral telomerase RNA
VZV	Varicella zoster virus
w/o	Without
WF	Wide-field
wt	Wild type

x

Prolog

As a virologist, I cannot neglect the situation about the coronavirus pandemic that started in December 2019. This virus affected every one of us in some ways. Most of us have already experienced pandemics – mainly the ones caused by influenza viruses. Common human coronaviruses cause predominantly seasonal respiratory diseases. In the last 20 years, however, there have been two epidemics caused by highly pathogenic coronaviruses – severe acute respiratory syndrome coronavirus (SARS-CoV) in 2003 and Middle East respiratory syndrome coronavirus (MERS-CoV) in 2013. However, this time the scenario was pretty different. One of the problems was, that infected patients with SARS-CoV-2, the causative agent of coronavirus disease 2019 (COVID-19), were already shedding the virus a few days before symptom onset. This resulted in a rapid spread of the virus on a global scale. Moreover, during the first year, no vaccines and effective treatments were available. Therefore, several "new" public health precautions have been implemented to protect individuals at highest risk – wearing face masks in public places, social distancing, lockdown and stay-at-home orders, enforced quarantines, contact tracings, travel restrictions, and even closing of international borders. Coronavirus disease was a main media topic and it felt like everyone was suddenly an expert on viruses. And what was the outcome? Before the pandemic, every time when people heard that I am "working with (herpes)viruses", they were interested and frequently asked me questions like "Oh, that's cool. Can you tell me more about this virus?". Now, people are either trying to lecture me about virus-related matters or they are arguing over some bizarre piece of information they found somewhere on the Internet. Of course, this pandemic demonstrated how important research is. However, it also showed how important science communication is. Therefore, in such situations it is up to us – virologists – to pull our weight. We are expected not only to do high-quality research, but also to be a trustworthy source of information to educate people, prevent panic, and preclude disinformation during future pandemics.

1 Introduction

1.1 Viruses

Viruses are obligate intracellular parasites absolutely dependent on the metabolic machinery of the host cell for reproduction. They are the most abundant biological entities on Earth found literally everywhere. Just the average human body contains approximately 100 fold more virus particles than human cells. Viruses infect everything living such as bacteria, fungi, plants, animals or humans. Their uncontrolled replication can induce disease or even death of the host. Moreover, viruses possess extraordinary abilities to adapt themselves to their hosts. Therefore, all vertebrates evolved immune system to protect themselves against virus infections.

Although viruses are generally considered infectious agents causing diseases, they proved to be useful as well. Studies on viruses provided us insights into cellular, molecular, and structural biology. In medicine, transforming viruses helped us to understand the genetic bases of cancer diseases. Viral vectors are commonly used in gene therapy as delivery vehicles to replace defective genes by a working copy. Interestingly, five to eight percent of our entire DNA consist of fossil viral fragments which were accumulated during millions of years of co-evolution (Lander et al., 2001). Latest studies even implicate that endogenous retroviruses, which are vertically inherited viral DNA sequences integrated into host DNA, also played an important role in the development of mammalian placenta (Imakawa et al., 2015; Mi et al., 2000).

1.2 Herpesviruses

Herpesviruses are relatively large viruses infecting animals and humans. Almost every one has ever been infected by a herpesvirus – just the prevalence of human herpesvirus 6 in adults is estimated around 90 % (Chan et al., 2001; Levy et al., 1990). Typical for herpesviruses is their lifelong persistence in the host after primary infection called latency or quiescence. The latent virus can be triggered by stress, co-infection, tissue injury, and/or weakened immune system leading to recurring infections and virus spread. Many herpesvirus infections are unnoticeable. However, if the host's immune system is compromised, the virus can cause serious or even devastating health problems. Until now, herpesvirus infections cannot be cured. Vaccines and antiviral drugs can only reduce the severity of the symptoms, frequency of virus reactivation, and shedding of the virus into the environment. Last but not least, the significance of herpesvirus research is also enhanced by the fact that some herpesviruses are even able to induce cancer.

1.2.1 Taxonomy and classification

In October 2020, the International Committee on Taxonomy of Viruses (ICTV) updated the classification of the order *Herpesvirales* including now 130 species distributed into three families, three subfamilies and 23 genera (ICTV Reports, 2021). The family *Alloherpesviridae* is mainly infecting fish and frogs, *Herpesviridae* are found in mammals, birds, and reptiles. The members of the family *Malacoherpesviridae* invade gastropods and bivalves.

The complex *Herpesviridae* family is further divided into *Alpha*-, *Beta*- and *Gammaherpesvirinae* subfamilies. In their latest report, ICTV introduced new species nomenclature within the complex *Herpesviridae* family referring to the subfamily categorization. Until now, nine human herpesviruses exist among these three subfamilies: human alphaherpesvirus 1 and 2 (HHV-1 and HHV-2; formerly herpes simplex virus 1 and 2, HSV-1 and HSV-2), human alphaherpesvirus 3 (HHV-3; also known as varicella zoster virus, VZV), human betaherpesvirus 5 (HHV-5; earlier human cytomegalovirus, HCMV), human betaherpesvirus 6A, 6B, and 7 (HHV-6A, HHV-6B, and HHV-7), human gammaherpesvirus 4 (HHV-4; or Epstein-Barr virus, EBV) and human gammaherpesvirus 8 (HHV-8; known as Kaposi's sarcoma-associated herpesvirus, KSHV) (Fields et al., 2007; ICTV Reports, 2021).

1.2.2 Structure of herpesviruses

All herpesviruses are enveloped viruses with a diameter of 150 – 200 nm in size with a spherical to pleomorphic shape (Fig. 1). The lipid envelope is derived from a host intracellular membrane and contains mature viral glycosylated envelope proteins. These proteins form spike structures on the virus surface. They are necessary for the attachment of virus at the host extracellular membrane and entry into the host cell upon interaction with specific cellular receptors. Underneath the lipid envelope is an amorphous protein matrix called tegument. It contains multiple copies of ca 20 viral proteins, viral RNAs, as well as some cellular proteins. Each herpesvirus has a specific tegument protein composition based on the viral particular needs and the cell type they are infecting. Within the tegument floats an icosahedral nucleocapsid which consists of 162 major structural protein subunits called capsomers. 150 of these capsomers are hexameric, 11 are pentameric and one serves as a portal through which the linear double stranded DNA (dsDNA) enters and exits the nucleocapsid. The herpesviral dsDNA is monopartite and ranges from 120 to 295 kilobase pairs (kbp) in size (Brown and Newcomb, 2011; Flint et al., 2015; Grunewald et al., 2003; Liu and Zhou, 2007).
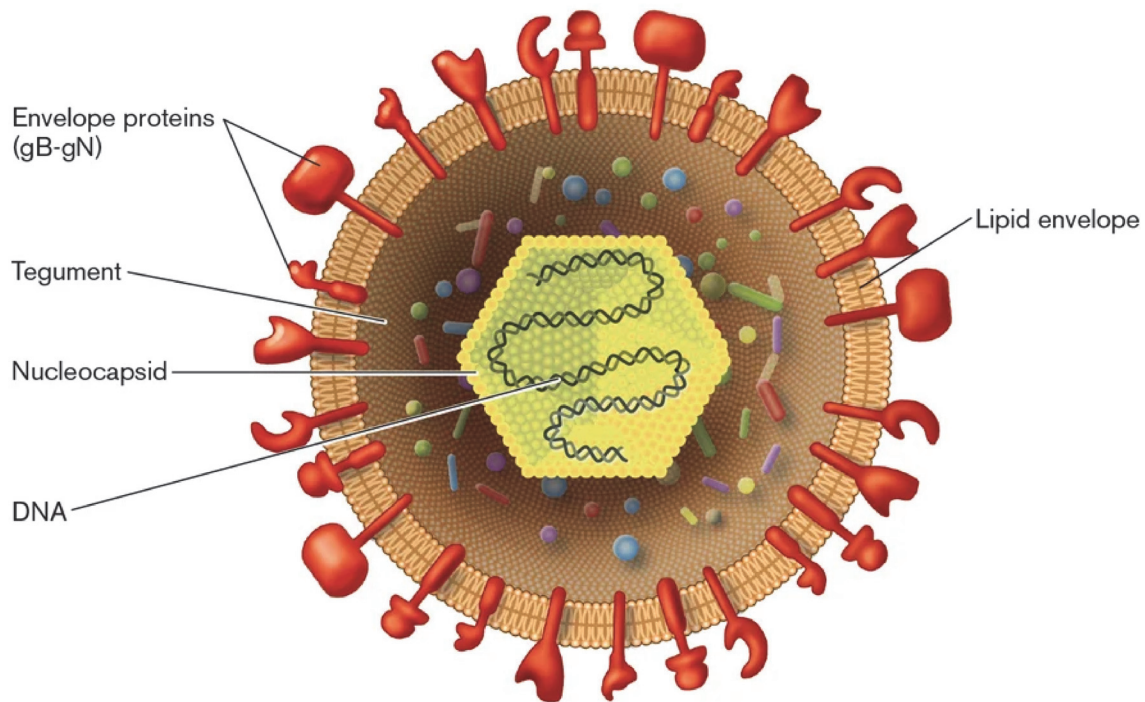
Figure 1: Schematic representation of a herpesvirus virion. All herpesviruses possess a monopartite double stranded DNA that is protected by an icosahedral nucleocapsid. The proteinaceous tegument surrounds the nucleocapsid. The lipid envelope contains envelope proteins called glycoproteins that are protruding out from the lipid bilayer. (Image from https://microbenotes.com/herpes-simplex-virus-1-hsv-1/)

1.2.3 The herpesvirus genome

All herpesviruses possess a monopartite linear dsDNA molecule that varies in size from 120 kbp to 295 kbp. Depending on the herpesvirus species, the viral DNA encodes from 70 to more than 160 viral proteins. Moreover, the genome of most herpesvirus species consists not only of unique DNA, it characteristically contains also direct or inverted repeats. Interestingly, some herpesviruses even possess a stretch of telomeric repeats (TMRs) in their DNA that facilitate virus genome integration into host telomeres (Kaufer et al., 2011). According to different DNA sequence arrangements, genomes of herpesviruses are divided into six groups designated by the letter A to F (Fig. 2). Notably, different types of genome arrangements can be found within one subfamily.
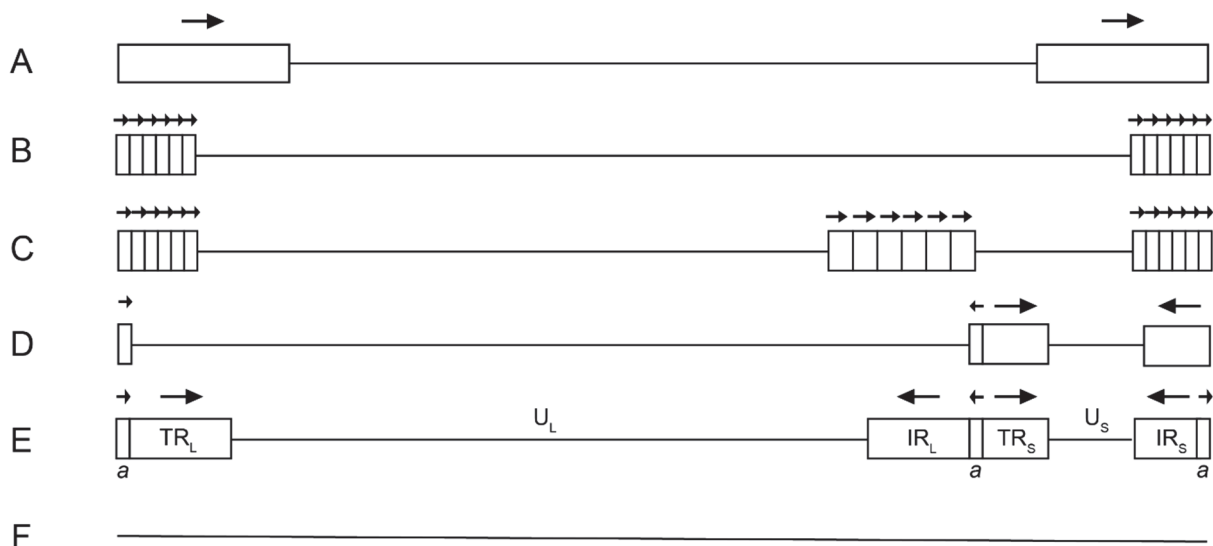
Figure 2: Genome arrangements in herpesviruses. Horizontal lines depict unique regions within the virus genome, boxes represent repetitive sequences and arrows show the orientation of repeats. The nomenclature is shown for the most complex E class genome that is extensively discussed in this work. The unique region long and short (U_L and U_S, respectively) are flanked by terminal and internal repeat long and short (TR_L, TR_S, IR_L and IR_S). Short a-like sequences are located between the repeat regions.

1.2.4   The replication cycle of herpesviruses

1.2.4.1   Lytic cycle and virus genome replication

The reproductive cycle has been most extensively studied in human alphaherpesvirus 1 (HHV-1, HSV-1). To initiate infection, virion binds via envelope proteins (glycoproteins) to the extracellular matrix. The interaction of glycoproteins with cellular receptors leads to fusion of viral lipid envelope with the plasma membrane and entry of the virus. After membrane fusion, tegument proteins and the nucleocapsid are released into the cytoplasm. In the next step, the nucleocapsid associates with microtubules and is actively transported to a nucleopore. After docking at the nucleopore, the viral DNA, which is coiled in the capsid under high pressure, is released through the portal into the nucleus where it rapidly circularizes. The tegument protein VP16 is also transported into the nucleus and is responsible for recruiting of the host RNA polymerase II and initiation of gene transcription. In general, there are three phases of herpesvirus gene expression: immediate early (IE), early (E), and late (L). The translated IE proteins are involved in regulation of the subsequent gene transcription and antagonizing of intrinsic host defenses. Early proteins are mainly involved in viral DNA replication, whereas late proteins are primarily structural proteins and additional proteins for virion packaging and assembly. Inside the nucleus, the newly synthesized viral concatemer DNA is cleaved into unit length molecules and injected into procapsids through the portal. Filled nucleocapsids and tegument proteins then bud at the inner nuclear membrane forming enveloped vesicles within

4

the perinuclear lumen. These immature vesicles subsequently fuse with the outer nuclear membrane releasing the nucleocapsid and tegument proteins into cytoplasm. This structure is then transported either to the *trans*-Golgi apparatus or to endosomes both containing mature viral envelope proteins. In the next step, the nucleocapsid and tegument proteins bud into the Golgi or endosomes acquiring the lipid envelope with viral glycoproteins. When the virus exits from Golgi, it receives another membrane bilayer forming a vesicle around the enveloped virus. These Golgi-derived vesicles and endosomes are then transported to the plasma membrane and release the virus from the cell through exocytosis (Fields *et al.*, 2007; Flint *et al.*, 2015; Liu et al., 2019).

All herpesviruses replicate their genome in the nucleus. During nuclear entry, the genome is injected from the capsid in form of a naked linear DNA with nicks and gaps where the ends resemble DNA double strand breaks (DSB). However, the ends of HSV-1 genome possess long repeats that are homologous to each other enabling rapid genome circularization by the homologous recombination (HR) repair pathway (Full and Ensser, 2019). Prior to any gene expression, the naked DNA is complexed with acetylated H3 histones forming nucleosomes. In the next step, the origin-binding protein (UL9) disrupts the dsDNA structure allowing the single-strand binding infected cell protein eight (ICP8 or UL29) to bind. Together, they are responsible for the formation of a hairpin loop that is recognized by the viral helicase/primase complex (UL5 and UL52). This complex starts to unwind the double helix and synthesize short RNA primers. After binding of the helicase/primase-associated protein (UL8) at the replication fork, viral DNA dependent DNA polymerase (UL30 and UL42) is recruited. The replication starts as a bidirectional theta replication which is then by an unknown mechanism switched to a rolling-circle amplification generating concatemeric viral DNA. Interestingly, the newly replicated viral genomes do not associate with histones which simplifies DNA packaging into procapsids. In alphaherpesviruses, DNA replication and recombination are interconnected. During replication, multiple random DSB, nicks, and gaps in DNA are produced which stimulates recombination events leading to replication intermediates with highly branched viral DNA. For these replication intermediates is responsible the recombination complex consisting of alkaline nuclease (UL12) and UL29 proteins. Moreover, homologous recombination plays an important role in the repair of damaged or deleted DNA (Engel et al., 2012; Oh and Fraser, 2008; Perez-Losada et al., 2015; Severini et al., 1996; Weller and Sawitzke, 2014).

The DNA replication in herpesviruses, as in other DNA viruses, is sequestered at distinct foci within the nucleus known as viral replication compartments (VRCs). VRCs are membrane-less assemblies providing the virus a protective environment. Here, viral processes are regulated by enrichment of necessary factors and by elimination of factors that would

otherwise abrogate viral replication. Recent studies revealed that each single incoming viral genome can form its own VRC that will subsequently coalesce into bigger VRCs (Dembowski and DeLuca, 2018; Sekine et al., 2017; Taylor et al., 2003). Under experimental conditions, HSV-1 initiates from one up to 15 multiple VRCs depending on the multiplicity of infection (MOI) and the cell type infected (Cohen and Kobiler, 2016; Tomer et al., 2019). Moreover, to overcome spatial barriers of cellular chromatin, it is assumed that herpesviruses re-organize the nuclear environment and the replicating viral DNA is then phase-separated from chromosomal DNA. VRCs possess properties of liquid phase separated condensates such as spherical shapes, the ability to fuse, and association with enrichment of viral tegument or IE proteins with intrinsically disordered domains. It was shown, that in VRCs proteins can freely diffuse, whereas DNA seems to move much slower within these assemblies (de Bruyn Kops and Knipe, 1994; Kobiler and Weitzman, 2019; McSwiggen et al., 2019; Seyffert et al., 2021).

1.2.4.2 Latency and reactivation

A characteristic feature of all herpesviruses is the life-long persistence of viral genome in host cells called latency. The viral genome persists in the host nucleus either in form of episomal DNA or it integrates into host telomeres. Until now, only HHV-6 and MDV have been confirmed with certainty to integrate (Arbuckle et al., 2010; Kaufer *et al.*, 2011). Importantly, to avoid recognition and elimination by the host immune system, the viral transcription activity is suppressed, but not entirely silenced during latency. For example, in HSV-1, only non-protein coding RNAs called latency-associated transcripts (LATs) are being expressed and spliced into stable introns which then further repress the viral gene expression (Cohen, 2020; Flint *et al.*, 2015; Nicoll et al., 2016). Interestingly, human herpesviruses establish latency in different cell types depending on the subfamily. Alphaherpesviruses (HSV-1, HSV-2 and VZV) primarily target sensory and cranial neurons, whereas betaherpesviruses (HCMV, HHV-6A, HHV-6B and HHV-7) and gammaherpesviruses (EBV and KSHV) persist in myeloid progenitor cells, monocytes, as well as in lymphocytes.

A very important aspect of latent herpesviruses is the ability to reactivate from the quiescence and start producing new viral progenies. This alteration between lytic and latent stages of infection is regulated epigenetically. After nuclear entry, the incoming naked viral DNA associates immediately with histones forming nucleosomes. Histone post-translational modifications play crucial roles in alteration of viral gene transcription activities. Nucleosomes found on transcriptionally silent heterochromatin had different modifications as nucleosomes on actively transcribed euchromatin (discussed in detail later). This epigenetic regulation of gene transcription serves as an excellent mechanism for rapid response of latent virus to

cellular stress or other stimuli followed by reactivation (Coleman et al., 2008; Kennedy et al., 2015; Oh and Fraser, 2008).

1.3 Marek's disease virus

This thesis is focused on a chicken herpesvirus called Marek's disease virus (MDV). MDV is an avian alphaherpesvirus belonging to the *Mardivirus* genus. Six virus species belong into this genus: Anatid alphaherpesvirus 1 and Columbid alphaherpesvirus 1 infecting quails and pigeons, Spheniscid alphaherpesvirus 1 found in pinguins, Gallid alphaherpesvirus 2 (GaHV-2/MDV), Gallid alphaherpesvirus 3 (GaHV-3/MDV serotype 2), and Meleagrid alphaherpesvirus 1 (HVT) (ICTV Reports, 2021). MDV is a highly contagious virus causing immunosuppression, ataxia and paralysis, blindness, chronic wasting, and formation of fatal T cell lymphomas in various visceral organs in susceptible birds. Therefore, MDV is also being used as a small-animal model for virus-induced cancer studies and tumor formation.

The annual economic impact of MDV on poultry industry was estimated in 2002 in the range of one to two billion US dollars. This corresponded to a loss of about 1% of the total profit. Since then, according to the Food and Agriculture Organization (FAO), the worldwide poultry meat production almost doubled in 2019 from 64 to 118 million tons and egg production increased from 54 to 83 million tons per year (Davison and Nair, 2004; FAO, 2021a; b). And although vaccines are widely used and efficiently protect chickens against tumor formation, they do not prevent chickens from becoming infected nor block the further transmission of virus. Hence, continuous evolution of MDV virulence and overcoming of vaccine barriers still poses a serious problem and threat to the poultry industry (Conradie et al., 2020; Fakhrul Islam et al., 2008; Padhi and Parcells, 2016).

1.3.1 MDV genome

MDV genome is approximately 180 kbp long dsDNA molecule arranged, similarly as HSV-1, as a E-class genome. It consists of unique region long and short (U_L and U_S, respectively) which are flanked by terminal (TR_L and TR_S), and internal repeat long and short (IR_L and IR_S). *A-like* sequences harboring telomeric repeats, packaging signals and genome cleavage site are located at the junctions between neighboring repeat regions (Greco et al., 2014). Both unique regions are mainly encoding for genes associated with DNA replication and the lytic replication cycle. These genes are highly conserved amongst all alphaherpesviruses. On the contrary, the repeat regions comprise primarily of MDV-specific genes that are involved in pathogenesis, cellular tropism, latency and tumorigenesis (Bertzbach et al., 2018; Lee et al., 2000; Tulman et al., 2000). Genes encoded in repeat regions are also called diploid genes because they are found twice in the genome – one copy is in the terminal repeat region and

the second inverted copy is placed in the internal repeat region (except for phosphoproteins pp24 and pp38 which are overlapping from repeat regions into unique regions) (Tulman et al., 2000). However, it is still unclear if the virus needs both copies of those MDV-specific genes and how the absence of one set of repeats affects the virus pathogenesis.

MDV life cycle and pathogenesis

MDV has a complex life cycle and the well-established model for the viral replication cycle is also known as *the Cornell model*. The model describes the course of disease from initial infection to the productive generation of infectious progenies in feather follicles (Calnek, 2001). The life cycle can be divided into four phases: (i) entry, (ii) replication, (iii) latency and (iv) spread (Fig. 3).

Furthermore, MDV is a cell-associated virus transmitted inside the infected bird by cell-to-cell contact. In cell culture, cell-free infectious MDV virion particles cannot be detected in supernatant nor purified from infected cell lysates which makes MDV unique among all herpesviruses (Denesvre et al., 2007). The only place where cell-free viruses are produced is the feather follicle epithelium (FFE) of infected chickens.
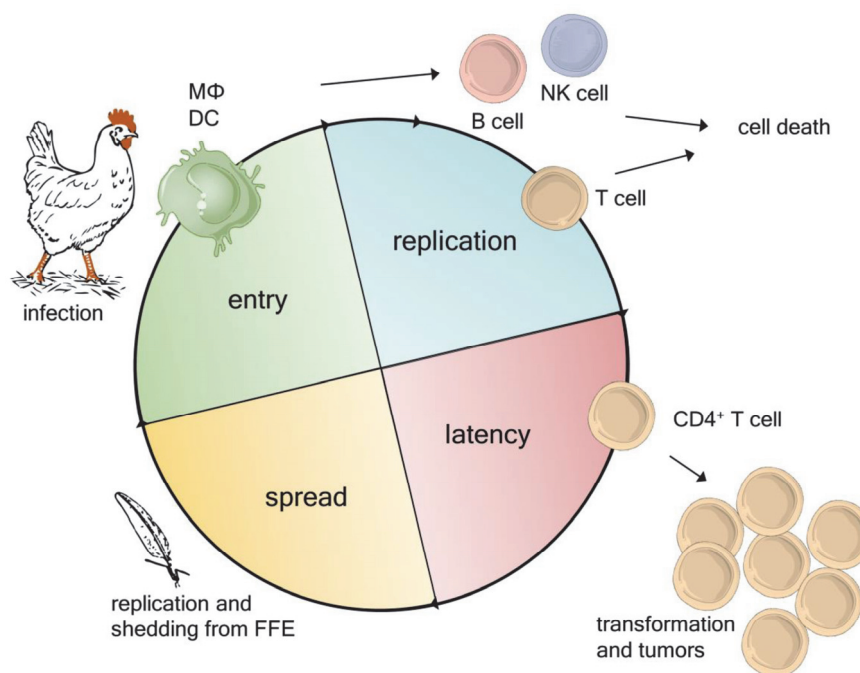
Figure 3: Life cycle of Marek's disease virus. MDV infection starts with inhalation of virus particles in dust from infectious environment. Macrophages (MΦ) and dendritic cells (DC) transfer the virus from lungs through the bloodstream to the primary lymphoid organs (the bursa of Fabricius, thymus and spleen) and pass the virus mainly on B cells, T cells or natural killer (NK) cells where the virus replicates. Latency is established in activated CD4$^+$ T cells which further transport the virus to the feather follicle epithelial (FFE), where the virus replicates again and produces cell-free MDV that is shed into the environment. Another faith

of the infected CD4^{+} T cells is transformation resulting in malignant lymphomas. (Image obtained from Bertzbach et al., 2020 (Bertzbach et al., 2020))

1.3.1.1 MDV entry

The natural route of infection is by inhalation of cell-free virus particles that are shed into the environment from the FFE of infected chickens. This infectious dust, poultry dander and feather debris can be inhaled by other chickens. After inhalation of virus particles, macrophages and dendritic cells (DC) deliver the virus from lungs through the bloodstream to primary lymphoid organs: the bursa of Fabricius, thymus and spleen (Barrow et al., 2003; Chakraborty et al., 2017). MDV secrets the viral interleukin-8 (vIL-8) chemokine, which name was recently changed to viral CXCL13 (from here on referred as vIL-8/vCXCL13) based on its function similarities with chicken CXC ligand 13 (CXCL13) (Haertle et al., 2017). The vIL8/vCXCL13 is an almost 700 bp long gene consisting of three exons separated by two introns. The gene is spliced into many splice variants and the deletion of entire vIL8/CXCL13 results in abrogated disease and tumorigenesis. Exon I likely serves as a signal peptide, whereas exon II and exon III are translated into the secreted chemokine protein (Cui et al., 2004; Parcells et al., 2001). Recently, another internal splice form called exon 3' was identified; however, it was shown that the expressed protein is dispensable for MDV replication, pathogenesis, and tumor formation (You et al., 2021b). Interestingly, nearby genes such as MDV major oncogene *meq*, RLORF5a, and/or RLORF4 also splice to vIL8/vCXCL13 exons II and III giving rise to multiple splice variants which are likely involved in MDV pathogenesis (Engel *et al.*, 2012; Jarosinski and Schat, 2007). In lymphoid organs, the vIL8/vCXCL13 chemokine recruits primary target cells to the infected macrophages and DCs which further pass the virus directly via cell-to-cell contact.

1.3.1.2 MDV replication

The primary target cells recruited by vIL-8/vCXCL13 are mainly B cells, CD4^{+} CD25^{+} T cells (Engel *et al.*, 2012) or natural killer (NK) cells (Bertzbach et al., 2019b) where MDV lytically replicates. B cells; however, represent the majority of infected cells with the highest viral load (Baaten et al., 2009). The primary replication takes place 2 – 7 days post-infection (dpi) and is accompanied by increased apoptosis, inhibition of cell proliferation and reduction of circulating blood B cells. Such immunosuppression increases the susceptibility of infected chickens to other infectious pathogens (Berthault et al., 2018). At around 14 – 21 dpi, a second wave of lytic replication results in severe atrophy of the bursa of Fabricius and thymus leading to permanent immunosuppression.

1.3.1.3   MDV latency and transformation

Around 7 – 10 dpi, MDV establishes latency in T cells, predominantly in activated CD4$^+$ T cells. The viral DNA integrates into host telomeres and serves as a reservoir of latent MDV genomes. Telomeric repeat arrays located in *a-like* sequences facilitate this integration process which occurs via homologous recombination (Kaufer *et al.*, 2011). During latency, gene transcription is limited to latency associated transcripts (LATs) and the MDV major oncogene *meq*. Typically between 21 - 28 dpi, small fractions of or even single infected T cells are subsequently transformed leading to formation of deadly, mostly clonal lymphomas in multiple visceral organs (Mwangi et al., 2011). However, the efficiency of lymphoma formation depends on the virus strain, virulence, as well as the genetic background of the chickens (Haq et al., 2013).

As already mentioned above, only a limited number of viral genes are expressed during latency. LAT is a complex family of spliced RNAs which is encoded antisense to the ICP4 immediate early gene and is thus considered to suppress lytic infection. Over 20 alternatively spliced LAT transcripts and a cluster of microRNAs (miRNA) at the 5' end of LAT involved in the post-transcriptional gene regulation were identified and play a key role in the switch between lytic and latent infection (Burnside et al., 2006; Cantello et al., 1994; Strassheim et al., 2012). *Meq* is the most consistently expressed latency gene playing an important role in maintaining latency and tumor development. *Meq* is a homolog of c-Jun/c-Fos oncogenes with an anti-apoptotic property that probably serves as a protection of infected cells from destruction by cellular apoptosis. Furthermore, *meq* was shown to be essential for the transformation process (Conradie et al., 2019; Heidari et al., 2008; Lupiani et al., 2004; Parcells *et al.*, 2001). Apart of the full-length *meq* form, another two spliced transcripts were described: *meq*/vIL-8 and *meq*/RLORF5a. Although these splice forms were shown to be expressed in MDV-induced tumor cells, their role remains poorly understood (Heidari *et al.*, 2008; Jarosinski and Schat, 2007).

Another crucial components in lymphoma formation are the viral telomerase RNA (vTR) and, in part, the phosphoprotein 38 (pp38) splice variant SplA. In MDV-transformed cells, vTR is the most abundant viral transcript. Telomeres are protected from shortening by the telomerase complex which adds telomeric repeats (TMRs) at the 3' end of chromosomes. The ribonucleoprotein consists of telomerase reverse transcriptase (TERT) and telomerase RNA molecule (TR) serves as a template for telomere elongation. The absence of vTR manifested in severely impaired disease development and tumorigenesis independently of its telomerase activity. On the other hand, overexpression of vTR promotes cell proliferation and dissemination of transformed T cells to various organs mediated by increased level of cell-

surface adhesion molecule integrin αv (Chbab et al., 2010; Kaufer et al., 2010; Trapp et al., 2006). Lastly, pp38 is an IE protein playing a role in apoptosis during the cytolytic infection. Besides the full-length protein, pp38 is also spliced into SplA and SplB which are expressed from 4 – 14 dpi. Although the splice variant SplA was indicated to be involved in tumor formation, the exact mechanism still remains unclear (Schat et al., 2013).

1.3.1.4 MDV spread

Around 10 – 14 dpi, infected CD4+ T cells transport the virus to the skin where the virus reactivates and infects the FFE cells. In FFE cells, virus replication is fully productive resulting in production of enveloped cell-free viral particles. These infectious particles are released throughout the life of an infected bird upon passive disintegration of FFE cells into the environment and can persist there for several months (Jarosinski et al., 2006).

In cell culture, the escape of virus seems to be rather ineffective. Detection of virus particles by electron microscopy in infected chicken embryo cells (CECs) during the late stage of virus egress showed that only a small fraction of newly assembled nucleocapsids are able to escape from the nucleus into the cytoplasm (Denesvre *et al.*, 2007). Controversially, a striking cell-blebbing phenomenon resulting in infected apoptotic bodies was reported in both early and heavily MDV infected cells posing an alternative model for MDV spread. These apoptotic bodies are thought to be cleared by neighboring cells leading to further virus dissemination. However, this theory remains speculative and needs to be confirmed in further studies (Harmache, 2014).

1.3.2 MDV integration

During latency, MDV integrates its genome into host telomeres which are protecting the ends of chromosomes. Telomeres comprise tandem repeats of DNA sequence 5′–TTAGGG–3′. It was proposed that integration into telomeres provides MDV several advantages: (i) efficient entry into host genome, (ii) efficient mobilization from latency due to highly recombinogenic disposition of telomeres and their sensitivity to large amount of stress factors resulting in activation of DNA damage response (DDR) machinery, as well as (iii) gene silencing as telomeres are enriched in post-translational histone modifications repressing gene expression. In tumor cells, MDV was found integrated in up to 15 chicken chromosomes including macro-, intermediate-, and micro-chromosomes (Delecluse and Hammerschmidt, 1993; Robinson et al., 2014; Robinson et al., 2010).

As already mentioned in chapter 6.3.1.3., MDV harbors telomeric repeats that facilitate integration into chicken chromosomes (Delecluse and Hammerschmidt, 1993; Kaufer et al., 2011; Robinson et al., 2010). In the *a-like* sequences between both IR_L/IR_S and TR_L/TR_S are

two TMR regions – multiple telomeric repeats (mTMRs), with a large but variable number of repeats, and short telomeric repeats (sTMRs), with exact 6 repeats of 5′–TTAGGG–3′ sequence. Although sTMRs were shown to play rather minor role in the integration process, mTMRs are essential for integration into telomeres and are also required for virus reactivation from latency (Greco et al., 2014; Kaufer et al., 2011). In the absence of mTMRs, MDV integrates as concatemers elsewhere in chromosomes resulting in severely impaired pathogenesis, tumor formation, and reactivation in infected chickens (Kaufer et al., 2011).

As the integration of MDV genome into host telomeres is thought to be facilitated by homologous recombination, apart from TMRs, also some viral and cellular factors have been proposed to be involved in MDV integration. Starting with viral factors, two viral proteins conserved among herpesviruses, namely UL12 and UL29, were previously shown to aid the recombination during HSV-1 genome replication by strand exchange (Schumacher et al., 2012). UL12 is an alkaline nuclease with 5'-3' exonuclease activity interacting also with MRN (Mre11, Rad50, and Nbs1) complex sensing DSBs. UL29 is a multifunctional single-strand binding protein with recombinase activity promoting strand invasion and annealing of complementary ssDNA (Balasubramanian et al., 2010; Makhov and Griffith, 2006; Perez-Losada et al., 2015; Weller and Sawitzke, 2014). It was thus suspected that MDV could have adapted the recombination mechanism also for its genome integration. However, this hypothesis seems to be improbable as we recently demonstrated that both UL12 and UL29 are dispensable for MDV integration into host telomeres (Previdelli et al., 2019). Coming to the cellular factors, many cellular proteins are involved in homologous recombination as a repair mechanism after DNA DSBs. In this context, especially two cellular proteins are hypothesized to foster the MDV integration – Rad51 and Rad52. Rad51 binds to single-stranded DNA and catalyzes the invasion of dsDNA by the single strand filament, whereas Rad52 mediates the extension of invasion strand followed by D-loop inversion during synthesis-depended strand annealing (Arnaudeau et al., 1999; Li and Heyer, 2008; Nogueira et al., 2019). Similarly, the shelterin complex protecting telomeres and consisting of TRF1, TRF2, RAP1, TIN2, TPP1, and POT1 proteins was also proposed to play a role in herpesvirus integration. As TRF1 and TRF2 proteins are known to bind directly to chromosomal TTAGGG repeats, scientists speculated whether these proteins might be also somehow involved in the integration process. Moreover, TRF2 is able to mediate strand invasion during homologous recombination (Mao et al., 2007). Based on these facts, a recent study on HHV-6 showed not only that TRF2 interacts with viral TMRs during infection, but its presence is even required for HHV-6 chromosomal integration (Gilbert-Girard et al., 2020). Therefore, it is possible that TRF2, as well as some other shelterin proteins, could also play an important role in MDV integration. Last but not least, activation of human CD4^{+} T cells was recently shown to be

associated with immense chromatin changes leading to increased chromatin accessibility (Bediaga et al., 2021). If this behavior is true also for chicken CD4$^+$ T cells, then probably even the nature of cells itself might facilitate MDV integration. Nevertheless, these theories remain to be proven experimentally.

1.3.3 MDV and epigenetic modifications

In infected birds, MDV induces significant posttranslational modifications of histones during early cytolytic and latent stage of infection. The nucleosome core contains two copies of each histones H2A, H2B, H3, and H4 that can be modified by methylation, acetylation, ubiquitination, sumoylation, and phosphorylation. These posttranslational modifications influence chromatin condensation and accessibility of DNA to other proteins. Some of the important chromatin changes include acetylation of lysine 9 of histone H3 (H3K9ac), methylation and trimethylation of lysine 4 of histone H3 (H3K4me and H3K4me3, respectively), which are associated with active genes. Another important modification is trimethylation of lysine 9 and/or 27 of histone H3 (H3K9me3 and H3K27me3, respectively) which mark silenced regions. Large amount of immune-related pathways, e.g. ubiquitin-mediated proteolysis pathway, focal adhesions (playing a critical role in cell migration and angiogenesis) or MAP kinase signaling pathway (regulating many cellular processes such as cell proliferation or apoptosis) appear to be hotspots of epigenetic regulation upon MDV infection. Moreover, they showed significant variations in H3K4me3 and H3K27me3 levels. In addition, some cancer-related miRNAs exhibited strong H3K4me3 marks and thus might contribute to higher MD-susceptibility (Luo et al., 2012; Mitra et al., 2015). Another recent studies showed that even *meq* protein plays a role in epigenetic regulation. Besides mediating the proteasome-dependent degradation of chicken histone deacetylases (chHDAC1 and 2) (Liao et al., 2021), MAP kinase is targeted by *meq* protein (Subramaniam et al., 2013) and showed significant variations in H3K27me3 levels in susceptible birds leading to increased transformation and tumorigenesis (Mitra *et al.*, 2015).

As previously mentioned, integrating into telomeres provides MDV the advantage of gene silencing as telomeres are involved in plethora of epigenetic modifications. Telomere silencing is a reversible and very complex mechanism regulated by cellular metabolism. One of the important silencing mechanisms that MDV could benefit from is the spread of heterochromatin over several kilobases and silencing nearby promoters known as the telomere position effect. Moreover, redistribution of shelterin proteins is another possible mechanism of regulating gene expression. In chromosomes with short telomeres, more TRF2 protein is available to bind at promoters outside telomeres which can result in TRF2-mediated gene silencing

through histone modifications (Mukherjee et al., 2018; Song and Johnson, 2018; Vinayagamurthy et al., 2020; Ye et al., 2014).

1.4 Optical detection of viral nucleic acids in living cells

Once a virus enters into the host cell, numerous interactions take place between viral and cellular factors, eventually leading to an exploiting of the host cell by the virus. Some of these interactions are already well studied; however, the majority of them are still poorly understood. Many questions regarding MDV genomes are still waiting to be answered: Do all incoming virus particles give rise to a replication compartment? Does MDV have to replicate before it integrates into telomeres? Can we identify in real-time which cells harbor the latent virus? Can we excise integrated virus from the host genome? What happens with the viral DNA during reactivation? Which cellular or viral proteins do interact with viral genomes during different stages of infection? Today, protein labeling is commonly used to visualize protein localization, trafficking, metabolic pathways, protein synthesis, and other interactions within a living cell. As some proteins, both viral and cellular, are interacting with and binding to viral DNA (vDNA), there is also a need to somehow label the vDNA. Fluorescent *in situ* hybridization (FISH) is a commonly used method to visually detect viral nucleic acids within infected cells. However, FISH is performed on fixed cells which leads to observation of a static state of infection. Fortunately, many labeling approaches were discovered and invented to specifically tag viral genomes in living cells allowing to observe the dynamic host-virus interplay during the whole infection process in real time. These approaches can aid to identify key players as well as to reveal the underlying mechanisms of these complex processes.

This thesis is focused on tracking DNA genomes of MDV in living cells. For this purpose, we utilized the well-established operator/repressor system. In the meantime, another two labelling techniques, namely the ANCHOR™ and SunTag systems, were also used to visualize herpesvirus genomes. Therefore, both systems are introduced in the next chapter as they are abundantly discussed in this thesis. However, in the past few years, genomes of many different RNA and DNA viruses have been visualized using also alternative approaches such as molecular beacons (Cui et al., 2005; Ma et al., 2019; Santangelo et al., 2006; Yeh et al., 2010), aptamers (Nilaratanakul et al., 2017; 2020), fluorogenic probes (Luo et al., 2019) or metabolic labeling by intercalating dyes (Mok and Yakimovich, 2019; Muller et al., 2019; Wang et al., 2013).

1.4.1 Operator/repressor system

In a typical operon, the operator is a segment of DNA located in a close proximity of a gene promoter to which a repressor protein can bind. The bound repressor is hindering RNA polymerase to tether with the gene promoter and thus blocks gene transcription. However, an

inducer molecule can interact with the bound repressor leading to conformational change and release of the repressor from the operator allowing the RNA polymerase to bind to the promoter.

The operator/repressor system for direct visualization of specific DNA loci is a modified technique utilizing the strong specific interaction of repressor with its operator. The repressor protein is fused with a fluorescent protein allowing visual detection of the protein with a microscope. Today, there are two variants of the system that are commonly used for visualization – lactose (Lac) and tetracycline (Tet) operator/repressor system. The first direct visualization of specific chromosomal loci in living cells was done in 1996 using modified Lac operator/repressor system. Here, a 10 kb long Lac operator (*LacO*) consisting of 256 tandem repeats was cloned into the yeast chromosome. Despite the large number of tandem repeats, the *LacO* remains stable in the chromosome and the size of repeats does not change even after 25 cell divisions. Each single operator repeat can bind two subunits of the Lac repressor fused with green fluorescence protein (LacI-GFP) (Straight et al., 1996). In 1997, a similar technique using the tetracycline operator/repressor system was developed (Michaelis et al., 1997). The construction of tetracycline operators (*tetO*) was achieved by amplifying 350 bp long fragments containing seven 42 bp long $TetO_2$ element sequences and a short spacer. After gradual head-to-tail multimerization, a tandem repeat of 112 *tetO* was cloned into the plasmid pRS306 resulting in approximately 5.5 kbp long *tetO* repeats (Gossen and Bujard, 1992; Sikorski and Hieter, 1989). To generate a tetracycline repressor fused with GFP (TetR-GFP), TetR was amplified by PCR introducing nuclear localization sequence (NLS) from the SV-40 large T-antigen right after the ATG start codon. In the next step, GFP was fused with the C terminus of TetR. Lastly, to ensure an efficient transcription termination, alcohol dehydrogenase I terminator was introduced right after the stop codon (Michaelis *et al.*, 1997). Similarly as in *LacO*/LacI, TetR-GFP forms a dimer that recognizes and attaches to a single $TetO_2$ element resulting in maximum 224 TetR-GFP molecules binding to the 112 tandem repeats of *tetO*. In the presence of tetracycline antibiotics, the inducer molecule triggers in TetR rearrangements of helices α4 and α6 ensuring a conformational change followed by release of TetR from *tetO* (Orth et al., 1998) (Fig. 4).

Both, the *LacO*/LacI and *tetO*/TetR systems were already used to investigate spatial dynamics of chromosomes and to visualize genomic loci in yeast, fly, nematodes, and mammalian cells (Bystricky et al., 2004; Gonzalez-Serricchio and Sternberg, 2006; Lisby et al., 2003; Robinett et al., 1996; Roukos et al., 2014; Roukos et al., 2013; Strukov and Belmont, 2008; Vazquez et al., 2002). In 2002, the *tetO*/TetR system was adapted to visualize parental HSV-1 genomes in living cells. Tandem *tetO* repeats and TetR fused with enhanced yellow fluorescent protein

(TetR-eYFP) were inserted into amplicon plasmids (Sourvinos and Everett, 2002). Amplicon plasmids are *E. coli* plasmids carrying minimal DNA replication origin (OriS) and HSV-1 packaging signals in addition to the genes of interest. In the presence of a helper virus, amplicon plasmids are replicated as concatemers that are normally packaged into viral particles (Epstein, 2005; Spaete and Frenkel, 1982). Similarly, recombinant adeno-associated virus-2 (rAAV) vectors utilizing *LacO*/LacI system were used to monitor spatial and temporal organization of AAV DNA replication in the presence of a helper virus (Fraefel et al., 2004; Glauser et al., 2007).
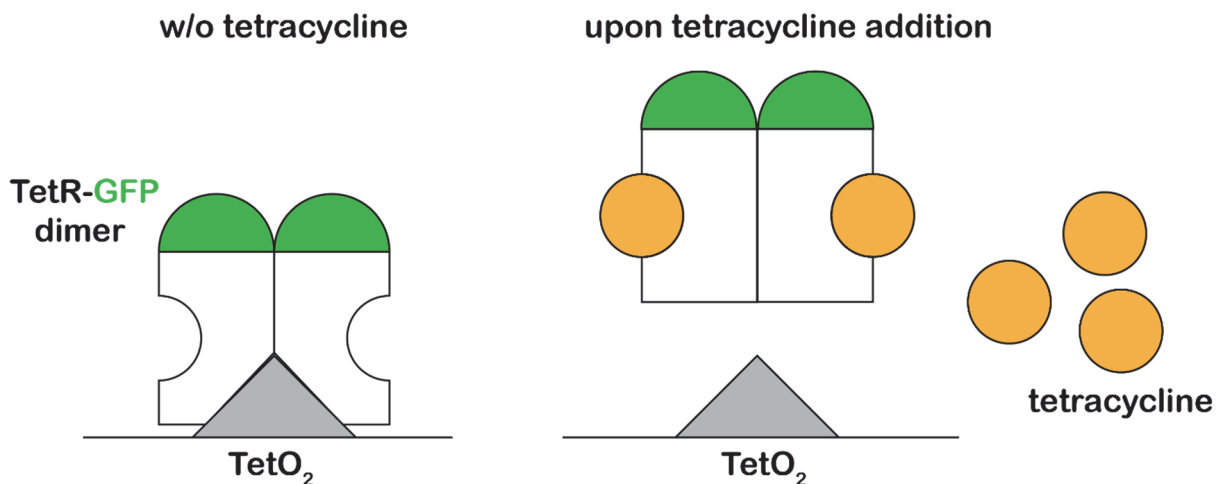
Figure 4: The tetracycline operator/repressor system. A tetracycline repressor fused with a green fluorescence protein (TetR-GFP) binds as a dimer to the $TetO_2$ element. In the presence of tetracycline, the inducer molecule (yellow circles) binds to the repressor triggering a conformational change of TetR resulting in release of the TetR-GFP dimer from $TetO_2$ element.

1.4.2 ANCHOR™ system

The patented ANCHOR™ DNA labelling technology is derived from a bacterial parABS chromosome segregation machinery. The ANCHOR™ system consists of an approximately 1 kbp long palindromic DNA sequence called ANCH (originally parS) and fluorescently labelled OR proteins (originally parB protein). OR proteins specifically bind through nucleation sites to the ANCH sequence. For that, the ANCH DNA sequence needs to be inserted in the target DNA of interest. The OR protein expression can be done from the whole ANCHOR™ cassette or from a separate plasmid. After binding of OR protein dimers to the ANCH DNA sequence, the OR proteins spread on the DNA and multimerize with newly recruited OR dimers to form a large nucleoprotein complex with up to 500 molecules of OR protein per 1 ANCH sequence. This results in signal amplification of fluorescently labelled OR proteins allowing detection of the target DNA sequence where the ANCH sequence was inserted (Fig. 5). Although the OR proteins do not possess any NLS, they are small in size and can freely

diffuse through nucleopores from cytoplasm into the nucleus. This system was already used for DNA tracking of the herpesvirus human cytomegalovirus (HCMV) and adenovirus type 5 during their replication cycles in living cells, to localize vaccinia virus (VACV) replication occurring in the cytoplasm in viral factories with immunofluorescently stained cellular compartments, and even for tracking baculovirus *Autographa californica* multiple nucleopolyhedrovirus (AcMNPV) in insect larvae *in vivo* (Bystricky et al., 2012; Gallardo et al., 2020; Hinsberger et al., 2020; Komatsu et al., 2018; Mariame et al., 2018).
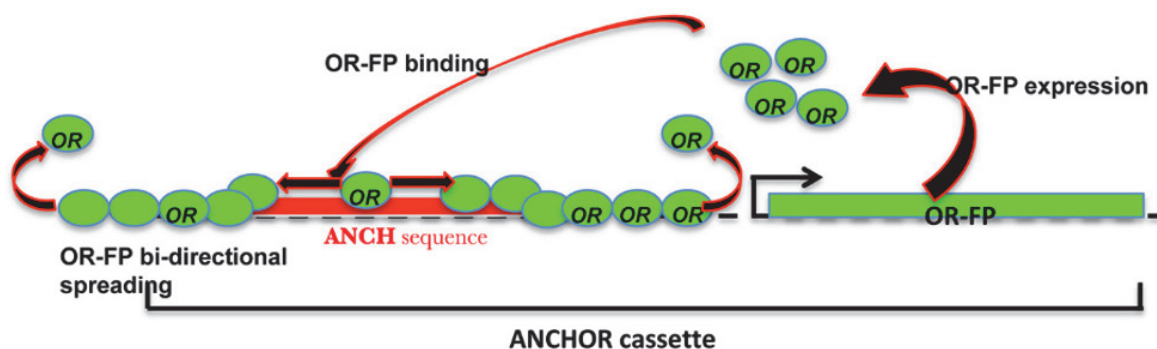
Figure 5: Principle of the ANCHOR^TM DNA labelling system. The ANCHOR cassette consists of a specific DNA sequence (ANCH sequence) and a protein expression cassette (OR fused with a fluorescence protein; OR-FP). After protein expression, OR-FP binds to ANCH DNA and multimerizes into a large nucleoprotein complex. (Image from Mariame et al., 2018 (Mariame *et al.*, 2018))

1.4.3 SunTag system

This tagging system was named after a very bright supernova stellar explosion (Tanenbaum et al., 2014). The SunTag system came with an elegant solution how to amplify fluorescent signal while overcoming RNA/DNA motifs or protein multimerization. The working principle of this method is based on the interaction between short unstructured peptides with antibodies that are binding to them with both high affinity and specificity. Single-chain variable fragment (scFv) antibodies, recombinant molecules that have fused epitopes of the light and heavy immunoglobulin chains into a single polypeptide, were fused to green fluorescent protein (GFP). They are co-expressed with the cognate GCN4 multimerized peptide resulting in recruitment of 24 copies of scFv-GFP molecules to a single peptide chain. To visualize a desired genomic sequence, an array of GCN4 peptides was fused to a nuclease-deficient mutant of the CRISPR-associated protein Cas9 (dCas9), which can bind to any at least 20 nucleotide-long genome sequence using sequence-specific small guide RNAs (sgRNAs; Fig. 6) (Tanenbaum *et al.*, 2014). This system was further adapted for detection of single RNA molecules of coxsackievirus B3 (Boersma et al., 2020) and can be also used in DNA viruses.
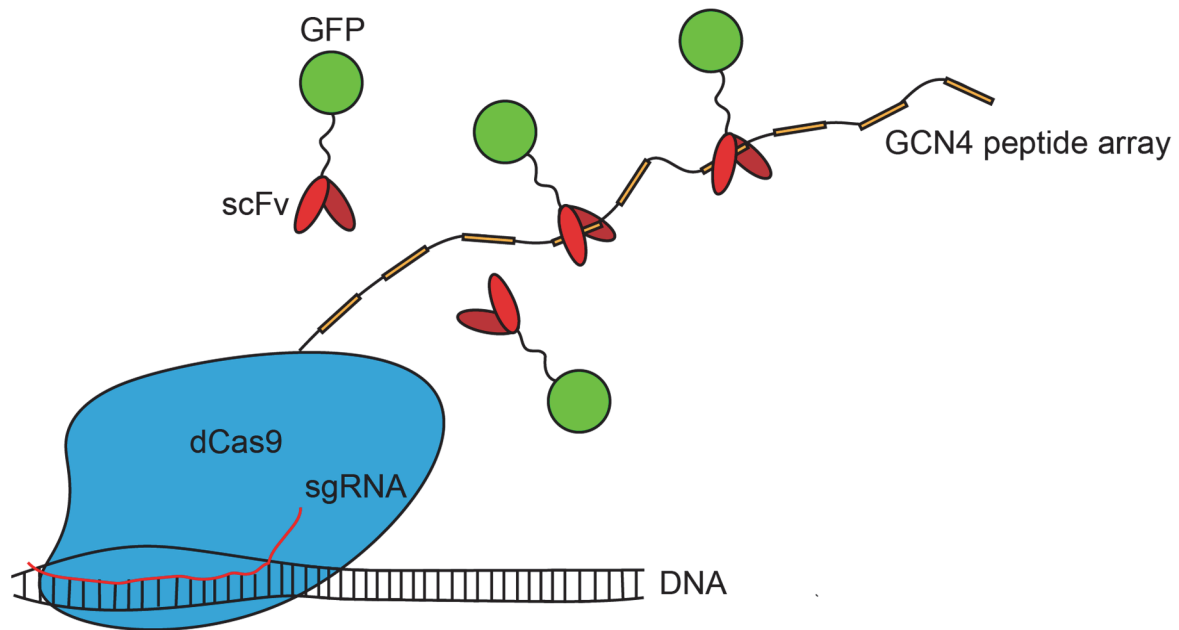
Figure 6: Schematic representation of the SunTag labelling method. A stretch of GCN4 peptides is recruiting up to 24 copies of single-chain variable fragment (scFv) antibodies fused with GFP to a single endonuclease deficient Cas9 (dCas9) protein. dCas9 is targeted to a specific genome sequence by sequence-specific small-guide RNA (sgRNA; depicted as red line), preferably to a repetitive sequence to amplify the GFP signal.

1.5   Project aims

In this cumulative PhD thesis, two specific aims were addressed and the findings contributed to better understanding of Marek's disease virus. In this thesis, we set out:

1.5.1   To investigate whether Marek's disease virus requires both copies of the inverted repeat regions

Marek's disease virus belongs into the group of herpesviruses with E class genome. The genome is arranged into two unique regions (long and short; U_L and U_S, respectively). Each unique region is flanked by identical inverted repeat regions called terminal and internal repeats. The terminal and internal U_L repeat regions (TR_L and IR_L, respectively) are 13 kbp long and the terminal and internal repeats flanking the U_S region (TR_S and IR_S, respectively) are 11 kbp long. Genes found within the repeat regions are involved in MDV pathogenesis, latency and tumor formation (Bertzbach *et al.*, 2018; Tulman *et al.*, 2000). Since two identical copies of these genes exist within the virus genome, it is tedious and time consuming to mutate both copies as two rounds of mutagenesis and subsequent analysis have to be performed. If only one copy of a gene is amended, the virus repairs such alteration by homologous recombination (HR) using the second unchanged gene copy as a template. In all probability,

this repair mechanism happens during the cleavage of concatemeric DNA into unit-length molecules as many DNA breaks are generated. Therefore, I focused on the generation and characterization of platform viruses that can be used for straightforward mutation of the repeat regions in the first paper of this cumulative dissertation. Utilizing the feature of HR, any mutation within the repeat region will be copied into the second inverted segment during virus reconstitution. One of the platform viruses was then further employed for generation of recombinant viruses used in the second project. Moreover, we investigated whether only one set of the repeats and diploid genes is sufficient for the pathogenesis, tumor formation, and spread of MDV.

1.5.2   To establish a system to visualize Marek's disease virus genomes in living cells

In the past years, visualization of viral genomes in living cells has become more and more attention since it allows to study the dynamics of host-viral interplay in real-time. So far, only ANCHOR™, the commercial approach of labeling DNA, was applied into the herpesvirus full genome to investigate the behavior of HCMV during infection and lytic replication (Mariame *et al.*, 2018). In addition, the operator/repressor system has been implemented into HSV-1 amplicon plasmids to explore the details of replication compartments and HSV-1 recombination in living cells (Glauser *et al.*, 2007; Seyffert *et al.*, 2021; Sourvinos and Everett, 2002). Based on the previous studies using the operator/repressor system also in yeast, we decided to utilize this well-established system to visualize MDV genomes during both lytic replication as well as latency.

2   Marek's disease virus requires both copies of the inverted repeat regions for efficient *in vivo* replication and pathogenesis

Tereza Vychodil[a,#], Andelé M. Conradie[a,#], Jakob Trimpert[a], Amr Aswad[a], Luca D. Bertzbach[a,*] and Benedikt B. Kaufer[a,*]

[a]Institut für Virologie, Freie Universität Berlin, Robert von Ostertag-Str. 7-13, 14163 Berlin, Germany

[#]T.V. and A.M.C. contributed equally to this work. Author order was determined chronologically when the authors joined the project and by decreasing seniority.

*Corresponding authors

Marek's disease virus requires both copies of the inverted repeat regions for efficient *in vivo* replication and pathogenesis

2.1 Abstract

Marek's disease virus (MDV) is an oncogenic alphaherpesvirus of chickens. The MDV genome consists of two unique regions that are both flanked by inverted repeat regions. These repeats harbor several genes involved in virus replication and pathogenesis, but it remains unclear why MDV and other herpesviruses harbor these large sequence duplications. In this study, we set to determine if both copies of these repeat regions are required for MDV replication and pathogenesis. Our results demonstrate that MDV mutants lacking the entire internal repeat region (ΔIR_{LS}) efficiently replicate and spread from cell-to-cell *in vitro*. However, ΔIR_{LS} replication was severely impaired in infected chickens and the virus caused significantly less frequent disease and tumors compared to the controls. In addition, we also generated recombinant viruses that harbor a deletion of most of the internal repeat region, leaving only short terminal sequences behind (ΔIR_{LS-HR}). These remaining homologous sequences facilitated rapid restoration of the deleted repeat region, resulting in a virus that caused disease and tumors comparable to the wild type. Therefore, ΔIR_{LS-HR} represents an excellent platform for rapid genetic manipulation of the virus genome in the repeat regions. Taken together, our study demonstrates that MDV requires both copies of the repeats for efficient replication and pathogenesis in its natural host.

2.2 Importance

Marek's disease virus (MDV) is a highly oncogenic alphaherpesvirus that infects chickens and causes losses in the poultry industry of up to $2 billion per year. The virus is also widely used as a model to study alphaherpesvirus pathogenesis and virus-induced tumor development in a natural host. MDV and most other herpesviruses harbor direct or inverted repeats regions in their genome. However, the role of these sequence duplications in MDV remains elusive and has never been investigated in a natural virus-host model for any herpesvirus. Here, we demonstrate that both copies of the repeats are needed for efficient MDV replication and pathogenesis *in vivo*, while replication was not affected in cell culture. With this, we further dissect herpesvirus genome biology and the role of repeat regions in Marek's disease virus replication and pathogenesis.

2.3 Introduction

Across the Herpesviridae family, six different genome arrangements exist that are termed class A to class F (1). Five of these genome classes harbor direct or inverted repeats, but the importance of these sequence duplications in replication and pathogenesis remains largely elusive. We set out to investigate their role in alphaherpesvirus infections, using a well-established natural virus-host infection model.

The highly oncogenic avian alphaherpesvirus Marek's disease virus (MDV) naturally infects chickens and replicates in various lymphocyte populations (2, 3). Upon primary infection, the virus establishes latency and integrates into the telomeres of latently infected T cells. Telomere integration provides the basis for rapid T-cell transformation and lymphoma formation, resulting in high mortality in unvaccinated hosts (4–6). MDV has a class E genome of 180 kbp in length that consists of a unique long segment (U_L) and a unique short segment (U_S) flanked by inverted terminal repeats (TR_L and TR_S) and internal repeats (IR_L and IR_S) (Fig. 7) (7). The unique regions mainly harbor genes that are conserved among alphaherpesviruses. In contrast, the repeat regions contain many MDV-specific protein-coding genes, RNAs, and other sequence elements that play a role in MDV pathogenesis, cellular tropism, tumorigenesis, and latency (8). We previously demonstrated that deletion of a large part of the MDV IR_L is readily restored during the first passages *in vitro* (9). This occurs most likely by homologous recombination (HR) during virus replication. In the present study, we set out to determine whether both copies of the repeat regions are required for MDV replication and pathogenesis *in vitro* and *in vivo*. Our data conclusively demonstrate that mutant viruses lacking the entire internal repeat regions were unable to restore these sequences but were able to efficiently replicate and spread cell to cell *in vitro*. In contrast, they poorly replicated in infected animals and caused significantly less frequent disease and tumors than the control viruses. Taking the results together, our report reveals that both copies of the repeat regions are crucial for pathogenesis in the natural host and provides important insights into herpesvirus genome biology.
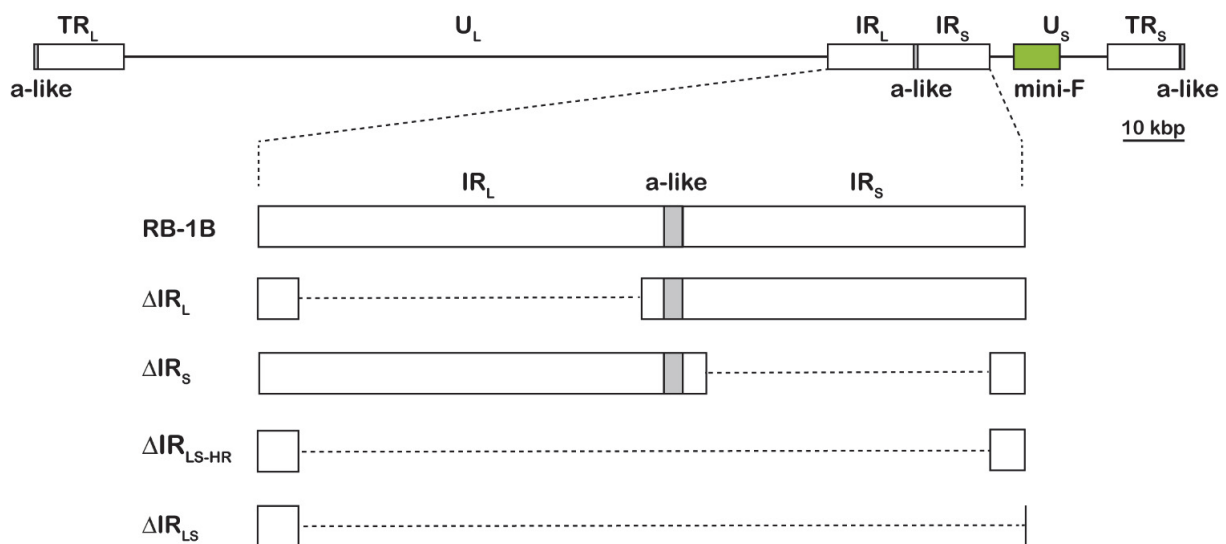
Figure 7: Overview of the MDV genome and the recombinant viruses. The figure presents an overview of the MDV RB-1B genome with its unique long region (U_L) and unique short region (U_S) harboring the mini-F cassette containing the pTK-eGFP cassette. The unique regions are flanked by a long terminal repeat and long internal repeat (TR_L and IR_L, respectively) and by a short terminal repeat and a short internal repeat (TR_S and IR_S,

respectively). The mutant viruses used in this study are depicted, and the respective deletions are shown as dashed lines. Deleted regions were confirmed by Illumina MiSeq analysis.

2.4 Results

2.4.1 Generation and characterization of deletion mutants *in vitro*

To determine if and how efficiently different repeat regions in the virus genome are restored upon reconstitution, we generated four recombinant viruses using a bacterial artificial chromosome (BAC) of the very virulent RB-1B strain (10). We deleted either most of the IR_L (ΔIR_L) or most of the IR_S (ΔIR_S), leaving only terminal sequence behind, which should have facilitated the restoration of the region as published previously for the IR_L (9). In addition, we generated mutants that lacked the entire IR_L and IRs regions with (ΔIR_{LS-HR}) or without (ΔIR_{LS}) the homologous sequences at both ends (Fig. 7). All viruses were efficiently reconstituted, resulting in stocks with comparable titers.

To examine the effect of each deletion on virus replication, we performed plaque size assays and multistep growth kinetics analyses. Plaque size assays performed after transfections (Fig. 8A) or infection with 100 plaque-forming units (PFU) (Fig. 8B) revealed that the ΔIR_{LS} deletion caused slightly smaller plaques (80.7% ± 28.1% standard deviation [SD]), while the spread of the other viruses in culture was comparable to that seen with the wild type (wt). Growth kinetics results did not show any significant differences between the viruses (Fig. 8C). Next, real-time quantitative PCR (RT-qPCR) performed on a panel of relevant genes showed that RNA expression levels in cells infected with the recombinant viruses were comparable to those seen with cells infected with the wt (Fig. 8D). Moreover, to ensure that protein expression of pp38 was not affected by the deletion of the repeats in its close proximity, we performed Western blotting and observed no difference in the levels of pp38 expression between mutant and wt viruses (Fig. 8E and F).

To further investigate if and how efficiently each of the deletions can be restored, recombinant BACs were transfected into chicken embryo cells (CECs) and the virus was propagated for 10 passages. DNA was isolated at passages 1, 5, and 10 and the deletion site assessed by quantitative PCR (qPCR). These qPCR results demonstrated that deletion of the IR_L in ΔIR_L virus was efficiently restored as described previously (Fig. 9A). Surprisingly, the restoration kinetics were much slower for the IR_S region, and the deletion was still detectable in 8.9% of the genomes at passage 10 (Fig. 9B), suggesting that there is very little selective pressure to restore the IR_S region. The deletion of entire IR_L and IR_S region in ΔIR_{LS-HR} virus was restored as rapidly as in ΔIR_L virus (Fig. 9C), indicating that the selection pressure for the restoration is mostly driven by the IR_L. Importantly, the deletion in ΔIR_{LS} virus was not restored throughout

the experiment (Fig. 9D), likely due to the absence of homologous sequences for recombination.
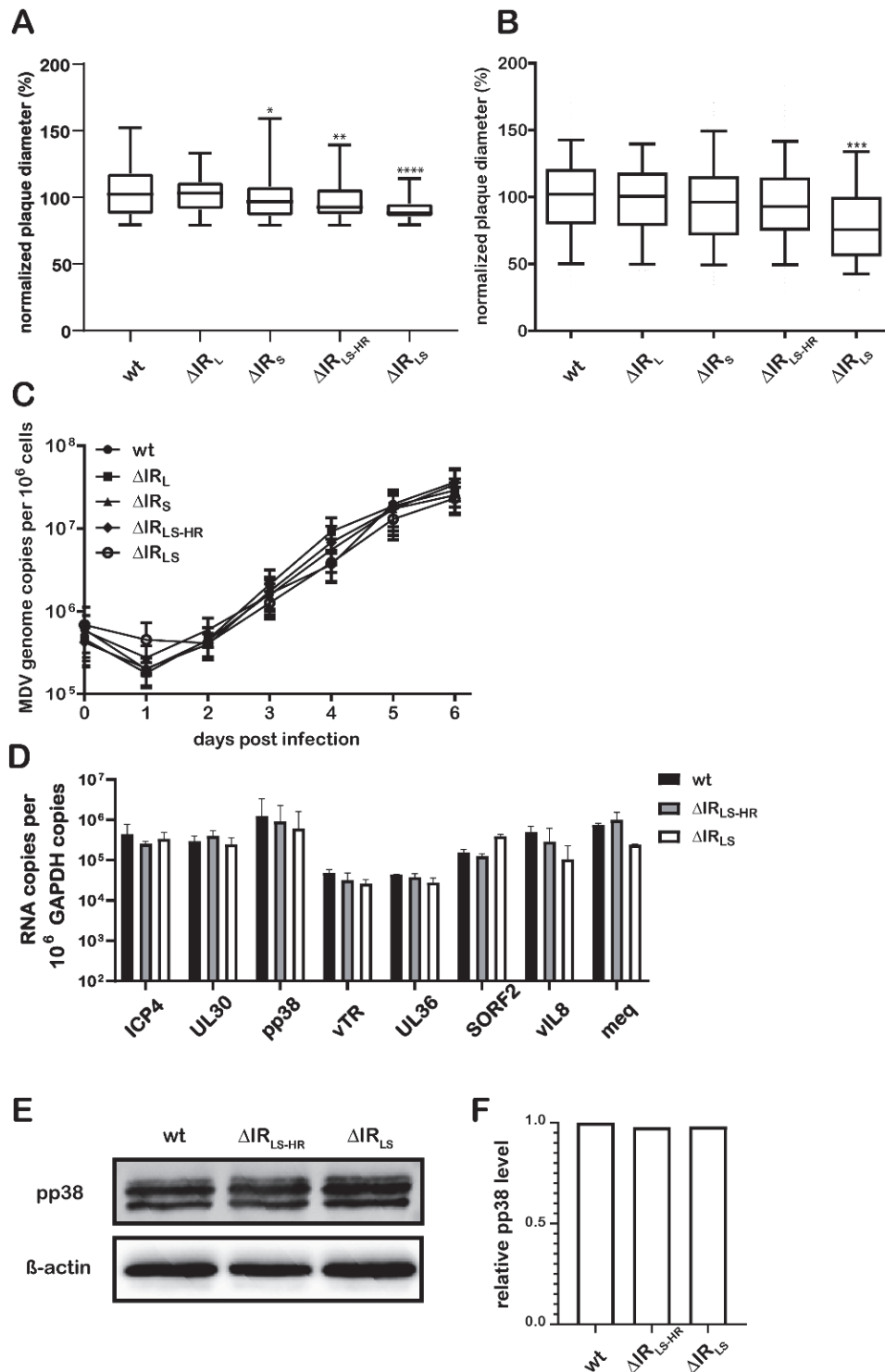
Figure 8: In vitro characterization of the recombinant viruses. Replication properties of the indicated viruses were assessed by plaque size assays after transfection (A) or inoculation of 100 pfu (B) and by multi-step growth kinetics (C). Data are shown as means of results from three independent experiments (B and C) with standard deviations. Asterisks indicate significant differences from the wt virus (*, $p < 0.1$; **, $p < 0.01$; ***, $p < 0.001$; and ****, $p < 0.0001$; one-way analysis of variance [ANOVA] Dunnett's test (A and B) or Kruskal-Wallis test

(C)). (D) CECs were infected with 4,000 pfu and harvested at 5 dpi. RNA levels of ICP4, UL30, pp38, vTR, UL36, SORF2, vIL8, and meq genes were measured by RT-qPCR. Data are shown as means with standard deviations. (E) pp38 and β-actin protein expression was detected by Western blotting. Cell lysates were prepared at 5 dpi, and proteins were separated by SDS-PAGE. (F) Relative signal intensities were quantified using BIO-1D software, and the pp38 signal intensity was normalized against that of the corresponding β-actin signal.
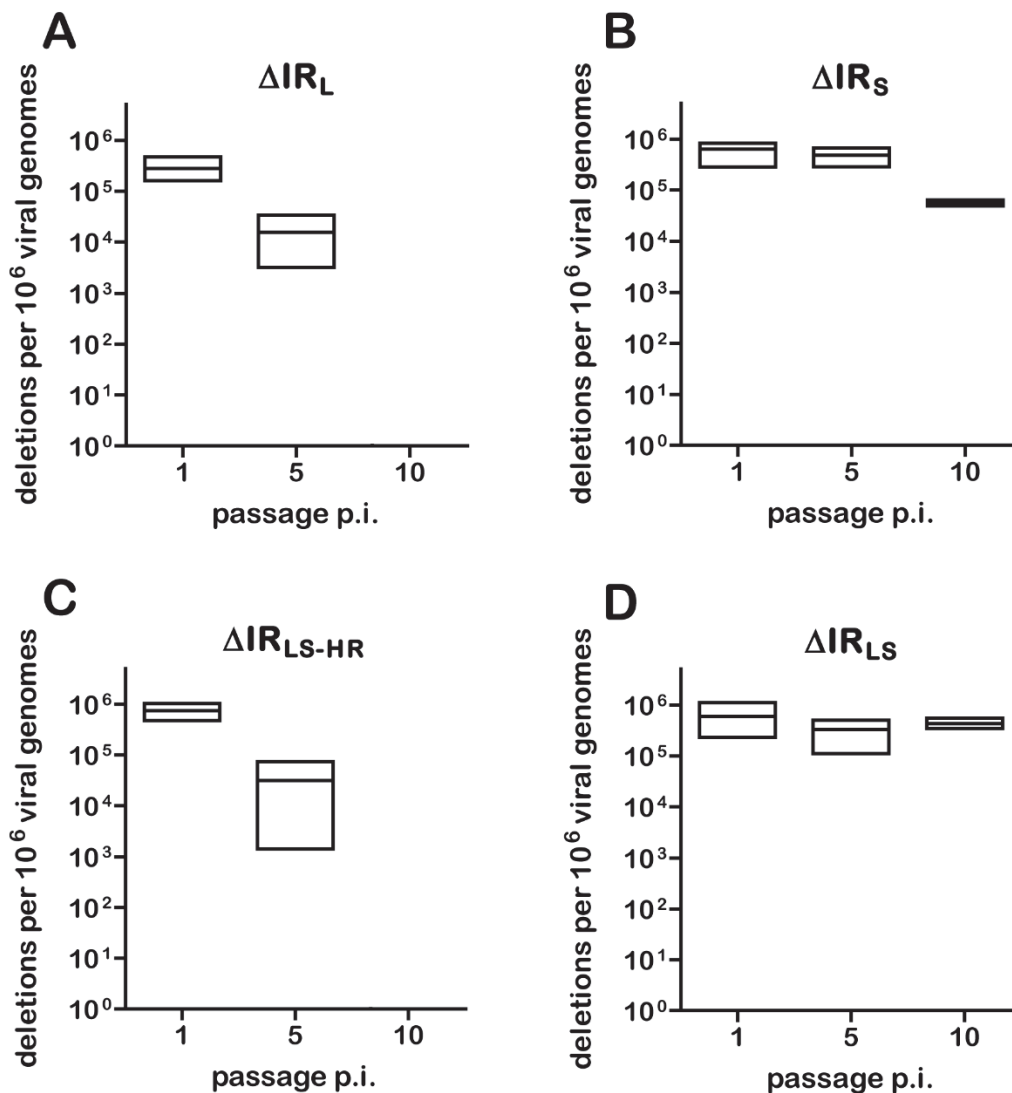
Figure 9: Assessment of the restoration in the recombinant virus genomes in vitro. Restoration of the deletion sites in (A) ΔIR$_L$, (B) ΔIR$_S$, (C) ΔIR$_{LS-HR}$, and (D) ΔIR$_{LS}$ virus was analyzed. The presence of the deletion was assessed by qPCR at passages 1, 5, and 10. Mean numbers of deletions per 10^6 viral genomes are shown as floating bars (minimum to maximum, with a line at the mean, n = 3).

2.4.2   Replication of IR$_{LS-HR}$ and IR$_{LS}$ virus in infected animals.

To determine if the duplication of the repeat regions plays a role in MDV replication *in vivo*, we infected 1-day-old chickens with 4,000 PFU of ΔIR$_{LS-HR}$, ΔIR$_{LS}$, or wt virus. Numbers of MDV genome copies in whole-blood samples were determined by qPCR at different time points postinfection (pi). Surprisingly, we observed that replication of ΔIR$_{LS}$ virus was significantly impaired in infected animals compared to wt virus-infected and ΔIR$_{LS-HR}$ virus-infected animals at almost all time points (Fig. 10A). We corroborated this replication defect by measuring RNA expression of ICP4 genes (MDV084; located in the IR$_S$), UL30 genes (MDV043; located in the U$_L$), and pp38 genes (MDV073, overlapping from IR$_L$ into U$_L$) in the blood of infected animals. The expression levels of ICP4 and UL30 genes were highly reduced at 10 days postinfection (dpi) as observed for the viral genome copies, while gene pp38 expression levels were not affected by the deletion of repeats in its close proximity (Fig. 10B). Since MDV is shed from the feather follicle epithelia, we sampled feathers at 91 dpi to further assess if the virus is delivered to the skin. Interestingly, although ΔIR$_{LS}$ virus was delivered to the skin, the viral load was significantly lower than that seen with wt and ΔIR$_{LS-HR}$ virus (Fig. 10C).

To further analyze if the viruses shed from feather follicles were able to infect naive contact chickens, we conducted qPCR on whole-blood samples. Viral load in the blood of ΔIR$_{LS}$ contact chickens was significantly lower than that seen with the contact chickens of the ΔIR$_{LS-HR}$ group (Fig. 10D). Taken together, these results demonstrate that the duplication of the repeat regions not only plays a crucial role in MDV replication in infected animals but also is required for horizontal spread.
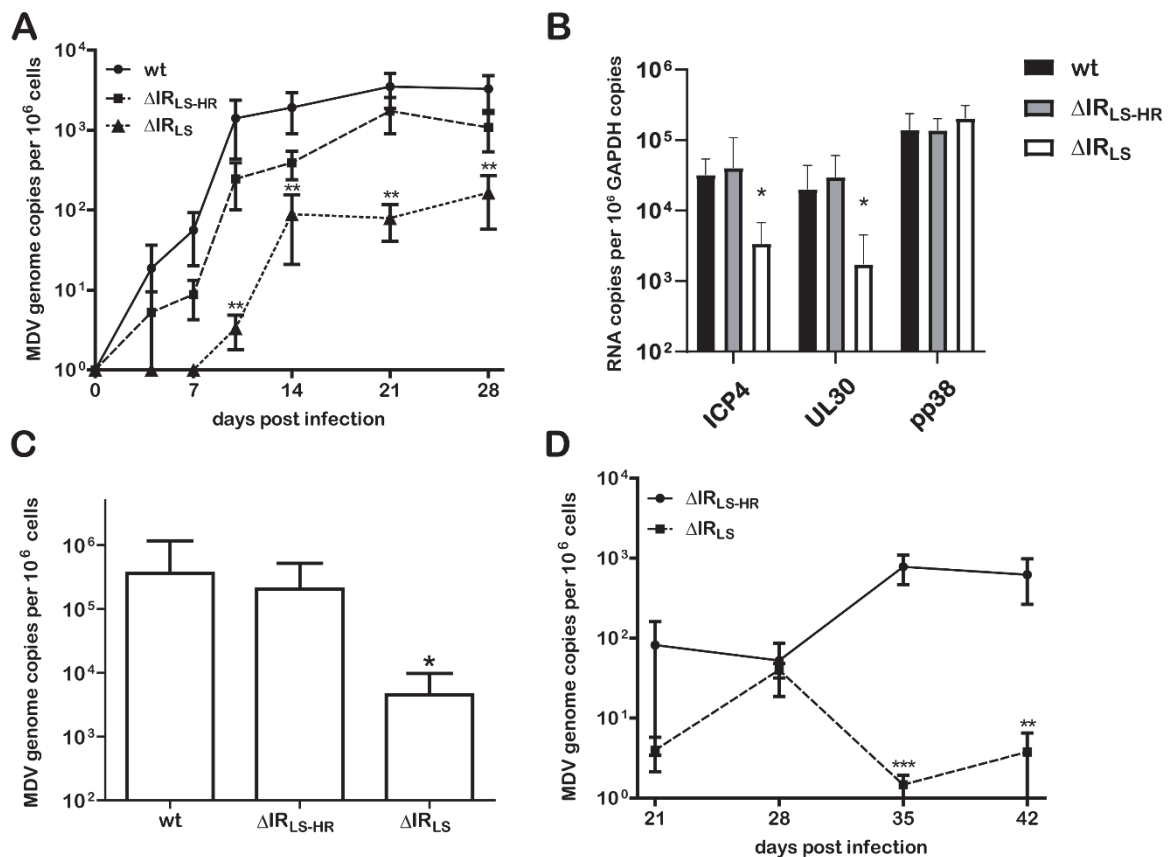
Figure 10: In vivo characterization of the recombinant viruses. (A) MDV genome copy numbers of indicated viruses in peripheral blood mononuclear cells (PBMCs) of experimentally infected chickens were assessed by qPCR (means ± standard deviations). Asterisks indicate significant differences (**, $p < 0.01$; Kruskal-Wallis test). (B) RNA expression levels of ICP4, UL30 and pp38 in the blood in eight infected chickens per group at 10 dpi. Data are shown as means with standard deviations. An asterisk indicates significance ($p < 0.05$; Kruskal-Wallis test). (C) Viral genome copy numbers in feather follicle DNA of at least five infected chickens per group at 91 dpi. Data are shown as means with standard deviations. An asterisk indicates significance ($p < 0.05$; Kruskal-Wallis test). (D) MDV genome copy numbers of indicated viruses in PBMCs of naïve contact animals assessed by qPCR (means ± standard deviations). Asterisks indicate significant differences (**, $p < 0.01$; ***, $p < 0.001$; Mann-Whitney test).

2.4.3 Pathogenesis induced by IR$_{LS-HR}$ and IR$_{LS}$ virus.

Next, we assessed the pathogenesis of and tumor incidence induced by ΔIR_{LS-HR} and ΔIR_{LS} virus throughout the 91 days of the experiment. Interestingly, disease incidence in the ΔIR_{LS} group was severely reduced compared to the wt and ΔIR_{LS-HR} virus groups. Most animals (75% to 90%) succumbed to disease upon infection with wt and ΔIR_{LS-HR} virus, whereas only 20.9% of the chickens developed disease in the ΔIR_{LS} group (Fig. 11A and B). Consistently, the overall tumor incidence was significantly reduced in the ΔIR_{LS} virus-infected chickens (16.7%) compared to those infected with wt virus (80%) and ΔIR_{LS-HR} virus (76%) (Fig. 11C). To

investigate if the IR_L and IR_S sequences were still deleted in ΔIR_{LS} virus and in restored $\Delta IR_{LS\text{-}HR}$ virus, we isolated viral DNA from tumor-derived viruses and used the DNA for Illumina MiSeq sequencing, which confirmed the sequences of the recombinant viruses.

As observed in subcutaneously infected animals, disease incidence in the contact chickens was drastically reduced in the absence of the IR_{LS} (9.09%) compared to the $\Delta IR_{LS\text{-}HR}$ virus with restored repeats (54.55%; Fig. 11B). Moreover, none of the animals infected with ΔIR_{LS} virus via the natural route developed tumors whereas $\Delta IR_{LS\text{-}HR}$ virus efficiently induced tumors (45.45%; Fig. 11C). Taken together, these data showed the importance of duplicated repeat regions in disease development and tumor formation.
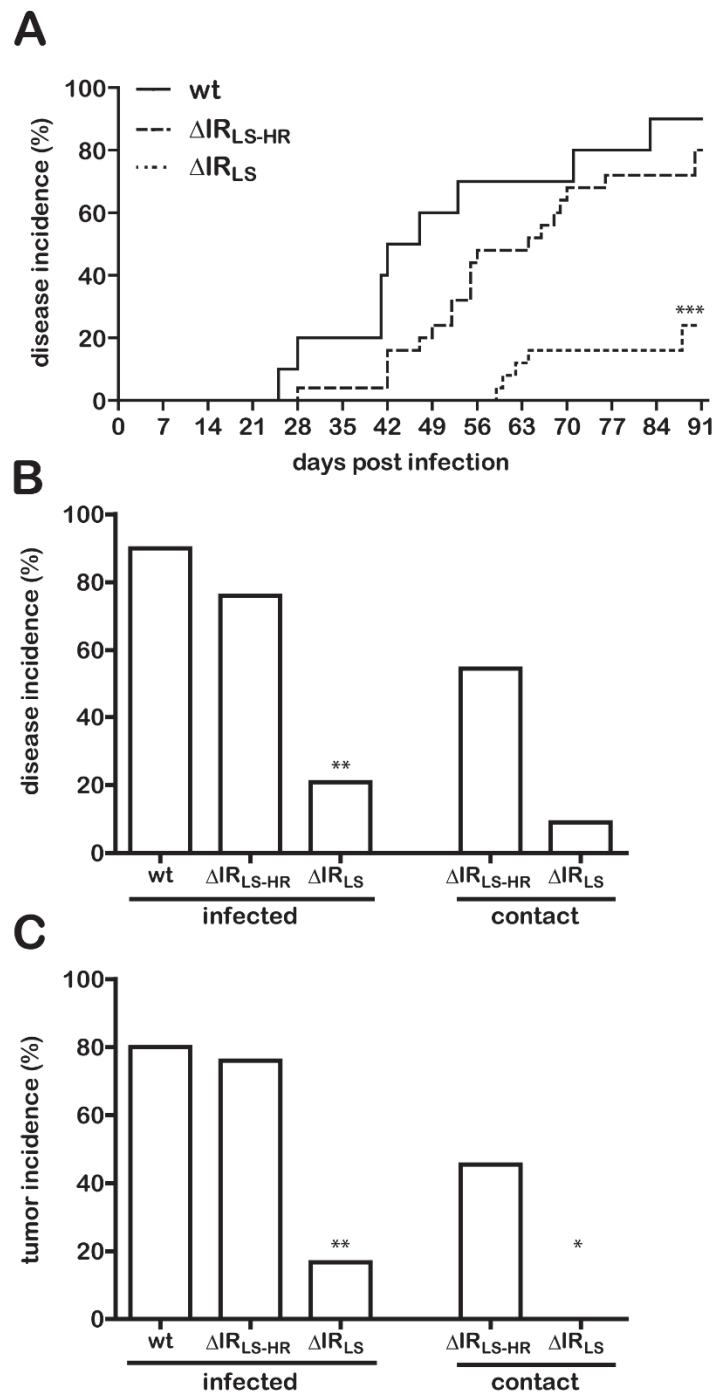
Figure 11: Marek's disease and tumor incidence of infected chickens. (A) Kaplan-Meier analysis of Marek's disease incidence in chickens infected with indicated recombinant viruses (***, $p < 0.001$; Mantel-Cox test). (B) Disease and (C) tumor incidence are shown for the different viruses as percentage of subcutaneously infected and contact chickens. Asterisks indicate significant differences (*, $p < 0.05$; **, $p < 0.01$; Fisher's exact test).

2.5 Discussion

In this study, we investigated the role of the inverted repeat regions in the complex class E herpesvirus genome using MDV and the chicken as a natural virus-host model. We previously demonstrated that a deletion of most of the IR_L in the MDV genome is rapidly restored upon reconstitution (9). This restoration is most likely facilitated by homologous recombination between the intact TR_L and the remaining terminal IR_L sequences during virus replication. This ΔIR_L virus is extensively used as a platform to generate recombinant viruses harboring mutations or deletions in genes harbored in the IR_L such as viral telomerase RNA (vTR), MDV encoded CXCL13 chemokine viral interleukin-8 (vIL-8), or the major oncogene meq (9, 11–13). Therefore, we set out to investigate if this approach could be also used for the IR_S and generated a recombinant virus lacking most of this repeat region (ΔIR_S, Fig. 7). Surprisingly, we observed that the repair efficiency of the IR_S was much lower than that of the IR_L. Whereas more than 90% of the IR_L deletions were already repaired at passage 5, hardly any restoration was detected for the IR_S (Fig. 9A and B). While the IR_L deletion was no longer detectable at passage 10, 8.9% of the ΔIR_S genomes still retained the IR_S deletion. Despite the low restoration efficiency of ΔIR_S, the virus replicated comparably to wt virus *in vitro*. This was quite surprising as the crucial transcriptional regulator ICP4 gene is located in IR_S, suggesting that the presence of only one copy of the gene is sufficient for efficient MDV replication *in vitro*. This phenomenon will be addressed in future studies.

To analyze whether two copies of the repeat region are needed for MDV replication and pathogenesis, we deleted both the IR_L and IR_S, preserving homologous sequences at both ends for homologous recombination. Here, we observed that the IR_L-IR_S deletion in ΔIR_{LS-HR} virus was restored as rapidly as the IR_L deletion in ΔIR_L virus (Fig. 9C), indicating that it is the IR_L region that mostly drives the selection pressure for the restoration. ΔIR_{LS-HR} virus replicated *in vivo* and caused disease comparable to that seen with the wt virus. Moreover, Illumina MiSeq sequencing confirmed that the virus genome was completely restored. Therefore, ΔIR_{LS-HR} virus represents an excellent platform for the manipulation of genes located in the IR_L and IR_S, as only a single locus needs to be manipulated. This approach could also be used for other E class herpesvirus genome such as herpes simplex virus 1 (HSV-1) and human cytomegalovirus (HCMV). The resulting virus then efficiently restores the deleted IR_{LS} sequence and harbors the introduced mutation in both copies of the repeats as shown previously (9, 11–13).

Furthermore, we generated an IR_L-IR_S deletion virus that cannot restore the deleted region (IR_{LS} virus; Fig. 9). ΔIR_{LS} virus replicated *in vitro* similarly to the wt virus and had plaques that were only slightly smaller than those seen with all other viruses in this study. Our data are

thereby consistent with previous publications on similar deletions in HSV-1 or HCMV (14, 15). Next, we assessed if one copy of the IR_L-IR_S region is sufficient for MDV replication and pathogenesis in this natural virus-host model. Our data demonstrate that lytic replication in animals infected with ΔIR_{LS} virus was severely impaired (Fig. 10A). Consequently, disease and tumor incidence were significantly reduced. This could have been due either to the less efficient virus replication or to lower expression levels of genes harbored in the IR_L-IR_S region, such as the vTR, vIL-8, and meq genes, that play a crucial role in pathogenesis (9, 16–19). Another reason could be the inability of the virus to undergo genome isomerization as previously shown for HSV-1 and HCMV (14, 15). Moreover, the observed drastic effect on MDV replication and pathogenesis in this natural virus-host model is consistent with previous studies on HSV-1 infection of mice (20 , 21). Taken together, our data demonstrate the importance of the inverted repeat regions in MDV replication and pathogenesis and provide the basis for further assessment of repeat regions in MDV and related herpesviruses.

2.6   Materials and methods

2.6.1   Ethics statement

All animal work was conducted according to relevant international and national guidelines for the humane use of animals and was approved by the LAGeSo (Landesamt für Gesundheit und Soziales), Berlin, Germany (approval number G0294-17).

2.6.2   Cells

CECs were prepared from Valo specific-pathogen-free (SPF) 11-day-old embryonated chicken eggs (Valo BioMedia, Osterholz-Scharmbeck, Germany) as described previously (22). Cells were maintained in minimum essential medium (Pan Biotech, Aidenbach, Germany) supplemented with 1% or 10% fetal bovine serum (FBS; Pan Biotech) and 1% penicillin (100 U/ml)/streptomycin (100 g/ml) (AppliChem, Darmstadt, Germany) at 37°C under a 5% CO_2 atmosphere.

2.6.3   Generation of mutant viruses

To determine the role of the repeat regions, we generated several recombinant viruses by two-step Red recombination system-mediated mutagenesis as described previously (23, 24). As a basis, we used the BAC of the very virulent RB-1B strain (GenBank accession no. MT797629) that expresses enhanced green fluorescent protein (eGFP) driven by the HSV-1 thymidine kinase (TK) promoter in the mini-F vector (Fig. 7) (25). In addition to the previously published IR_L deletion mutant (9), we generated a similar mutant lacking most of the IR_S region, retaining only the ends of the IR_S region (0.6 and 1 kbp; see Fig. 7) for its restoration upon reconstitution. In addition, we generated two mutants that lacked both the IR_L and IR_S

regions. The ΔIR_{LS-HR} mutant still contained the ends of the IR_L and IR_S regions (1.5 and 0.6 kbp, respectively; Fig. 7) to facilitate restoration of the deleted sequences by homologous recombination. In contrast, the entire IR_L and IR_S regions were deleted in ΔIR_{LS} virus, except for sequences of the IR_L region that are part of the pp38 gene that spans the sequence from the U_L into the IR_L region (1.5 kbp). All recombinant virus genomes were confirmed by restriction fragment length polymorphism (RFLP) analyses, Sanger sequencing, and next-generation sequencing (NGS; Illumina MiSeq) of the entire virus genome. All primers used for mutagenesis and sequencing can be found in Table 1.

2.6.4 Virus reconstitution and propagation

Recombinant viruses were reconstituted by transfection of CECs with MDV BACs using the calcium-phosphate method (26). To remove the mini-F sequences in the recombinant viruses used for the animal experiment, we cotransfected the CECs with MDV BACs and pCAGGS-NLS/Cre plasmid (9 , 27). Removal of mini-F sequences resulted in the loss of eGFP, and the results were assessed by fluorescence microscopy.

2.6.5 Plaque size assay and growth kinetics

MDV replication properties and spread were determined by plaque size assay and multistep growth kinetics. For plaque size assays, the areas of 100 randomly selected plaques for each titrated virus were measured using ImageJ (https://imagej.nih.gov/ij/). Next, plaque diameters were calculated and compared to those seen with the wt control. In addition, plaques were also measured 6 days after BAC DNA transfection (Fig. 8A) and plaque diameters were analyzed using a Bioreader 6000 system (Bio-Sys, Karben, Germany). Multistep growth kinetics were evaluated by qPCR. Here, 1 million CECs were infected with 100 PFU in 6-well plates and cultured for 6 days. Every day, the contents of one 6-well plate were harvested for qPCR and stored at –20°C. After 6 days, DNA of all samples was extracted using an RTP DNA/RNA virus minikit (Stratec, Berlin, Germany) according to the manufacturer's instructions. MDV genome copy numbers were determined by qPCR using specific primers and probe for the UL30 gene, which encodes the MDV polymerase located in the U_L region. UL30 copy numbers were normalized to chicken inducible nitric oxide synthase (iNOS) as described previously (27). Primers and probes used in this work are listed in Table 1.

Marek's disease virus requires both copies of the inverted repeat regions for efficient *in vivo* replication and pathogenesis

Table 1: Primers and probes used in this study

Construct		Sequence (5' → 3')
ΔIR$_S$, ΔIR$_L$IR$_S$	ep for	GTTCCCATTGCCCTGGGACACATCCAAAATATCAAAGTGTCGGGAAT CGAGGAATGTCGTAGGGATAACAGGGTAATCGATTT
	ep rev	CTGCATGATCTTCTTTAATTGGACGACATTCCTCGATTCCCGACACTT TGATATTTTGGGCCAGTGTTACAACCAATTAACC
ΔIR$_{LS-HR}$	ep for	GTATGTGTGGGAGAAAGTATGTCGATTTTAAATGTAGTTGACACTTTG ATATTTTGGATGTAGGGATAACAGGGTAATCGATTT
	ep rev	GTTCCCATTGCCCTGGGACACATCCAAAATATCAAAGTGTCAACTAC ATTTAAAATCGACGCCAGTGTTACAACCAATTAACC
ΔIR$_{LS}$	ep for	GTATGTGTGGGAGAAAGTATGTCGATTTTAAATGTAGTTGATATTTTT ATTAGCCAAATCTAGGGATAACAGGGTAATCGATTT
	ep rev	TGTCAAACTTCCAGGAATACGATTTGGCTAATAAAAATATCAACTACA TTTAAAATCGACGCCAGTGTTACAACCAATTAACC
GFP in mini-F	ep for	GGTGACACGCGCGGCCTCGAACACAGCTGCAGGCCATGGTGAGCA AGGGCGAGG
	ep rev	CGTCGACCCGGGTACCTCTAGATCCGCTAGCGCTTTACTTGTACAGC TCGTCCATGCC
iNOS (qPCR)	for	GAGTGGTTTAAGGAGTTGGATCTGA
	rev	TTCCAGACCTCCCACCTCAA
	Probe	FAM-CTCTGCCTGCTGTTGCCAACATGC-TAMRA
IR$_S$ detection in ΔIR$_S$ (qPCR)	for	GATCTTCTTTAATTGGACGACATTCC
	rev	GGAATTCGAAAGTGATTGCTGTT
	Probe	FAM-TTTGGATGTGTCCCAGGGCAATGG -TAMRA
IR$_L$ detection in ΔIR$_L$ (qPCR)	for	TTCTGCGAATGTTGATTACATGG
	rev	TCCAATAACTCGAACGCTCTT
	Probe	FAM-TGTATGTGTGGGAGAAAGTATGTCGA-TAMRA
IR detection in ΔIR$_{LS-HR}$ (qPCR)	for	TGTATGTGTGGGAGAAAGTATGT
	rev	GGCTGAAGGAATTCGAAAGTG
	Probe	FAM-TTTGGATGTGTCCCAGGGCAATGG -TAMRA
IR detection in ΔIR$_{LS}$ (qPCR)	for	AAATGGGAAGGTTTATTCTGC
	rev	CCTCCCATAATGATTTATAGTGATGC
	Probe	FAM-TGTATGTGTGGGAGAAAGTATGTCGA-TAMRA
UL30 (qPCR)	for	AAGCGGAATCGGTTTACAAG
	rev	GGAGTTGCTGTTAGAATACGGA
	Probe	FAM-TCGACGAGTTTCTTCCTCCTCGTTG-TAMRA
GAPDH (qPCR)	for	GGTGCTAAGCGTGTTATCATCTCA
	rev	CATGGTTGACACCCATCACAA
	Probe	FAM-TGTGCCAACCCCCAAT-TAMRA
meq (qPCR)	for	TTGTCATGACCCAGTTTGCCCTAT
	rev	AGGGAGGTGGAGGAGTGCAAAT

	Probe	FAM-GGTGACCCTTGGACTGCTTACCATGC-TAMRA
ICP4 (qPCR)	for	CGTGTTTTCCGGCATGTG
	rev	TCCCATACCAATCCTCATCCA
	Probe	FAM- CCCCCACCAGGTGCAGGCA-TAMRA
pp38 (qPCR)	for	GAGCTAACCGGAGAGGGAGA
	rev	CGCATACCGACTTTCGTCAA
	Probe	FAM-CTCCCACTGTGACAGCC-TAMRA
vTR (qPCR)	for	CCTAATCGGAGGTATTGATGGTACTG
	rev	CCCTAGCCCGCTGAAAGTC
	Probe	FAM-CCCTCCGCCCGCTGTTTACTCG-TAMRA
UL36 (qPCR)	for	GACAAGCTACTACAAATTGCA
	rev	GACGTCGATTTATCTCTTAACA
	Probe	FAM-AAGAACTACATCGAACGCACCCATGCTAGC-TAMRA
SORF2 (qPCR)	for	AGCGCCAAACCGGACAT
	rev	GTCCCCTGCGATTCCAAAC
	Probe	FAM-TGGAAGACAAAAAGAGAAC-TAMRA
vIL8 (qPCR)	for	CGCACAAGGAAGGAAAATCTG
	rev	GTCCCACGGTCGATTTGC
	Probe	FAM-TGGTTGGAGAAGATGG-TAMRA

En-passant mutagenesis primer, ep; forward primer, for; reverse primer, rev; 6-carboxyfluorescein, FAM; tetramethylrhodamine, TAMRA.

2.6.6 Western blotting

For Western blot analysis of pp38, 1 million CECs were infected with 4,000 PFU of wt RB-1B, ΔIR_{LS-HR}, and ΔIR_{LS} virus. At 5 dpi, cell lysates were prepared using glycoprotein denaturating buffer (NEB, Ipswich, MA, USA). Samples were boiled, loaded, and separated by SDS–15% polyacrylamide gel electrophoresis. Next, proteins were transferred onto a polyvinylidene difluoride (PVDF) membrane (Carl Roth, Karlsruhe, Germany) by dry transfer and blocked with 5% skimmed milk–phosphate-buffered saline (PBS)–Tween. Proteins were incubated with a mouse anti-pp38 antibody (BD1; generated at The Pirbright Institute, Woking, United Kingdom) (1:200) and a mouse anti-β-actin antibody (Thermo Fisher, Waltham, MA, USA) (1:1,000) followed by anti-mouse IgG horseradish peroxidase (HRP) secondary antibody (Sigma-Aldrich, St. Louis, MO, USA) (1:10,000). HRP was visualized by enhanced chemiluminescence using Pierce ECL Plus substrate (Thermo Fisher Scientific) and detected by the use of a Fusion-SL system (Vilber, Collegein, France). BIO-1D v12.14 software (Vilber) was used to quantify band intensities by utilizing the thresholding algorithm. pp38 optical densities were normalized against β-actin (Fig. 8E and F).

2.6.7 Restoration assay

CECs were transfected with MDV BACs using the calcium-phosphate method as described above. In every passage, cells were trypsinized and split at a ratio of 1:100. In addition, a sample of these cells was frozen for subsequent DNA extraction. Restoration efficiency was assessed from passage 1 to passage 10, which corresponded to a final dilution factor of 10^{20}. To detect restoration of the deleted repeat sequences, DNA was extracted from infected cells as described above. The numbers of genomes still harboring the deletion site were determined by qPCR using specific primers and probes that span the deletion sites of the respective mutant viruses. Copies were then normalized against UL30 DNA copy numbers (Fig. 9; see also Table 1).

2.6.8 *In vivo* experiment

To assess *in vivo* replication and induction of disease, 1-day-old specific-pathogen-free Valo chickens (Valo BioMedia) lacking maternal antibodies against MDV were subcutaneously infected with 4,000 PFU of wt RB-1B virus (n = 10), $\Delta IR_{LS\text{-}HR}$ virus (n = 25), and ΔIR_{LS} virus (n = 25). With each group, 11 noninfected contact animals of the same age were housed together to assess the natural transmission of the respective viruses. Importantly, all inoculated viruses were subjected to NGS to confirm genome integrity (Illumina MiSeq, v3 chemistry for 600-bp paired-end reads; Illumina, San Diego, CA, USA). As the $\Delta IR_{LS\text{-}HR}$ genome was identical to that of the wt virus upon passaging (Fig. 10D), we had contacts only for this group following the 3R (replacement, reduction, and refinement) principle. Groups were housed in separate units, and water and food were provided ad libitum. Chickens were evaluated daily for clinical signs, humanely euthanized as soon as clinical symptoms of Marek's disease were evident, and examined for tumor lesions. To eliminate bias, the examining veterinarian had no knowledge of the viruses in the different groups throughout the experiment. The experiment was terminated at 91 dpi, and all remaining animals were evaluated for tumor lesions.

2.6.9 Quantification of MDV genome copy numbers in chicken blood and feather tips

Whole-blood samples from eight animals of each group were taken from the brachial vein at 4, 7, 10, 14, 21, and 28 dpi (infected chickens) and 21, 28, 35, and 42 dpi (contact chickens). DNA was isolated from all blood samples using an E-Z96 96-well blood DNA isolation kit (Omega Biotek, Norcross, GA, USA) following the manufacturer's instructions. Feather tips were taken at final necropsy to determine if the virus had been delivered to and had replicated in the skin. DNA was extracted by proteinase K lysis at 55°C overnight followed by phenol-chloroform extraction and ethanol precipitation as described previously (28). Determination of

MDV genomic copy numbers by qPCR was performed as described above using primers specific for the meq oncogene (Table 1) (29).

2.6.10 Quantification of MDV RNA copies in chicken blood and CECs

To assess the expression of MDV genes, we quantified the gene expression levels in the blood at 10 dpi and in cell lysates prepared at 5 dpi using RT-qPCR. For *in vitro* infection, 1 million CECs were infected with 4,000 PFU of the same wt RB-1B, ΔIR_{LS-HR}, and ΔIR_{LS} inocula that were used for the *in vivo* experiment. Total RNA was extracted with an RNeasy Plus minikit (Qiagen, Hilden, Germany) according to the manufacturer's instructions. The samples were treated with DNase I (Promega, Fitchburg, WI, USA), and cDNA was generated using a High-Capacity cDNA reverse transcription kit (Applied Biosystems/Thermo Fisher, Waltham, MA, USA). ICP4, UL30, vTR, pp38, UL36, vIL-8, meq, and SORF2 RNA levels were measured and normalized against cellular GAPDH (glyceraldehyde-3-phosphate dehydrogenase) (Table 1).

2.6.11 Reisolation of viruses from tumor cells

To isolate viruses from latently infected cells, lymphocytes from tumorous organs or from whole-blood samples were subjected to Ficoll purification as previously described (30). Subsequently, 2.5×10^5 MDV lymphocytes were used to infect fresh CECs and viruses were harvested at 6 dpi. Virus DNA was extracted from nucleocapsids that were protected from micrococcal nuclease treatment as described previously (31). The DNA was used for Illumina MiSeq sequencing with 350-fold-to-450-fold coverage to confirm the sequence and integrity of tumor cellderived virus genomes (32). The generated Illumina reads were processed with Trimmomatic v.0.36 (33) and mapped against the RB-1B strain using Burrows-Wheeler aligner v.0.7.12 (34). The presence of single nucleotide polymorphisms (SNPs) and deletions was assessed with FreeBayes v.1.1.0-333 (35), and the data were merged by position and mutation using R v.3.2.3. The coverage was additionally assessed and generated using Geneious R11 software.

2.6.12 Statistical analyses

Statistical analyses were performed using GraphPad Prism software (v. 5), and data were considered significantly different for P values of ≤ 0.05. Descriptions of all applied statistical tests can be found in the respective figure legends. All *in vitro* experiments were repeated at least three independent times.

2.6.13 Data availability

GenBank accession numbers of the recombinant viruses are listed in Table 2.

Marek's disease virus requires both copies of the inverted repeat regions for efficient *in vivo* replication and pathogenesis

Table 2: GenBank accession numbers

Name	BAC / virus	Accession number
$\Delta IR_{LS\text{-}HR}$	BAC	MT955328
ΔIR_{LS}	BAC	MT994392
wt RB-1B and $\Delta IR_{LS\text{-}HR}$	Reconstituted virus	MT797629
ΔIR_{LS}	Reconstituted virus	MT872313

2.7 Competing interests

The authors declare no competing interests.

2.8 Acknowledgement

2.9 Author contributions

T.V., A.M.C., L.D.B. and B.B.K. designed the experiments; T.V., A.M.C., J.T., and L.D.B. conducted the experiments; T.V., A.M.C., and L.D.B. analyzed the data; T.V., A.M.C., A.A., L.B.D. and B.B.K. drafted the manuscript and all authors edited and approved the final version.

2.10 Supplementary figure
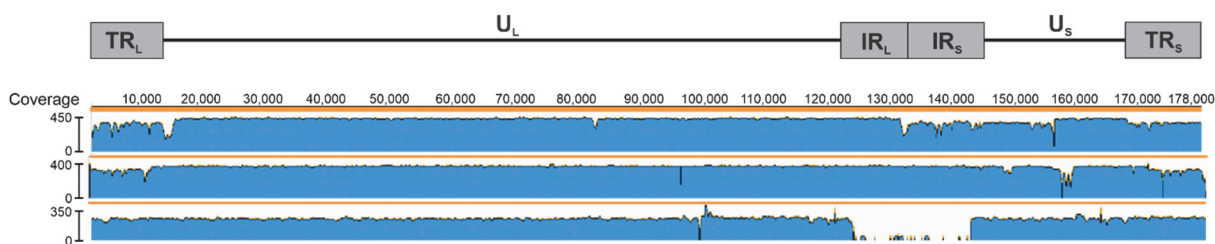
Figure 12: Genome sequence alignment of the recombinant viruses from infected chickens. Schematic representation of the MDV genome with representative coverage of Illumina MiSeq NGS reads from wt (top), $\Delta IR_{LS\text{-}HR}$ (middle) and ΔIR_{LS} (bottom). Indicated viruses were isolated from virus-induced tumors and used for NGS.

2.11 References

1. Pellet PE, Roizman B. 2001. The family Herpesviridae: a brief introduction, p 2479 – 2499. In Knipe DM, Howley PM, Griffin DE, Lamb RA, Martin MA, Roizman B, Straus SE (ed), Fields virology, 4th ed. Lippincott Williams & Wilkins, Philadelphia, PA, USA.

2. Bertzbach LD, Conradie AM, You Y, Kaufer BB. 2020. Latest insights into Marek's disease virus pathogenesis and tumorigenesis. Cancers 12:647. https://doi.org/10.3390/cancers12030647.

3. Bertzbach LD, Laparidou M, Härtle S, Etches RJ, Kaspers B, Schusser B, Kaufer BB. 2018. Unraveling the role of B cells in the pathogenesis of an oncogenic avian herpesvirus. Proc Natl Acad SciUSA 115:11603–11607. https://doi.org/10.1073/pnas.1813964115.

4. Kaufer BB, Jarosinski KW, Osterrieder N. 2011. Herpesvirus telomeric repeats facilitate genomic integration into host telomeres and mobilization of viral DNA during reactivation. J Exp Med 208:605– 615. https://doi.org/10.1084/jem.20101402.

5. Nair V, Gimeno I, Dunn J, Zavala G, Williams SM, Reece RL, Hafner S. 2020. Neoplastic diseases, p 548 –715. In Swayne DE, Boulianne M, Logue CM, McDougald LR, Nair V, Suarez DL, de Wit S, Grimes T, Johnson D, Kromm M, Prajitno TY, Rubinoff I, Zavala G, (ed), Diseases of poultry, 14th ed. John Wiley & Sons, Inc, Hoboken, NJ, USA.

6. Greco A, Fester N, Engel AT, Kaufer BB. 2014. Role of the short telomeric repeat region in Marek's disease virus replication, genomic integration, and lymphomagenesis. J Virol 88:14138 –14147. https://doi.org/10.1128/ JVI.02437-14.

7. Osterrieder N, Wallaschek N, Kaufer BB. 2014. Herpesvirus genome integration into telomeric repeats of host cell chromosomes. Annu Rev Virol 1:215–235. https://doi.org/10.1146/annurev-virology-031413-085422.

8. Lee LF, Wu P, Sui D, Ren D, Kamil J, Kung HJ, Witter RL. 2000. The complete unique long sequence and the overall genomic organization of the GA strain of Marek's disease virus. Proc Natl Acad SciUSA 97:6091–6096. https://doi.org/10.1073/pnas.97.11.6091.

9. Engel AT, Selvaraj RK, Kamil JP, Osterrieder N, Kaufer BB. 2012. Marek's disease viral interleukin-8 promotes lymphoma formation through targeted recruitment of B

cells and CD4+ CD25+ T cells. J Virol 86:8536–8545. https://doi.org/10.1128/JVI.00556-12.

10. Petherbridge L, Brown AC, Baigent SJ, Howes K, Sacco MA, Osterrieder N, Nair VK. 2004. Oncogenicity of virulent Marek's disease virus cloned as bacterial artificial chromosomes. J Virol 78:13376–13380. https://doi.org/ 10.1128/JVI.78.23.13376-13380.2004.

11. Kheimar A, Trimpert J, Groenke N, Kaufer BB. 2019. Overexpression of cellular telomerase RNA enhances virus-induced cancer formation. Oncogene 38:1778–1786. https://doi.org/10.1038/s41388-018-0544-1.

12. Conradie AM, Bertzbach LD, Bhandari N, Parcells M, Kaufer BB. 2019. A common live-attenuated avian herpesvirus vaccine expresses a very potent oncogene. mSphere 4:e00658-19. https://doi.org/10.1128/mSphere.00658-19.

13. Kheimar A, Kaufer BB. 2018. Epstein-Barr virus-encoded RNAs (EBERs) complement the loss of Herpesvirus telomerase RNA (vTR) in virusinduced tumor formation. Sci Rep 8:209. https://doi.org/10.1038/s41598 -017-18638-7.

14. Jenkins FJ, Roizman B. 1986. Herpes simplex virus 1 recombinants with noninverting genomes frozen in different isomeric arrangements are capable of independent replication. J Virol 59:494 – 499. https://doi.org/ 10.1128/JVI.59.2.494-499.1986.

15. Sauer A, Wang JB, Hahn G, McVoy MA. 2010. A human cytomegalovirus deleted of internal repeats replicates with near wild type efficiency but fails to undergo genome isomerization. Virology 401:90–95. https://doi.org/10.1016/j.virol.2010.02.016.

16. Trapp S, Parcells MS, Kamil JP, Schumacher D, Tischer BK, Kumar PM, Nair VK, Osterrieder N. 2006. A virus-encoded telomerase RNA promotes malignant T cell lymphomagenesis. J Exp Med 203:1307–1317. https://doi.org/10.1084/jem.20052240.

17. Kaufer BB, Trapp S, Jarosinski KW, Osterrieder N. 2010. Herpesvirus telomerase RNA(vTR)-dependent lymphoma formation does not require interaction of vTR with telomerase reverse transcriptase (TERT). PLoS Pathog 6:e1001073. https://doi.org/10.1371/journal.ppat.1001073.

18. Lupiani B, Lee LF, Cui X, Gimeno I, Anderson A, Morgan RW, Silva RF, Witter RL, Kung HJ, Reddy SM. 2004. Marek's disease virus-encoded Meq gene is involved in transformation of lymphocytes but is dispensable for replication. Proc Natl Acad SciUSA 101:11815–11820. https://doi.org/10.1073/pnas.0404508101.

19. Bertzbach LD, Kheimar A, Ali FAZ, Kaufer BB. 2018. Viral factors involved in Marek's disease virus (MDV) pathogenesis. Curr Clin Micro Rep 5:238–244. https://doi.org/10.1007/s40588-018-0104-z.

20. Jenkins FJ, Martin JR. 1990. Role of the herpes simplex virus 1 internal repeat sequences in pathogenicity. Intervirology 31:129–138. https://doi.org/10.1159/000150147.

21. Jenkins FJ, Donoghue AM, Martin JR. 1996. Deletion of the Herpes simplex 1 internal repeat sequences affects pathogenicity in the mouse. Front Biosci 1:a59–a68. https://doi.org/10.2741/a106.

22. Schat KA, Purchase HG. 1998. Cell-culture methods, p 223–234. In Swayne D, Glisson JR, Jackwood MW, Pearson JE, Reed WM (ed), A laboratory manual for the isolation and identification of avian pathogens, 4th ed. American Association of Avian Pathologists, Kennett Square, PA, USA.

23. Tischer BK, von Einem J, Kaufer B, Osterrieder N. 2006. Two-step redmediated recombination for versatile high-efficiency markerless DNA manipulation in Escherichia coli. Biotechniques 40:191–197. https://doi.org/10.2144/000112096.

24. Tischer BK, Kaufer BB. 2012. Viral bacterial artificial chromosomes: generation, mutagenesis, and removal of mini-F sequences. J Biomed Biotechnol 2012:472537. https://doi.org/10.1155/2012/472537.

25. Bertzbach LD, van Haarlem DA, Härtle S, Kaufer BB, Jansen CA. 2019. Marek's disease virus infection of natural killer cells. Microorganisms 7:588. https://doi.org/10.3390/microorganisms7120588.

26. Schumacher D, Tischer BK, Fuchs W, Osterrieder N. 2000. Reconstitution of Marek's disease virus serotype 1 (MDV-1) from DNA cloned as a bacterial artificial chromosome and characterization of a glycoprotein B-negative MDV-1 mutant. J Virol 74:11088 –11098. https://doi.org/10.1128/jvi.74.23.11088-11098.2000.

27. Jarosinski KW, Margulis NG, Kamil JP, Spatz SJ, Nair VK, Osterrieder N. 2007. Horizontal transmission of Marek's disease virus requires US2, the UL13 protein kinase, and gC. J Virol 81:10575–10587. https://doi.org/10.1128/JVI.01065-07.

28. Bello N, Francino O, Sanchez A. 2001. Isolation of genomic DNA from feathers. J Vet Diagn Invest 13:162–164. https://doi.org/10.1177/104063870101300212.

29. Jarosinski KW, Yunis R, O'Connell PH, Markowski-Grimsrud CJ, Schat KA. 2002. Influence of genetic resistance of the chicken and virulence of Marek's disease virus (MDV) on nitric oxide responses after MDV infection. Avian Dis 46:636–649. https://doi.org/10.1637/0005-2086(2002)046[0636:IOGROT]2.0.CO;2.

30. Bertzbach LD, Pfaff F, Pauker VI, Kheimar AM, Höper D, Härtle S, Karger A, Kaufer BB. 2019. The transcriptional landscape of Marek's disease virus in primary chicken B cells reveals novel splice variants and genes. Viruses 11:264. https://doi.org/10.3390/v11030264.

31. Volkening JD, Spatz SJ. 2009. Purification of DNA from the cell-associated herpesvirus Marek's disease virus for 454 pyrosequencing using micrococcal nuclease digestion and polyethylene glycol precipitation. J Virol Methods 157:55–61. https://doi.org/10.1016/j.jviromet.2008.11.017.

32. Trimpert J, Groenke N, Kunec D, Eschke K, He S, McMahon DP, Osterrieder N. 2019. A proofreading-impaired herpesvirus generates populations with quasispecies-like structure. Nat Microbiol 4:2175–2183. https://doi.org/10.1038/s41564-019-0547-x.

33. Bolger AM, Lohse M, Usadel B. 2014. Trimmomatic: a flexible trimmer for Illumina sequence data. Bioinformatics 30:2114–2120. https://doi.org/10.1093/bioinformatics/btu170.

34. Li H, Durbin R. 2009. Fast and accurate short read alignment with Burrows-Wheeler transform. Bioinformatics 25:1754–1760. https://doi.org/10.1093/bioinformatics/btp324.

35. Garrison E, Marth G. 2012. Haplotype-based variant detection from short-read sequencing. arXiv:1207.3907. https://arxiv.org/abs/1207.3907.

Author contributions:

Name	Author's designation	Involved in:
Tereza Vychodil	1. First author	Conceptualization (50 %)
		Design of experiments (60 %)
		Investigation *in vitro* (90 %)
		Data analysis (50 %)
		Statistical analysis of *in vitro* experiments (100 %)
		Statistical analysis of *in vivo* experiments (30 %)
		Visualization (75 %)
		Manuscript writing (40 %)
Andelé M. Conradie	2. First author	Design of experiments
		Investigation *in vitro*
		Investigation *in vivo*
		Data analysis
		Statistical analysis of *in vivo* experiments
		Manuscript writing
Jakob Trimpert	Co-author	Investigation *in vitro*
Amr Aswad	Co-author	Manuscript writing
Luca D. Bertzbach	Co-author and corresponding author	Design of experiments
		Investigation *in vivo*
		Data analysis
		Statistical analysis of *in vivo* experiments
		Visualization
		Manuscript writing
Benedikt B. Kaufer	Supervisor and corresponding author	Conceptualization
		Design of experiments
		Supervision
		Project administration
		Funding acquisition
		Manuscript writing
		Provided resources

3 Visualization of Marek's disease virus genomes in living cells during lytic replication and latency

Tereza Vychodil[1], Darren J. Wight[1], Mariana Nascimento[1], Fabian Jolmes[2], Thomas Korte[2], Andreas Herrmann[2,3]and Benedikt B. Kaufer[1,4,*]

[1] Institut für Virologie, Freie Universität Berlin, Robert von Ostertag-Straße 7-13, 14163 Berlin, Germany; tereza.vychodil@fu-berlin.de (T.V.); d.wight@fu-berlin.de (D.J.W.); m.nascimento@fu-berlin.de (M.N.)

[2] Department of Biology, Molecular Biophysics, Humboldt-Universität zu Berlin, Invalidenstraße 42, 10115 Berlin, Germany; jolmes@picoquant.com (F.J.); thomas.korte@rz.hu-berlin.de (T.K.); andreas.herrmann@rz.hu-berlin.de (A.H.)

[3] Institut für Chemie und Biochemie, Freie Universität Berlin, Altensteinstr. 23a, 14195 Berlin, Germany

[4] Veterinary Centre for Resistance Research (TZR), Freie Universität Berlin, 14163 Berlin, Germany

* Correspondence: b.kaufer@fu-berlin.de; Tel.: +49-30-838-51936

3.1 Abstract

Visualization of the herpesvirus genomes during lytic replication and latency is mainly achieved by fluorescence in situ hybridization (FISH). Unfortunately, this technique cannot be used for the real-time detection of viral genome in living cells. To facilitate the visualization of the Marek's disease virus (MDV) genome during all stages of the virus lifecycle, we took advantage of the well-established tetracycline operator/repressor (TetO/TetR) system. This system consists of a fluorescently labeled TetR (TetR-GFP) that specifically binds to an array of *tetO* sequences. This *tetO* repeat array was first inserted into the MDV genome (vTetO). Subsequently, we fused TetR-GFP via a P2a self-cleaving peptide to the C-terminus of the viral interleukin 8 (vIL8), which is expressed during lytic replication and latency. Upon reconstitution of this vTetO-TetR virus, fluorescently labeled replication compartments were detected in the nucleus during lytic replication. After validating the specificity of the observed signal, we used the system to visualize the genesis and mobility of the viral replication compartments. In addition, we assessed the infection of nuclei in syncytia as well as lytic replication and latency in T cells. Taken together, we established a system allowing us to track the MDV genome in living cells that can be applied to many other DNA viruses.

3.2 Introduction

Marek's disease virus (MDV), also known as Gallid alphaherpesvirus 2 (GaHV-2), is a highly oncogenic herpesvirus that belongs to the genus Mardivirus. MDV infects chickens and causes neurological disorders, immunosuppression, paralysis, and deadly T cell lymphomas in various organs [1]. The virus enters the host through the respiratory tract where it infects macrophages and dendritic cells [2,3] that transport the virus to lymphoid organs. Here, this cell-associated virus is passed on to B and T cells in which it can replicate lytically [4–6]. In addition, MDV establishes latency predominantly in CD4+ T cells [7,8] and integrates its genome into the host telomeres [9,10]. During latency, only a few genes are expressed, including the major oncogene Meq (MDV005 and MDV076), splice variants of the viral chemokine vCXCL13 (aka. vIL-8; MDV003 and MDV078), [11,12] and the viral telomerase RNA [13,14]. Latently infected cells can also be transformed, resulting in the rapid formation of T cell lymphomas [15]. In addition, these cells can transport the virus to the feather follicle epithelia, where the virus replicates, is shed into the environment, and, thereby, spreads to naïve chickens [9]. Despite many years of research, many molecular processes involved in MDV replication and integration remain poorly understood. This is mostly due to the cell associated nature of the virus, its slow replication cycle, and the limited availability of tools. In recent years, viruses harboring fluorescent proteins have drastically expanded our knowledge on MDV replication and other processes during infection [16–22]. While virus proteins can be

easily visualized in living infected cells by fusing them to, for example, green fluorescent protein (GFP), it remained impossible to visualize the virus genome in living cells. This genome visualization would provide valuable tools to assess the molecular processes including replication, integration, and latency. In this study, we used the well-established tetracycline operator/repressor (*tetO*/TetR) system to visualize MDV genomes in living cells. The *tetO*/TetR system consists of a fluorescently labeled TetR protein (TetR-GFP) that specifically binds *tetO* repeat sequences as a dimer and, thereby, provides an increased fluorescent signal at the *tetO* insertion site [23]. This tool is commonly used in cell biology where cellular chromosome loci harboring *tetO* repeats are visualized to assess chromosome dynamics [24,25]. To monitor the MDV genome during infection, we inserted 112× *tetO* repeats into the virus genome using two-step Red-mediated mutagenesis [26]. TetR-GFP or TetR-mCherry were either expressed from the virus genome or stably expressed by the host cells. This system allowed us to visualize the MDV genome during lytic replication and in latently infected cells, providing important insights into the formation of replication compartments (RC), the structures in the nucleus in which the viral genome is replicated, and the infection of T cells.

3.3 Materials and methods

3.3.1 Cells

Chicken embryo cells (CECs) were prepared from Valo specific-pathogen free (SPF) 11-day-old embryonated chicken eggs (Valo BioMedia, Osterholz-Scharmbeck, Germany), as described previously [27]. CECs were maintained in minimum essential medium (PAN Biotech, Aidenbach, Germany) supplemented with 10% fetal bovine serum (FBS, PAN Biotech) and 1% penicillin/streptomycin at 37°C in a 5% CO_2 environment. ESCDL-1, cell line derived from chicken embryonic stem cells [28] were maintained in DMEM Ham's F12 (PAN Biotech) and supplemented with 10% FBS and 1% penicillin/streptomycin at 37°C under a 5% CO_2 atmosphere. The reticuloendotheliosis virus-transformed chicken T-cell line 855-19 was kindly provided by Prof. Thomas Göbel (Ludwig Maximilian University of Munich, Germany). Cells were maintained in RPMI (PAN Biotech) and supplemented with 10% FBS, 1% sodium pyruvate (PAN Biotech), 1% non-essential amino acids (Biochrom; Berlin, Germany), and 1% penicillin/streptomycin at 41°C under a 5% CO_2 atmosphere. All stable cell lines were confirmed by PCR to be mycoplasma-free.

3.3.2 Generation of recombinant viruses

The recombinant viruses harboring the *tetO*/TetR system components were generated based on a previously generated bacterial artificial chromosome (BAC) clone of the very virulent RB1B strain [29], in which most of the internal repeat short and long regions were deleted ($\Delta IR_L \Delta IR_S$) [15]. This deletion is rapidly restored upon reconstitution and facilitates a rapid

manipulation of the repeat regions using two-step Red-mediated mutagenesis, as described previously [26,30]. First, transfer plasmids were generated that allowed the insertion of the components into the virus genome. To obtain the TetR-GFP transfer plasmid, the TetR-GFP cassette containing a nuclear localization signal (NLS) was amplified from the a p128tetR-GFP plasmid, kindly provided by Susan Gasser (Friedrich Miescher Institute, Switzerland) [25], and cloned into pcDNA3.1 using BamHI and EcoRI. The kanamycin selection cassette (kana_I-SceI) was amplified from pEPkan-S1, homologue sequences for its removal inserted via the primer overhangs and cloned into pcDNA3.1_TetR-GFP. This mutagenesis cassette was subsequently used to insert TetR-GFP (i) after the strong HSV-1 thymidine kinase (TK) promoter within the mini-F cassette (vTetR) or (ii) fused to the C-terminus of vCXCL13 via a P2A self-cleaving peptide (vTetO/TetR), resulting in expression of TetR-GFP and vCXCL13 as separate proteins, using two-step Red-mediated mutagenesis, as described previously [26,30].

To obtain the TetO transfer plasmid, the 112× *tetO* repeats array (4.5 kbp) of pRS306tet02x112 (Susan Gasser, Friedrich Miescher Institute, Switzerland) was cloned into a vector containing long homologue sequences of UL45 and UL46 (MDV058 and MDV059, respectively). The *tetO* sequence was inserted between UL45 and UL46 using BamHI and BglII. The kana_I-SceI cassette with homologue sequences for its removal were inserted into the UL45 homologue arm. This mutagenesis cassette was subsequently used to insert *tetO* between UL45 and UL46 of the virus genome using two-step Red-mediated mutagenesis (Figure 13A, vTetO and vTetO-TetR). This UL45/UL46 was chosen as it previously allowed the insertion of foreign genes without affecting the MDV replication [16]. In addition, either GFP or E2-Crimson, driven by the HSV-1 TK promoter, was inserted in the mini-F vector to facilitate the detection of infected cells (for vTetO and vTetO-TetR, respectively).
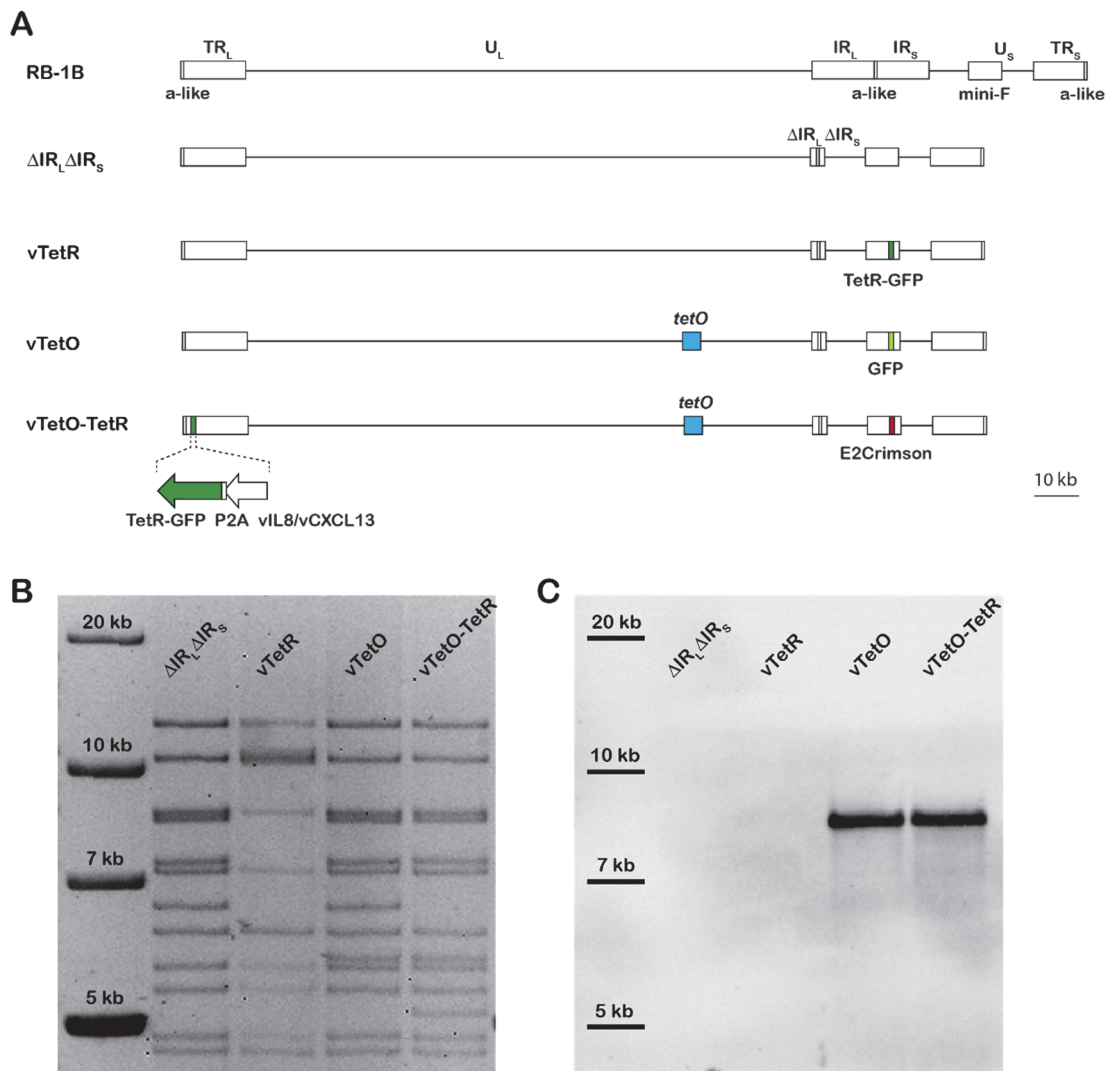
Figure 13. **Generation of recombinant viruses.** (**A**) Overview of the MDV genome and the recombinant BAC clones. The MDV genome consists of a unique long and short region (U$_L$ and U$_S$) flanked by the terminal repeat long and short (TR$_L$, TR$_S$) and the internal repeat long and short (IR$_L$, IR$_S$). The a–like sequences harboring the cleavage and packaging signals are indicated. The recombinant viruses were generated based in the ΔIR$_L$ΔIR$_S$ BAC lacking most of the IR$_L$ and IR$_S$ region, which is rapidly restored upon reconstitution. TetR-GFP is depicted in dark green, *tetO* sequence in blue, GFP in light green, and E2-Crimson in red; (**B**) RFLP of indicated recombinant BAC genomes using NdeI; (**C**) Southern blot of the same RFLP gel using a specific TetO probe to confirm the presence and length of the *tetO* sequences in the virus genome.

All recombinant virus genomes were confirmed by restriction fragment length polymorphism (RFLP) analyses, Southern blotting, Sanger sequencing, and next-generation sequencing (NGS; Illumina MiSeq) of the entire virus genome. All primers used for cloning and mutagenesis can be found in Table 3.

49

Table 3. Oligonucleotide sequences used in this study.

Construct/Steps	Direction	Sequence (5′ → 3′)
pCDNA3.1 TetR-GFP	for	TAGATGAGCTCGGATCCATGCCAAAGAAGAAGCGTAAG
	rev	GATGGATATCTGCAGAATTCTCATCCCATGCCATTGGT
TetR-GFP-kana transfer	for	TACAAGACACGTGCTGAAGTCAAGTTTGAAGGTAGGGATAACAGGGTAATCGATTT
	rev	ACTTCAGCACGTGTCTTGTAGTTCCCGTCATCGCCAGTGTTACAACCAATTAACC
TetR-GFP in mini-F (vTetR)	ep for	TTAAGGTGACACGCGCGGCCTCGAACACAGCTGCAGGCCGATGTACGGGCCAGATATACG
	ep rev	CGTCGACCCGGGTACCTCTAGATCCGCTAGCGCTTTATGTCTTCCCAATCCTCCCC
P2A-TetR-GFP into vIL-8/vCXCL13	ep for	ATTGAGCCCACACCTCCTACTATTGGTTCCCATATCTGTCTTGGTTCCGGAGCCACGAACTTCTCTCTGTTAAAGCAAGCAGGAGACGTGGAAGAAAACCCCGGTCCTATGCCAAAGAAGAAGCGTAAG
	ep rev	AAAGTGCCTTCTTTTAATTACAGGAGGTAGCAATTAATCATCCCATGCCATTGGTAATCC
TetO-kana transfer	for	GACAGTAGATCTACCTGTATACTACCCACCATTGTAGGGATAACAGGGTAATCGATTT
	rev	ACAGGTAGATCTACTGTCCCGTAGTCTAAATATGCCAGTGTTACAACCAATTAACC
eGFP in mini-F	ep for	GGTGACACGCGCGGCCTCGAACACAGCTGCAGGCCATGGTGAGCAAGGGCGAGG
	ep rev	CGTCGACCCGGGTACCTCTAGATCCGCTAGCGCTTTACTTGTACAGCTCGTCCATGCC
E2-Crimson into mini-F	ep for	TGCCCTTGCTAGGGTTCTTCACACGAGCCTCGCCTTATTAAATGGGCTCCGGTGCCCGTC
	ep rev	CCCGAGGCCTCGTGGGGCACCTATTTGCGCGGAGGAAGGCCCATAGAGCCCGGGCCATC
TetO DIG-probe		DIG-TCCCTATCAGTCATAGAGAAAAGTGAAAGTCGAGTTTACCAC
iNOS (qPCR)	for	GAGTGGTTTAAGGAGTTGGATCTGA
	rev	TTCCAGACCTCCCACCTCAA
	probe	FAM-CTCTGCCTGCTGTTGCCAACATGC-TAMRA
UL30 (qPCR)	for	AAGCGGAATCGGTTTACAAG
	rev	GGAGTTGCTGTTAGAATACGGA
	probe	FAM-TCGACGAGTTTCTTCCTCCTCGTTG-TAMRA
Mycoplasma test	for	GGGAGCAAACAGGATTAGATACCCT
	rev	TGCACCATCTGTCACTCTGTTAACCTC

ep, en passant mutagenesis primer; for, forward primer; rev, reverse primer; FAM, 6-carboxyfluorescein; TAMRA, 6-carboxytetramethylrhodamine; DIG, Digoxigenin

3.3.3 Southern blotting

To confirm the insertion of the *tetO* repeats, DNA of BAC clones were digested with indicated enzymes and separated on a 0.8% agarose gel. DNA in the agarose gel was denatured (0.5 M NaOH, 1.5 M NaCl) and transferred to a positively charged nylon membrane (Immobilon-NY+, Merck Millipore, Darmstadt, Germany) and incubated with TetO DIG-labeled probe (Table 3), as described previously [9]. *TetO* repeats were detected using an anti-DIG alkaline phosphatase-labeled antibody (Roche GmbH, Mannheim, Germany).

3.3.4 Illumina MiSeq sequencing

BAC DNA of the vTetO and vTetO-TetR clones were sequenced using Illumina MiSeq (Illumina, San Diego, CA, USA). Sequencing libraries were prepared using the NEBNext® Ultra™ II DNA Library Prep Kit for Illumina® (New England Biolabs, Ipswich, MA, USA). The generated Illumina reads were processed with Trimmomatic v.0.39 [31] and mapped against the RB-1B TetO (GenBank accession no. OM350391) and RB-1B TetO TetR-GFP (GenBank accession no. OM350392) GenBank references, respectively, using the BurrowsWheeler aligner v.0.7.17 [32]. Single nucleotide polymorphisms (SNPs), insertions, and deletions were assessed with FreeBayes v.1.1.0-333 [33]. Data were merged by position and mutation using R v.3.2.3; the coverage was additionally assessed and generated using Geneious R11 software.

3.3.5 Plaque size assay and growth kinetics

Recombinant viruses were reconstituted using calcium-phosphate transfection of CECs and ESCDL-1 with respective BAC clones, as described previously [34]. Spread of recombinant viruses and replication properties in vitro were determined by plaque size assay and multi-step growth kinetics. For plaque size assays, one million CECs were infected with 100 plaque forming units (PFU) of each virus (passage 5 and 7) and the area of 50 randomly selected plaques were measured using ImageJ (https://imagej.nih.gov/ij/, accessed on 4 June 2020) and normalized against $\Delta IR_L \Delta IR_S$. In addition, plaques were also measured 6 days after BAC DNA transfection. For multi-step growth kinetics, one million CECs were infected with 100 PFU in 6-well plates per virus and cultured for 6 days. Every day, one well per plate was harvested and stored at −80°C. After 6 days, DNA of all samples was extracted using Zymo Quick DNA Viral kit (Zymo Research Europe GmbH, Freiburg, Germany), according to the manufacturer's instructions. MDV genome copy numbers were determined by qPCR using specific primers and probe for the MDV polymerase (MDV043, UL30). UL30 copy numbers were normalized against the chicken inducible nitric oxide synthase (iNOS), as described previously [35]. Primers and probes used for qPCR are listed in Table 3.

3.3.6 Assessment of *tetO* stability by nanopore sequencing

To determine if the array of *tetO* repeats is stably maintained in the virus, extrachromosomal DNA of CECs infected with higher passages of vTetO and vTetO-TetR (passage 9) was extracted using Hirt extraction, as described previously [36,37]. Briefly, infected cells from 150 mm dishes were trypsinized and pelleted by centrifugation at 4°C and 800× g for 5 min. The pellet was washed with ice-cold PBS, centrifuged again, resuspended in 400 µL of Hirt lysis buffer (10 mM Tris-HCl, 20 mM EDTA, 1.2% SDS, pH 8.0) and incubated for 20 min at room temperature. Next, 200 µL of 5 M NaCl was added and incubated at 4°C for ≥16 h

followed by centrifugation at 4°C and 15.000× g for 30 min to pellet proteins and chromosomes. The extrachromosomal DNA in the supernatants was then purified by phenol-chloroform extraction, precipitated with isopropanol, and washed with ethanol. The obtained viral genomes were used for nanopore sequencing. Nanopore libraries were prepared using the SQK-LSK110 Ligation Sequencing Kit (Oxford Nanopore Technologies, Oxford, UK) and sequenced using a Flongle flow cell (FLO-FLG001, Oxford Nanopore Technologies, Oxford, UK) on a MinION sequencer (MK-1B, Oxford Nanopore Technologies, Oxford, UK). The resulting Nanopore reads were mapped against the RB-1B TetO and RB-1B TetO TetR-GFP GenBank references using Minimap2 [38] embedded on Nanopore's MinKNOW GUI. Alignments were viewed using IGV Web App [39,40].

3.3.7 Generation of t cell line stably expressing TetR-mCherry

To generate a cell line stably expressing TetR-mCherry, the 855-19 chicken T-cell line was transduced with the pQCXIN-TetR-mCherry retroviral system (kindly provided by Tom Misteli from National Cancer Institute, Addgene plasmid #59417) [41] and selected in the presence of 1200 µg/mL Geneticin (Roth, Karlsruhe, Germany). The newly generated cell line was confirmed to be mycoplasma-free by PCR.

3.3.8 Wide-field microscopy

To investigate if the recombinant viruses efficiently express TetR-GFP, we infected CECs and ESCDL-1 cells with vTetR and/or vTetO-TetR. At 4 dpi, we stained the nuclei with Hoechst 33342 (Invitrogen, Carlsbad, CA, USA) for 30 min and fixed the cells with 4% paraformaldehyde (PFA). Wide-field images of infected cells were taken using Axio Imager M1 (Zeiss, Oberkochen, Germany) equipped with Axio Cam MRm camera (Zeiss) with a 100×/1.4 Oil Plan-Apochromat objective (Zeiss). Images were further processed in ImageJ.

3.3.9 Confocal microscopy and live-cell imaging

For live imaging, cells were grown in pre-coated µ-Slide ibiTreat plates with polymer coverslip (Ibidi, Gräfelfing, Germany). Cells were maintained in medium supplemented with 0.2 M HEPES (Roth). 855-19 cells were also immobilized in 0.25% low melting-point agarose (Gibco BRL, Carlsbad, CA, USA). Nuclei were stained with Hoechst 33342 for 30 min. To confirm TetR binding specificity, cells were incubated with 2 µg/mL tetracycline (Roth) for 1 h. Live microscopy was performed using (i) a VisiScope spinning disk confocal system (Visitron Systems, Puchheim, Germany, CSU-W1; Yokogawa, Tokyo, Japan) built on a Nikon Eclipse Ti inverted microscope equipped with an iXon Ultra 888 EMCCD camera and an OkoLab gas and temperature controller (OkoLab, Ottaviano, Italy) to maintain a 5% CO_2 atmosphere at 37°C or (ii) a FluoView1000 inverted confocal microscope (Olympus, Tokyo, Japan). If not

indicated otherwise, the VisiScope spinning disc confocal microscope was used. Images were captured with (i) 60×/1.4 and 100×/1.45 Oil Plan-Apo objectives (Nikon) using VisiView software (v.4.3.0.6; Visitron Systems, Puchheim, Germany) or (ii) 60× water immersion objective (UPlanSApo) using Olympus FluoView software (v 4.02; Olympus, Tokyo, Japan). Z-step size between focal planes was 0.5 µm and final 2D images are visualized as maximum intensity projection. All images and videos were processed with ImageJ software.

3.3.10 Lymphocyte infection

To infect 855-19 T-cells expressing TetR-mCherry, one million CECs were infected with 10,000 PFU of vTetO. After 6 days, CECs were overlaid with one million T-cells and incubated together for 24 h in RPMI (PAN Biotech) supplemented with 10% FBS, 1% sodium pyruvate (PAN Biotech), 1% non-essential amino acids (Biochrom, Berlin, Germany), and 1% penicillin/streptomycin at 41°C under a 5% CO_2 atmosphere. The next day, T-cells were carefully harvested and the infection rate was determined by flow cytometry detecting eGFP expressed in infected cells using a CytoFLEX S system (Beckman Coulter, Krefeld, Germany). Infected T-cells were maintained in culture for 14 days to allow the virus to establish latency and integrate its genome into host chromosomes. Images were taken 1, 3, and 14 days post infection (dpi) using the VisiScope spinning disc confocal microscope.

3.3.11 Fluorescence *in situ* hybridization (FISH)

Interphase nuclei were prepared from infected 855-19 T-cells 3 dpi (lytic) and 14 dpi (latent), as described previously [42]. Briefly, MDV genomes were detected using a set of PCR-based MDV probes and visualized using Cy3 Streptavidin (1:1000 dilution; GE Healthcare, Munich, Germany) [43]. Images of interphases were taken using Axio Imager M1 (Zeiss) and analyzed with the ImageJ software.

3.3.12 Statistical Analysis

Statistical analyses were performed using GraphPad Prism software v.8.0.2. Data were considered significantly different for p values of ≤0.05. Description of all applied statistical tests can be found in the respective figure legends. If not noted differently, all experiments were repeated at least three independent times.

3.4 Results

3.4.1 Generation of recombinant viruses

To visualize MDV genomes in living cells, we generated recombinant viruses that harbor the *tetO*-repeats using the very virulent RB-1B strain [35,44]. The *tetO* repeat cassette (4.5 kbp) was inserted in between UL45 and UL46, a locus well established for the insertion of foreign

genes without affecting virus replication [16]. The TetR fused to a fluorescence protein and a nuclear localization signal (NLS) and was then either expressed by the virus or the cells depending on the application. To exclude that the TetR protein alone forms unspecific aggregates in the nucleus of chicken cells, we generated a virus expressing high levels of TetR-GFP driven by the strong TK promoter in the mini-F in the absence of *tetO* (vTetR). Since we observed that high expression levels of TetR-GFP driven by the TK promoter reduced the signal to noise ratio, we tested various loci for the insertion of the protein. The optimal expression was achieved by fusing TetR-GFP via a P2A self-cleaving peptide to the C-terminus of vCXCL13 (aka. vIL-8). This facilitated TetR-GFP expression during both lytic replication and latency at optimal levels. To identify infected cells, we inserted the GFP into the virus only containing *tetO* (vTetO) and the far-red protein E2-Crimson into the vTetO-TetR double insertion virus (vTetO-TetR) into the mini-F (Figure 13A). The resulting clones were analyzed by RFLP (Figure 13B) and Sanger sequencing. The presence and length of the *tetO* repeats in the viral genome were confirmed by Southern blotting (Figure 13C). The specific TetO probe detected the fragment with the expected size in both vTetO and vTetO-TetR, indicating that the full length *tetO* cassette was inserted during mutagenesis. Illumina MiSeq next generation sequencing was performed and confirmed that no additional mutations are present in the recombinant virus genomes.

3.4.2   Characterization of replication properties

To examine if the insertion of *tetO* and TetR-GFP affects virus replication, we performed plaque size assays and multi-step growth kinetics. No significant difference was observed in plaque size assays performed after transfection compared to the parental virus (Figure 14A). Similarly, no significant difference was detected in plaque size assays upon serial passaging of the viruses (passage 7; Figure 14B). These results were confirmed by multi-step growth kinetic analyses (Figure 14C), highlighting that insertion of *tetO* and TetR-GFP has no significant impact in MDV replication. To further investigate the stability of the *tetO* repeats in the viral genome, we isolated extrachromosomal DNA from CECs infected with high passaged virus (passage 9) and performed nanopore sequencing on the MDV genomes. The results from nanopore sequencing demonstrated that *tetO* is stably maintained in the UL45-UL46 locus in both vTetO and vTetO-TetR, highlighting that the system could even be used with high passage stocks.
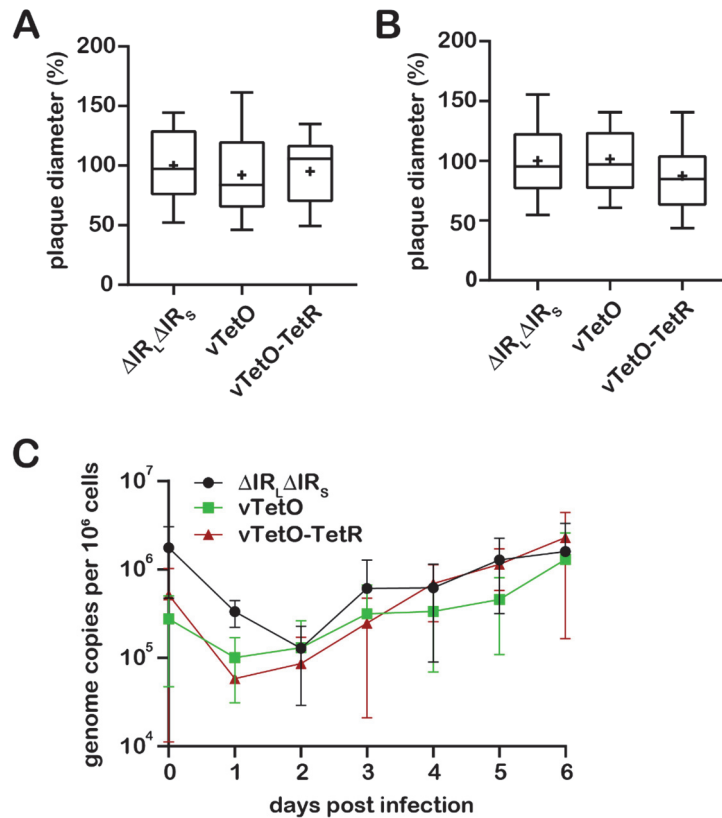
Figure 14. In vitro characterization of the recombinant viruses. Plaque size assays after (A) transfection and (B) infection with passaged viruses, as indicated. Data are shown as means of three independent experiments with means (+), medians (line within the bar), and standard deviations (p > 0.05, one-way analysis of variance (ANOVA) Dunnett's test). (C) Representative multi-step growth kinetics of indicated viruses with standard deviations (p > 0.05, one-way analysis of variance (ANOVA) Kruskal–Wallis test).

3.4.3 Visualization of the virus genome during lytic replication and specificity of TetR binding

To visualize MDV genomes during lytic replication, we infected primary CECs and the chicken ESCDL-1 cell line with 100 pfu of vTetO-TetR, counterstained with Hoechst 33342 at four dpi imaged the cells. In both CECs and ESCDL-1, we consistently observed one to two replication compartments (RCs) per nucleus that were visually separated from each other (Figure 15A). To ensure that TetR alone does not establish unspecific aggregates, we infected CECs with vTetR and vTetO-TetR. In cells infected with vTetR we observed a uniform TetR-GFP signal in the nucleus. In contrast, in cells infected with vTetO-TetR we detected specific signal for the virus genome, forming RCs within the nucleus (Figure 15B). To further validate the specificity of the TetO/TetR signal, we used tetracycline to induce a conformational change of the TetR DNA-binding domain, resulting in the dissociation of TetR-GFP from the *tetO* repeats [45]. CECs were infected with vTetO-TetR for 4 days and imaged before and after the addition of tetracycline. Neighboring infected cells harbored RCs in their nucleus before adding

tetracycline. Upon addition of the drug, TetR-GFP dissociates and the specific signal pattern was lost, highlighting that the observed genome staining is highly specific (Figure 15C).

3.4.4 Genesis and mobility of replication compartments

Next, we investigated the formation of the RCs in infected cells. We infected CECs with vTetO-TetR for 4 days, counterstained the nuclei with Hoechst 33342, and monitored the development of RCs in newly infected cells via live cell imaging for 21 h. Separated RCs in the nuclei were observed early in infection (Figure 16A). During the 21 h period, the RCs gradually increased in size (RC 1 from 6.6 µm^2 to 20.5 µm^2 ; RC 2 from 1.5 µm^2 to 5.7 µm^2). Based on the previous findings that RCs have properties of phase-separated condensates (liquid-liquid phase separation) and proteins move freely within RCs [46], we set out to investigate the mobility of the viral DNA in these structures. At 4 dpi, we tracked infected nuclei for 1 h and captured stacks of 15 focal planes and analyzed the maximum-intensity projection (MIP) (Figure 16B) and rendered 3D images (Supplementary Video S1) of a representative nucleus. Although the nuclei themselves were moving during the imaging period, we observed that the shape of the RCs did not change and many of the dotted structures stayed in the same place suggesting that the viral DNA is rather immotile.

3.4.5 Detection of both infected and uninfected nuclei inside a syncytium

MDV has been previously shown to induce syncytia in duck embryo fibroblasts (DEF) [47,48]. Using our vTetO-TetR expressing E2-Crimson in the cytoplasm, we frequently observed that MDV can also induce syncytia in infected primary CECs. We, therefore, infected CECs with vTetO-TetR to assess if all nuclei were infected and showed replication compartments. Nuclei of the cells were stained with Hoechst 33342 and we imaged the cells using a spinning-disk confocal microscope at 4 dpi. Interestingly, we observed that some nuclei harbor RCs while others did not. In some nuclei, single dots were detected (Figure 17A), suggesting that only one or few viral genomes were present. In other syncytia, no virus signal was detected in some of the nuclei (Figure 17B), indicating that MDV does not replicate its genome in all nuclei of a syncytium.

3.4.6 Visualization of viral genomes during lytic replication and latency in T cells

To assess lytic replication and latency in T cells, we co-seeded CECs highly infected with vTetO with uninfected 855-19 T cells stably expressing TetR-mCherry. Imaging started after the T cells settled on the infected CEC monolayer. Cells were imaged using the spinning-disk confocal microscope every ten minutes for 21 h. DNA replication was detectable at 8 hpi and gradually increased until 22 hpi (Figure 18A). Intriguingly, we observed smaller and sparse

RCs in T cells when compared with CECs and ESCDL-1 cells, indicating that MDV replication in T cells may differ.
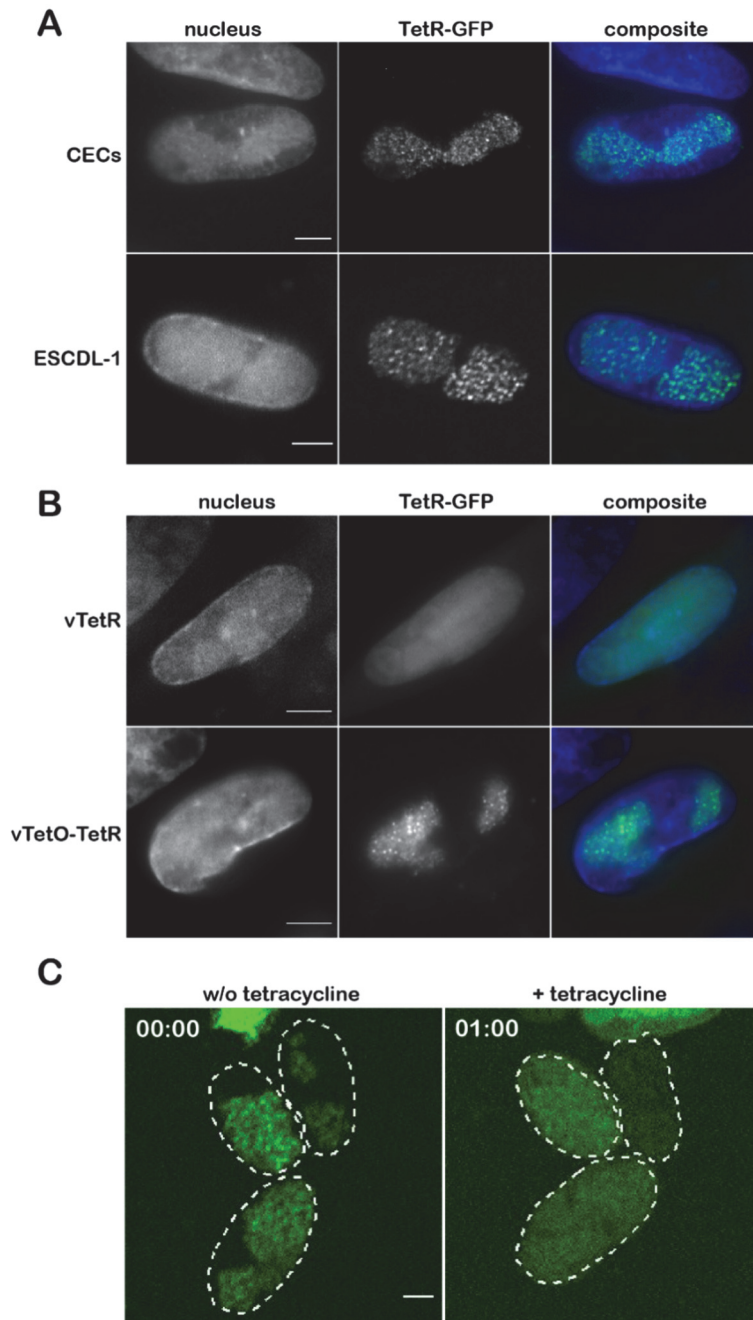

Figure 15. Detection of virus genomes in infected cells. (**A**) CECs and ESCDL-1 cells were infected with vTetO-TetR, fixed with 4% PFA at 4 dpi, and imaged with an Axio Imager M1 using a 100× oil objective. Scale bar corresponds to 5 µm; (**B**) CECs were infected with either vTetR or vTetOTetR, fixed at 4 dpi using VisiScope spinning-disk confocal microscope with a 100× oil objective. Scale bar corresponds to 5 µm; (**C**) CECs infected with vTetO-TetR were treated with tetracycline. Images are shown before (left panel) and 1 h after the addition of tetracycline (right panel). Image stacks of nine focal planes were captured with a z-step size of 0.5 µm and displayed as maximum-intensity projection (MIP). The perimeter of the nuclei are depicted as dotted lines. Time (in hh:mm) and scale bar (5 µm) are indicated.
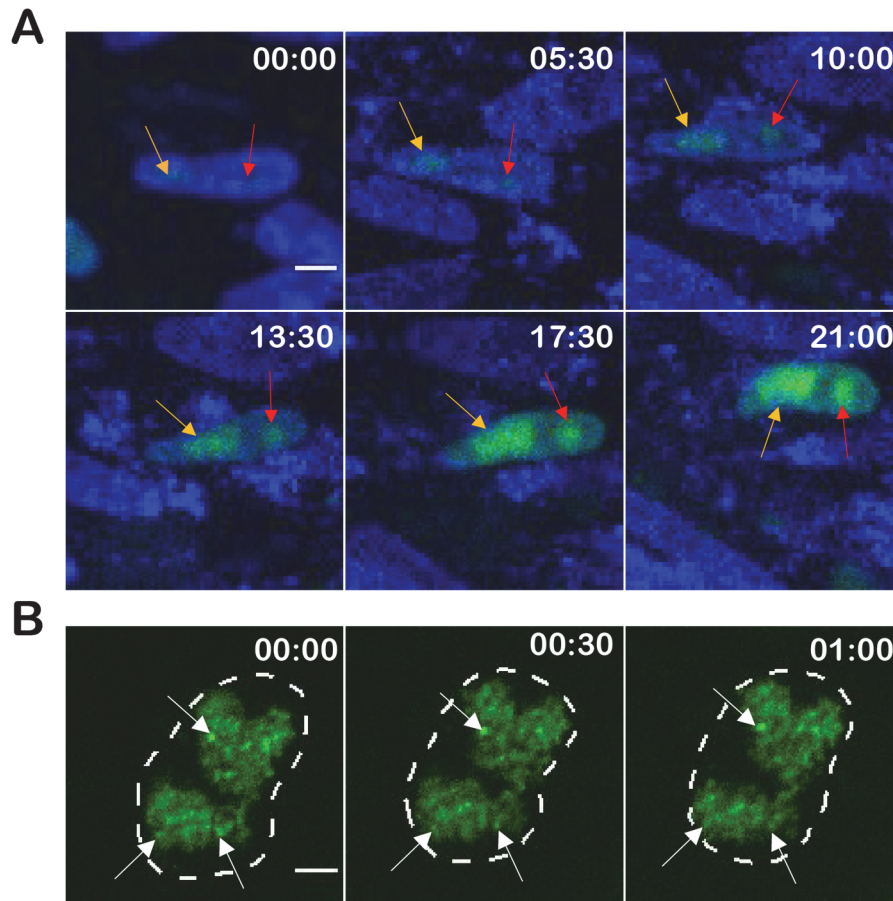
Figure 16. Genesis and mobility of replication compartments (RC). (**A**) The development of RCs in infected cells were monitored for 21 h. Sequential images were taken with spinning-disk confocal microscope using a 60× water immersion objective every ten minutes. Multiple Z-stacks were processed as maximum-intensity projection (MIP). RC 1 and RC 2 are indicated with an orange arrow and red arrow, respectively. Nuclei are shown in blue, TetR-GFP in green. Time in hh:mm, scale bar 5 µm; (**B**) the mobility of the RCs in infected cells was monitored for 1 h. Stacks of 15 focal planes with a z-step size of 0.5 µm were captured at 5 min intervals using a VisiScope microscope. Images represent the MIP of each time point. Nucleus contour is depicted as dotted line; white arrows indicate non-moving dotted structures. Time in hh:mm, scale bar 3 µm.

To further investigate infection and the establishment of latency in T cells, vTetO infected lymphocytes were harvested at 24 hpi and maintained in cell culture for 14 days. At 3 dpi, few lytically infected cells were still observed (Figure 18B). Intriguingly, we also detected cells with a single dot in the nucleus (white arrow) after 3 dpi (Figure 18B). These pictures were confirmed with FISH preparations of infected cells and are consistent with recently published work done on 885-19 T cells [43]. Moreover, to ascertain that this single bright staining represents a latent virus genome, we analyzed the infected T cells also 14 dpi when no replication was observed. Single specific spots were observed during the latent phase upon infection of these T cells (Figure 18C, white arrow), highlighting that our system is sensitive enough to detect these latent virus genomes.
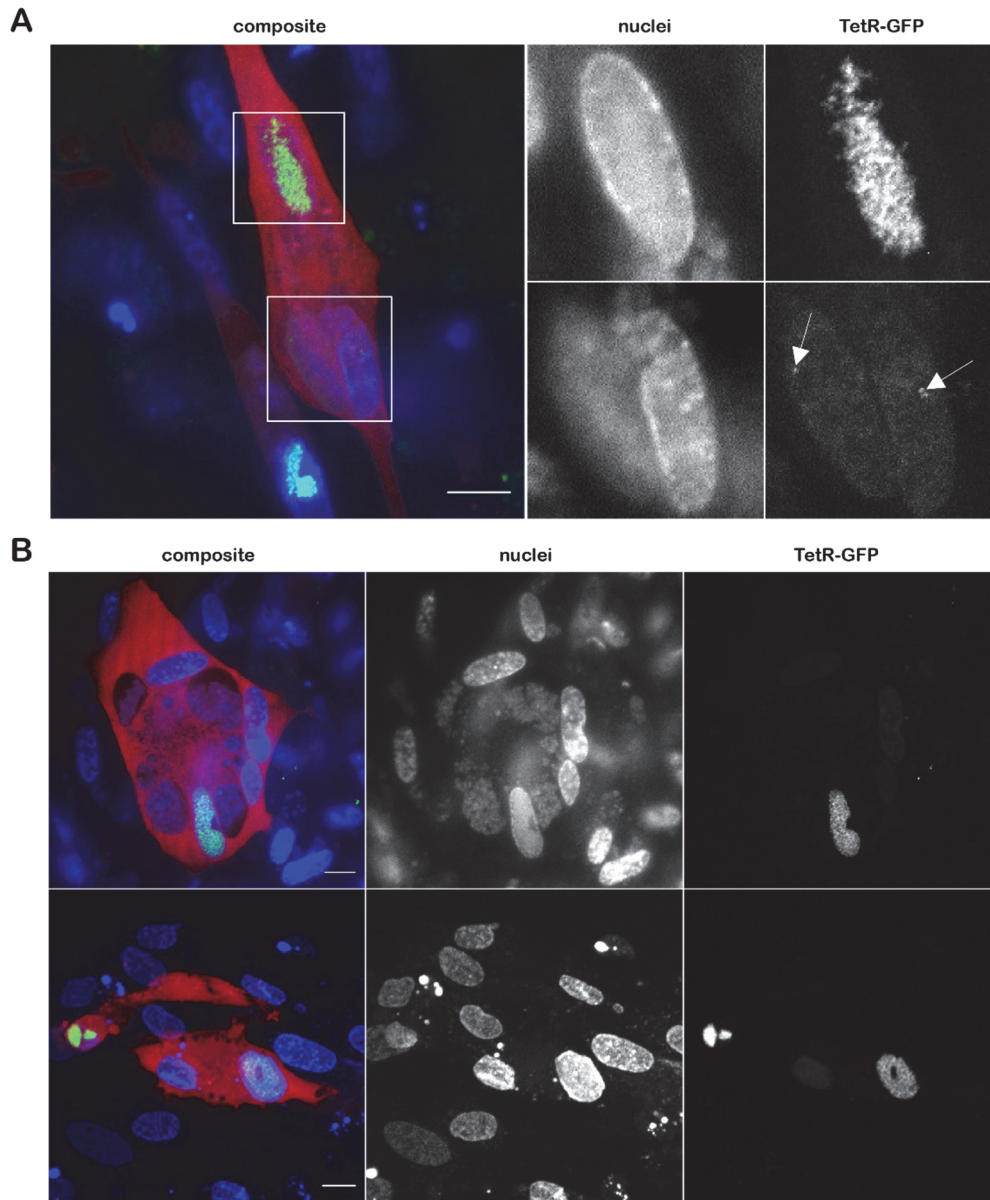
Figure 17. MDV can induce syncytia in CECs but replication is only detected in some of the nuclei. (**A**) Nuclei within a syncytium with varying TetR-GFP intensities. Image stacks of 21 focal planes with a z-step size of 0.5 µm are displayed as MIP. Nuclei were stained with Hoechst 33342 for 30 min and captured using WF-DAPI. Single or few MDV genomes are indicated by white arrows; (**B**) representative images of MDV syncytia. E2-Crimson in cytoplasm in red, nuclei in blue, and TetR-GFP in green. Scale bar 10 µm.
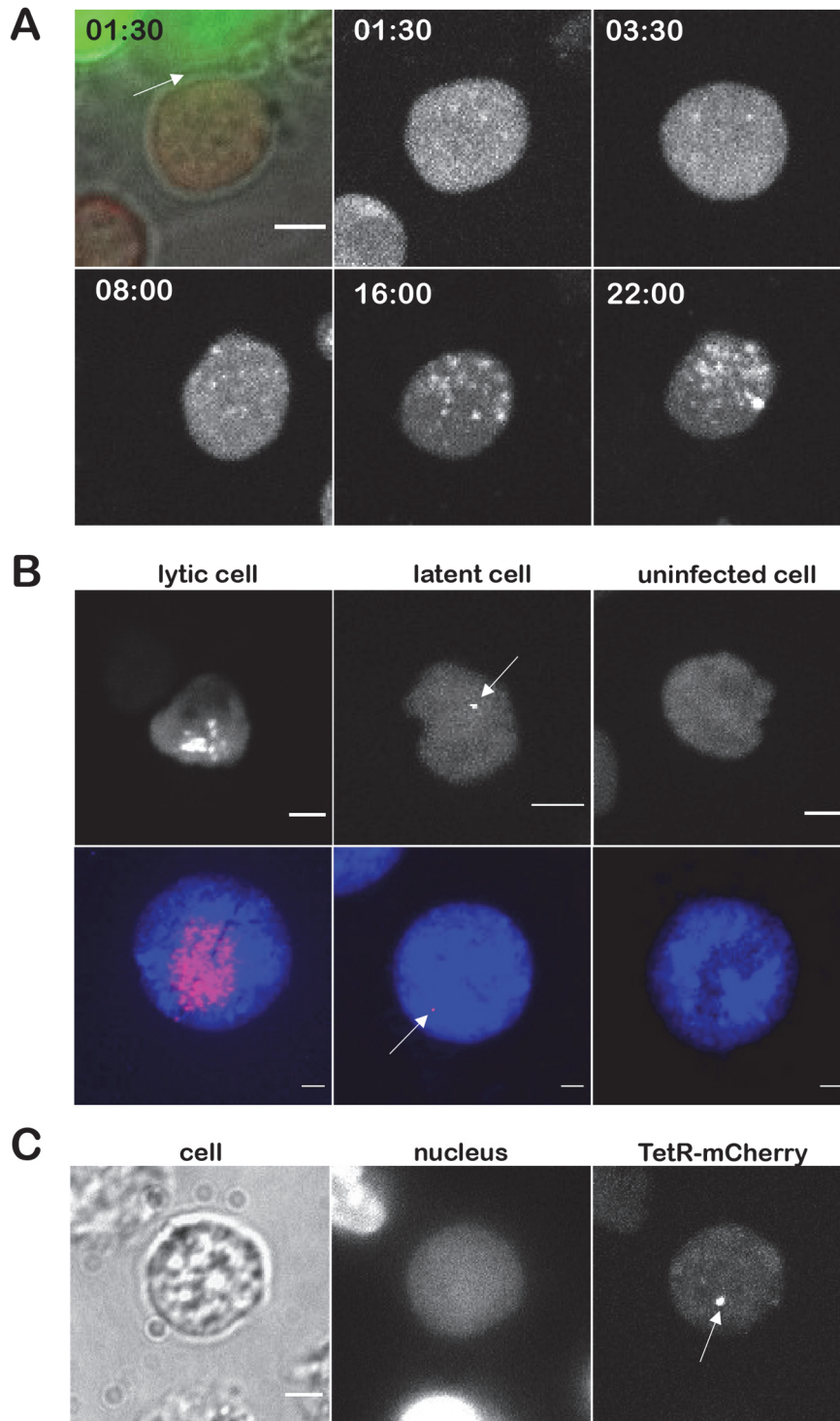
Figure 18. Lytic replication and latency in T cells. (**A**) 855-19 T cells stably expressing TetR-mCherry (multi-color image) were seeded on an infected CECs monolayer. The site of contact between infected CEC (green) and uninfected T cell (red) is shown with a white arrow. Time course images are shown as maximum intensity projections of the red channel (TetR-mCherry). Images were taken using a 60× Oil objective. 13 focal planes with a z-stack size of 1.7 µm were imaged every ten minutes for 21 h. Time in hh:mm, scale bar 3 µm (**B**) representative images of 855-19 T cells expressing TetR-mCherry three days after virus infection (upper line) in comparison with FISH images (lower line; DAPI in blue, viral DNA in red). Live cell images are shown as maximum intensity projection of z-stacks in the red channel. Arrows highlight single dots in the nucleus of latently infected cells. Scale bar 3 µm;

(**C**) representative image of infected T cells at 14 dpi. One specific dot (arrow) was detected in maximum-intensity projection of multiple focal planes in TetR-mCherry.

3.5 Discussion

The visualization of viral genomes in living cells has an immense potential in research on a broad range of processes including antiviral responses to the genome, viral replication, and genome maintenance in latently infected cells. Most processes involving the virus genome during MDV infection remain poorly understood. Therefore, we set out to develop a system that facilitates visualization of the MDV genome in living cells.

To visualize MDV genomes, we inserted the *tetO* repeats into the MDV genome between UL45 and UL46 genes (vTetO). Plaque size assays and multiple step growth kinetics revealed that insertion of the *tetO* repeats into this site does not affect MDV replication and cell-to-cell spread in culture. This was not surprising as this locus has been previously successfully used (e.g., for the insertion of a GFP expression cassette) [16]. Southern blotting confirmed the expected size of the *tetO* repeats and Illumina MiSeq NGS ensured that no additional SNPs were present in the recombinant viruses. More importantly, nanopore sequencing confirmed that the *tetO* repeats in the MDV genome are stable for at least nine passages, highlighting that the system could even be used with high passage viruses and for long-term analyses.

Next, we expressed the fluorescently tagged TetR either from the virus genome or from a plasmid stably maintained in the target cell. To ensure the reliability of the *tetO*/TetR system, we validated the specificity of the TetR staining by two independent approaches. First, we confirmed that overexpression of TetR-GFP driven by the strong TK promoter does not cause unspecific staining in the absence of *tetO*, for example, due to the formation of aggregates in the nucleus. In addition, we validated the TetR specificity via the addition of tetracycline, resulting in a conformational change of the TetR DNA-binding domain [45]. This resulted in the expected release of the TetR-GFP from the *tetO* repeats present in the virus and resulted in a diffuse staining observed in the absence of *tetO* (Figure 15C). Although we detected even distribution of TetR-GFP (Figure 15B) in the entire nucleus, the amount of TetR expressed from the TK-promoter was too high to be able to detect single viral genomes. In addition, most of the viral genes (including the TK promoter in the mini-F) are silenced during latency. Therefore, we decided to fuse TetR-GFP via a P2a self-cleaving peptide to the C-terminus of vCXCL13 in vTetO (Figure 13A), as splice variants containing the last exon (exon 3) are expressed during both lytic replication and latency at moderate levels [12,49].

Using the optimized *tetO*/TetR system, we could efficiently visualize RCs in lytically infected primary cells and cell lines (Figures 15A and 17A). We could also observe the establishment

and growth of the RCs using live-cell microscopy. In previous studies on HSV-1, it was shown that the vast majority of RCs are initiated from a single incoming viral genome at distinct sites in the nucleus [50,51]. Due to the strictly cell-associated nature of MDV, we could not perfectly time the infection, but could observe a similar phenotype. Our results indicate that it takes MDV RCs about 24 h to reach their full size upon entry into the nucleus. In addition, the observed one to two RCs within a nucleus possessed a different size and shape, although they were gradually growing (Figure 16A). In comparison, HSV-1 infected cells with a multiplicity of infection of 20 commonly harbor three to five RCs per nucleus depending on the cell line [52]. In T cells, MDV establishes usually just a diffuse RC that differs from the ones seen in fibroblasts. This could be due to the smaller size of T cell nuclei, their previously reported rigidity, and compact nature [53–55]. Our system, thereby, revealed a cell type dependent difference between the RCs.

Based on previous studies with HSV-1 [46,56], it is thought that viral genomes are phase-separated from chromosomal DNA and have the properties of liquid-liquid phase-separated condensates. It was shown that proteins can freely diffuse through RC, whereas the viral genomes appear to be much slower. However, these studies were done using HSV-1 amplicon plasmids that do not reflect the entire complexity of replicating herpesviruses [46,57]. Here, we observed that, although the infected cells and nuclei moved during the recording period, we detected only minimal changes in the shape of RC and position of the dotted structures within the RC (Figure 16B). This could be explained by the cohesion of concatemeric viral genomes during branched rolling circle replication, whereas proteins can freely diffuse through the RCs. We will assess the interaction of proteins with the MDV genome in this context using our MDV system in future studies.

Using the *tetO*/TetR system, we observed that MDV can induce fusion of cultured CECs, resulting in the formation of syncytia. We examined this CPE, which was previously only reported in DEFs, and observed that some nuclei within a syncytium do not possess RC (Figure 17A). We noticed a weak but diffuse TetR-GFP signal in those nuclei, indicating that the fusion protein was, to some extent, transported into the uninfected nuclei within the syncytium due to its NLS.

To shed more light on the course of infection in T cells and the establishment of latency, we set out to explore the behavior of viral genomes early in infection. Since almost all MDV genes are silenced during latency, we generated T cell line stably expressing TetR-mCherry independent of the virus life cycle (Figure 18B). Replication foci were detected around 8 hpi that increased over the course of time (Figure 18A), indicating that lytic replication progresses in some of the T cells, as shown previously [4–6]. After 14 dpi we were able to detect single

bright dots in the nucleus, as detected by FISH. This is consistent with previous studies that found only one or few integration sites in primary T cells and T cell lines latently infected *in vitro* [6,43], while multiple integration sites were detected in MDV-induced tumor cells [9,10]. Since no replication was detected at this time point, these most likely correspond to latent virus genomes (Figure 18B,C). Comparable signals were found in infected T cells already at 3 dpi, suggesting that MDV can enter in the quiescent stage early after infection. We will expand on these observations, especially in the context of MDV integration in the future.

Taken together, we established a system that facilitates the visualization of MDV genomes in living cells. This system provided exciting insights into the virus live cycle, including the number of RCs in different cell types, the establishment and expansion of RCs, the formation of syncytia, and the infection of T cells resulting in either lytic replication or latency. This *tetO*-TetR-based system, established in this study, will contribute to our understanding of MDV, replication, genome integration, and the establishment of latency in future studies.

3.6 Supplementary material

The following supporting information can be downloaded at: https://www.mdpi.com/article/10.3390/v14020287/s1, Video S1: 3D image of RC in nucleus.

3.7 Author contributions

Conceptualization, B.B.K. and T.V.; methodology, B.B.K., T.V. and D.J.W.; formal analysis, T.V. and M.N.; investigation, T.V., D.J.W., M.N. and F.J.; resources, B.B.K., T.K. and A.H.; writing—original draft preparation, T.V. and B.B.K.; writing—review and editing, T.V., B.B.K., M.N., D.J.W., F.J., A.H. and T.K.; visualization, T.V. and M.N.; supervision, B.B.K.; project administration, B.B.K.; funding acquisition, B.B.K. All authors have read and agreed to the published version of the manuscript.

3.8 Funding

This research was funded by European Research Council, grant number Stg 677673 awarded to B.B.K. The publication of this article was funded by Freie Universität Berlin.

3.9 Institutional review board statement

Not applicable.

3.10 Informed consent statement

Not applicable.

3.11 Data availability statement

Not applicable.

3.12 Acknowledgements

We are grateful to Ann Reum, Andelé Conradie, and Yu You for their technical assistance. We also thank Thomas Göbel for providing the chicken T cell line 855-19 used in this study.

3.13 Conflicts of interest

The authors declare no conflict of interest. The funders had no role in the design of the study; in the collection, analyses, or interpretation of data; in the writing of the manuscript; or in the decision to publish the results.

3.14 References

1. Schat, K.A.; Nair, V. Neoplastic diseases. In Diseases of Poultry, 13th ed.; Swayne, D.E., Ed.; John Wiley & Sons, Inc.: Hoboken, NJ, USA, 2013; pp. 513–673.

2. Barrow, A.; Burgess, S.C.; Baigent, S.J.; Howes, K.; Nair, V. Infection of macrophages by a lymphotropic herpesvirus: A new tropism for Marek's disease virus. J. Gen. Virol. 2003, 84, 2635–2645. [CrossRef] [PubMed]

3. Chakraborty, P.; Vervelde, L.; Dalziel, R.G.; Wasson, P.S.; Nair, V.; Dutia, B.M.; Kaiser, P. Marek's disease virus infection of phagocytes: A de novo in vitro infection model. J. Gen. Virol. 2017, 98, 1080–1088. [CrossRef] [PubMed]

4. Bertzbach, L.D.; Laparidou, M.; Härtle, S.; Etches, R.J.; Kaspers, B.; Schusser, B.; Kaufer, B.B. Unraveling the role of B cells in the pathogenesis of an oncogenic avian herpesvirus. Proc. Natl. Acad. Sci. USA 2018, 115, 11603–11607. [CrossRef] [PubMed]

5. Bertzbach, L.D.; Van Haarlem, D.A.; Härtle, S.; Kaufer, B.B.; Jansen, C.A.; Haarlem, V. Marek's Disease Virus Infection of Natural Killer Cells. Microorganisms 2019, 7, 588. [CrossRef] [PubMed]

6. Schermuly, J.; Greco, A.; Härtle, S.; Osterrieder, N.; Kaufer, B.B.; Kaspers, B. In vitro model for lytic replication, latency, and transformation of an oncogenic alphaherpesvirus. Proc. Natl. Acad. Sci. USA 2015, 112, 7279–7284. [CrossRef] [PubMed]

7. Jarosinski, K.W.; Tischer, B.K.; Trapp, S.; Osterrieder, N. Marek's disease virus: Lytic replication, oncogenesis and control. Expert Rev. Vaccines 2006, 5, 761–772. [CrossRef] [PubMed]

8. Schat, K.A.; Chen, C.L.; Calnek, B.W.; Char, D. Transformation of T-lymphocyte subsets by Marek's disease herpesvirus. J. Virol. 1991, 65, 1408–1413. [CrossRef] [PubMed]

9. Kaufer, B.B.; Jarosinski, K.W.; Osterrieder, N. Herpesvirus telomeric repeats facilitate genomic integration into host telomeres and mobilization of viral DNA during reactivation. J. Exp. Med. 2011, 208, 605–615. [CrossRef] [PubMed]

10. Greco, A.; Fester, N.; Engel, A.T.; Kaufer, B.B. Role of the Short Telomeric Repeat Region in Marek's Disease Virus Replication, Genomic Integration, and Lymphomagenesis. J. Virol. 2014, 88, 14138–14147. [CrossRef] [PubMed]

11. Parcells, M.S.; Arumugaswami, V.; Prigge, J.T.; Pandya, K.; Dienglewicz, R.L. Marek's disease virus reactivation from latency: Changes in gene expression at the origin of replication. Poult. Sci. 2003, 82, 893–898. [CrossRef] [PubMed]

12. Parcells, M.S.; Lin, S.-F.; Dienglewicz, R.L.; Majerciak, V.; Robinson, D.R.; Chen, H.-C.; Wu, Z.; Dubyak, G.R.; Brunovskis, P.; Hunt, H.D.; et al. Marek's Disease Virus (MDV) Encodes an Interleukin-8 Homolog (vIL-8): Characterization of the vIL-8 Protein and a vIL-8 Deletion Mutant MDV. J. Virol. 2001, 75, 5159–5173. [CrossRef] [PubMed]

13. Kaufer, B.B.; Trapp, S.; Jarosinski, K.W.; Osterrieder, N. Herpesvirus Telomerase RNA(vTR)-Dependent Lymphoma Formation Does Not Require Interaction of vTR with Telomerase Reverse Transcriptase (TERT). PLoS Pathog. 2010, 6, e1001073. [CrossRef] [PubMed]

14. Kheimar, A.; Previdelli, R.L.; Wight, D.J.; Kaufer, B.B. Telomeres and Telomerase: Role in Marek's Disease Virus Pathogenesis, Integration and Tumorigenesis. Viruses 2017, 9, 173. [CrossRef] [PubMed]

15. Mwangi, W.N.; Smith, L.P.; Baigent, S.J.; Beal, R.K.; Nair, V.; Smith, A.L. Clonal Structure of Rapid-Onset MDV-Driven CD4+ Lymphomas and Responding CD8+ T Cells. PLoS Pathog. 2011, 7, e1001337. [CrossRef]

16. Liu, Y.; Li, K.; Cui, H.; Gao, L.; Liu, C.; Zhang, Y.; Gao, Y.; Wang, X. Comparison of different sites in recombinant Marek's disease virus for the expression of green fluorescent protein. Virus Res. 2017, 235, 82–85. [CrossRef]

17. Denesvre, C.; Rémy, S.; Trapp-Fragnet, L.; Smith, L.P.; Georgeault, S.; Vautherot, J.-F.; Nair, V. Marek's disease virus undergoes complete morphogenesis after reactivation in a T-lymphoblastoid cell line transformed by recombinant fluorescent marker virus. J. Gen. Virol. 2016, 97, 480–486. [CrossRef]

18. Jarosinski, K.W.; Donovan, K.M.; Du, G. Expression of fluorescent proteins within the repeat long region of the Marek's disease virus genome allows direct identification of infected cells while retaining full pathogenicity. Virus Res. 2015, 201, 50–60. [CrossRef]

19. Rémy, S.; Blondeau, C.; Le Vern, Y.; Lemesle, M.; Vautherot, J.-F.; Denesvre, C. Fluorescent tagging of VP22 in N-terminus reveals that VP22 favors Marek's disease virus (MDV) virulence in chickens and allows morphogenesis study in MD tumor cells. Vet. Res. 2013, 44, 125. [CrossRef]

20. Mao, W.; Kim, T.; Cheng, H.H. Visualization of Marek's disease virus in vitro using enhanced green fluorescent protein fused with US10. Virus Genes 2013, 47, 181–183. [CrossRef]

21. Jarosinski, K.W.; Arndt, S.; Kaufer, B.B.; Osterrieder, N. Fluorescently Tagged pUL47 of Marek's Disease Virus Reveals Differential Tissue Expression of the Tegument Protein In Vivo. J. Virol. 2011, 86, 2428–2436. [CrossRef]

22. Prigge, J.T.; Majerciak, V.; Hunt, H.D.; Dienglewicz, R.L.; Parcells, M.S. Construction and Characterization of Marek's Disease Viruses Having Green Fluorescent Protein Expression Tied Directly or Indirectly to Phosphoprotein 38 Expression. Avian Dis. 2004, 48, 471–487. [CrossRef] [PubMed]

23. Fuchs, J.; Lorenz, A.; Loidl, J. Chromosome associations in budding yeast caused by integrated tandemly repeated transgenes. J. Cell Sci. 2002, 115, 1213–1220. [CrossRef] [PubMed]

24. Mirkin, E.V.; Chang, F.S.; Kleckner, N. Protein-Mediated Chromosome Pairing of Repetitive Arrays. J. Mol. Biol. 2014, 426, 550–557. [CrossRef] [PubMed]

25. Michaelis, C.; Ciosk, R.; Nasmyth, K. Cohesins: Chromosomal Proteins that Prevent Premature Separation of Sister Chromatids. Cell 1997, 91, 35–45. [CrossRef]

26. Tischer, B.K.; von Einem, J.; Kaufer, B.; Osterrieder, N. Two-step red-mediated recombination for versatile high-efficiency markerless DNA manipulation in Escherichia coli. Biotechniques 2006, 40, 191–197. [PubMed]

27. Schat, K.A.; Purchase, H.G.; Amer Assn of Avian Pathologist. Cell-culture methods. In A Laboratory Manual for the Isolation and Identification of Avian Pathogens, 4th ed.; Swayne, D.E., Ed.; American Association of Avian Pathologists: Kennett Square, PA, USA, 1998.

28. Vautherot, J.-F.; Jean, C.; Fragnet-Trapp, L.; Rémy, S.; Chabanne-Vautherot, D.; Montillet, G.; Fuet, A.; Denesvre, C.; Pain, B. ESCDL-1, a new cell line derived from chicken embryonic stem cells, supports efficient replication of Mardiviruses. PLoS ONE 2017, 12, e0175259. [CrossRef]

29. Petherbridge, L.; Brown, A.C.; Baigent, S.J.; Howes, K.; Sacco, M.A.; Osterrieder, N.; Nair, V.K. Oncogenicity of Virulent Marek's Disease Virus Cloned as Bacterial Artificial Chromosomes. J. Virol. 2004, 78, 13376–13380. [CrossRef] [PubMed]

30. Tischer, B.K.; Kaufer, B.B. Viral Bacterial Artificial Chromosomes: Generation, Mutagenesis, and Removal of Mini-F Sequences. J. Biomed. Biotechnol. 2012, 2012, 472537. [CrossRef]

31. Bolger, A.M.; Lohse, M.; Usadel, B. Trimmomatic: A flexible trimmer for Illumina sequence data. Bioinformatics 2014, 30, 2114–2120. [CrossRef]

32. Li, H.; Durbin, R. Fast and accurate short read alignment with Burrows–Wheeler transform. Bioinformatics 2009, 25, 1754–1760. [CrossRef]

33. Garrison, E.; Marth, G. Haplotype-based variant detection from short-read sequencing. arXiv 2012, arXiv:1207.3907.

34. Schumacher, D.; Tischer, B.K.; Fuchs, W.; Osterrieder, N. Reconstitution of Marek's Disease Virus Serotype 1 (MDV-1) from DNA Cloned as a Bacterial Artificial Chromosome and Characterization of a Glycoprotein B-Negative MDV-1 Mutant. J. Virol. 2000, 74, 11088–11098. [CrossRef] [PubMed]

35. Jarosinski, K.W.; Margulis, N.G.; Kamil, J.P.; Spatz, S.J.; Nair, V.K.; Osterrieder, N. Horizontal transmission of Marek's disease virus requires US2, the UL13 protein kinase, and gC. J. Virol. 2007, 81, 10575–10587. [CrossRef] [PubMed]

36. Trimpert, J.; Groenke, N.; Kunec, D.; Eschke, K.; He, S.; McMahon, D.; Osterrieder, N. A proofreading-impaired herpesvirus generates populations with quasispecies-like structure. Nat. Microbiol. 2019, 4, 2175–2183. [CrossRef] [PubMed]

37. Hirt, B. Selective extraction of polyoma DNA from infected mouse cell cultures. J. Mol. Biol. 1967, 26, 365–369. [CrossRef]

38. Li, H. Minimap2: Pairwise alignment for nucleotide sequences. Bioinformatics 2018, 34, 3094–3100. [CrossRef] [PubMed]

39. Robinson, J.T.; Thorvaldsdóttir, H.; Winckler, W.; Guttman, M.; Lander, E.S.; Getz, G.; Mesirov, J.P. Integrative genomics viewer. Nat. Biotechnol. 2011, 29, 24–26. [CrossRef]

40. Thorvaldsdóttir, H.; Robinson, J.T.; Mesirov, J.P. Integrative Genomics Viewer (IGV): High-performance genomics data visualization and exploration. Brief. Bioinform. 2013, 14, 178–192. [CrossRef]

41. Roukos, V.; Voss, T.C.; Schmidt, C.K.; Lee, S.; Wangsa, D.; Misteli, T. Spatial Dynamics of Chromosome Translocations in Living Cells. Science 2013, 341, 660–664. [CrossRef]

42. Kaufer, B.B. Detection of Integrated Herpesvirus Genomes by Fluorescence In Situ Hybridization (FISH). Program. Necrosis 2013, 1064, 141–152. [CrossRef]

43. You, Y.; Vychodil, T.; Aimola, G.; Previdelli, R.L.; Göbel, T.W.; Bertzbach, L.D.; Kaufer, B.B. A Cell Culture System to Investigate Marek's Disease Virus Integration into Host Chromosomes. Microorganisms 2021, 9, 2489. [CrossRef] [PubMed]

44. Gasser, S.M. Visualizing Chromatin Dynamics in Interphase Nuclei. Science 2002, 296, 1412–1416. [CrossRef] [PubMed]

45. Orth, P.; Cordes, F.; Schnappinger, D.; Hillen, W.; Saenger, W.; Hinrichs, W. Conformational changes of the Tet repressor induced by tetracycline trapping. J. Mol. Biol. 1998, 279, 439–447. [CrossRef] [PubMed]

46. Seyffert, M.; Georgi, F.; Tobler, K.; Bourqui, L.; Anfossi, M.; Michaelsen, K.; Vogt, B.; Greber, U.; Fraefel, C. The HSV-1 Transcription Factor ICP4 Confers Liquid-Like Properties to Viral Replication Compartments. Int. J. Mol. Sci. 2021, 22, 4447. [CrossRef]

47. Gupta, M.; Deka, D. Ramneek Sequence analysis of Meq oncogene among Indian isolates of Marek's disease herpesvirus. Meta Gene 2016, 9, 230–236. [CrossRef]

48. Boodhoo, N.; Gurung, A.; Sharif, S.; Behboudi, S. Marek's disease in chickens: A review with focus on immunology. Vet. Res. 2016, 47, 1–19. [CrossRef]

49. Jarosinski, K.W.; Schat, K.A. Multiple alternative splicing to exons II and III of viral interleukin-8 (vIL-8) in the Marek's disease virus genome: The importance of vIL-8 exon I. Virus Genes 2007, 34, 9–22. [CrossRef]

50. Sekine, E.; Schmidt, N.; Gaboriau, D.; O'Hare, P. Spatiotemporal dynamics of HSV genome nuclear entry and compaction state transitions using bioorthogonal chemistry and super-resolution microscopy. PLoS Pathog. 2017, 13, e1006721. [CrossRef]

51. Dembowski, J.A.; DeLuca, N.A. Temporal Viral Genome-Protein Interactions Define Distinct Stages of Productive Herpesviral Infection. mBio 2018, 9, e01182-18. [CrossRef]

52. Tomer, E.; Cohen, E.M.; Drayman, N.; Afriat, A.; Weitzman, M.D.; Zaritsky, A.; Kobiler, O. Coalescing replication compartments provide the opportunity for recombination between coinfecting herpesviruses. FASEB J. 2019, 33, 9388–9403. [CrossRef]

53. Jain, N.; Iyer, K.V.; Kumar, A.; Shivashankar, G.V. Cell geometric constraints induce modular gene-expression patterns via redistribution of HDAC3 regulated by actomyosin contractility. Proc. Natl. Acad. Sci. USA 2013, 110, 11349–11354. [CrossRef] [PubMed]

54. Borsos, M.; Torres-Padilla, M.-E. Building up the nucleus: Nuclear organization in the establishment of totipotency and pluripotency during mammalian development. Genes Dev. 2016, 30, 611–621. [CrossRef] [PubMed]

55. Skinner, B.M.; Johnson, E.E.P. Nuclear morphologies: Their diversity and functional relevance. Chromosoma 2017, 126, 195–212. [CrossRef] [PubMed]

56. McSwiggen, D.T.; Hansen, A.S.; Teves, S.S.; Marie-Nelly, H.; Hao, Y.; Heckert, A.B.; Umemoto, K.K.; Dugast-Darzacq, C.; Tjian, R.; Darzacq, X. Evidence for DNA-mediated nuclear compartmentalization distinct from phase separation. eLife 2019, 8, e47098. [CrossRef] [PubMed]

57. Sourvinos, G. Visualization of parental HSV-1 genomes and replication compartments in association with ND10 in live infected cells. EMBO J. 2002, 21, 4989–4997. [CrossRef]

Author contributions:

Name	Author's designation	Involved in:
Tereza Vychodil	First author	Conceptualization Formal analysis Investigation Data analysis Visualization Statistical analysis Writing – original draft preparation Writing – review and editing
Darren J. Wight	Co-author	Investigation Writing – review and editing
Mariana Nascimento	Co-author	Formal analysis Investigation Visualization Writing – review and editing
Fabian Jolmes	Co-author	Investigation Writing – review and editing
Thomas Korte	Co-author	Design of experiments Provided resources Writing – review and editing
Andreas Herrmann	Co-author	Provided resources Writing – review and editing
Benedikt B. Kaufer	Supervisor and corresponding author	Conceptualization Design of experiments Supervision Project administration Funding acquisition Writing – original draft preparation Writing – review and editing Provided resources

4 Discussion

4.1 General discussion

MDV causes one of the most frequent virus-induced cancers in animal kingdom. Scientists are using MDV as a versatile small-animal model virus for research on herpesvirus pathogenesis, integration, latency, and tumorigenesis in the natural host (Bertzbach *et al.*, 2020; Osterrieder et al., 2006). During latency, herpesviruses genomes persist in the host either in the form of extrachromosomal circular episomes or as integrated linear genomes in the host telomeres (Delecluse and Hammerschmidt, 1993; Kaufer *et al.*, 2011). Integration is facilitated by viral telomeric repeats (TMRs) which are identical to the host TMRs localized at the ends of the chromosomes. According to the NCBI database (taxid 548681; accessed on 11 April 2022), 18 herpesviruses out of 89 completely sequenced full length genomes harbor TMRs in their genome. Although HHV-7, GaHV-3 (SB-1 strain), and MeHV-1 (HVT) are speculated to integrate into host chromosomes (McPherson et al., 2016; Prusty et al., 2017), so far, mainly MDV (GaHV-2), HHV-6A, and HHV-6B were extensively studied and documented to establish latency by integrating their genomes into the host telomeres ensuring the maintenance of viral genomes in the host cell (Arbuckle *et al.*, 2010; Delecluse and Hammerschmidt, 1993; Kaufer *et al.*, 2011; Wallaschek et al., 2016). In MDV, there are two identical copies of TMRs which are located in a-like sequences between the repeat regions – one is located between the two internal repeats and the second is situated between the terminal repeats of the circular genome. In this thesis, we investigated the impact of an deletion of one of these sets of repeat regions, a-like sequence, and TMRs on MDV replication, integration, tumorigenesis, and virus spread.

Until now, almost everything we know about herpesvirus integration was explored utilizing the powerful single-cell fluorescent *in situ* hybridization (FISH) method. FISH provided us with very important insights into the mechanism of herpesvirus integration, e.g. that the absence of TMRs in MDV and HHV-6A leads to a severely impaired integration (Kaufer *et al.*, 2011; Wallaschek *et al.*, 2016). However, many and many hours were devoted to fix the infected cells, generate metaphase spreads, wash-out proteins and cell debris, and finally stain viral genomes. And only then, after 3 days of a hard work, one is able to evaluate whether the FISH method worked properly and to eventually analyze the results. As every other method, also FISH has its limitations and pitfalls. Firstly, during splashing of swollen cells on a glass slide for metaphase chromosomes spreads, a small fraction of lytically replicating cells can make such a background that we cannot reliably claim, if a signal localized on a chromosome really corresponds with an integrated virus or if it is a random virus genome that landed there from

another cell by accident. Secondly, since the method is time-consuming and it takes approximately 3 days to detect vDNA, we cannot use FISH for a real-time quantification of latently infected cells. Lastly, once we fix the cells, we cannot see what would further happen with the latently infected cell. Therefore, we were looking for an alternative method which would supplement FISH to gain deeper knowledge about the integration process.

Compared with FISH, live-cell imaging renders different kind of information. It provides insights into the infection dynamics: mobility, sequence of events, interaction partners, and current changes within an infected cell during a selected time period. Previous studies done on labeling viral genomes in infected living cells demonstrated the huge potential of this procedure. Real-time optical detection of vDNA provided us with new observations and broader understanding of replication kinetics and properties of viral replication compartments (VRCs) in different viruses (Gallardo *et al.*, 2020; Hinsberger *et al.*, 2020; Kieser et al., 2019; Mariame *et al.*, 2018; Seyffert *et al.*, 2021). Moreover, depending on the labeling method, background and microscope, it should be even possible to distinguish and detect single vDNAs (Mariame *et al.*, 2018).

To track the fate of both replicating and quiescent MDV genomes, we decided to employ the operator/repressor live-cell imaging method. During latency, the majority of MDV genes are silenced. The only few genes which were identified and detected to be expressed are located in repeat regions and thus twice in the genome. Since we were planning to generate a MDV recombinant virus expressing the labeled repressor also during latency, we first generated a versatile virus to modify both copies of diploid genes situated in the repeat regions with just one round of mutagenesis.

4.2   Platform viruses for a straight-forward mutation of diploid genes

In herpesviruses, the E class genome has the most complex arrangement consisting of two unique regions each of them flanked by two inverted copies of repeat regions. Most of the genes encoded by MDV have functional homologues also in other alphaherpesviruses, but these genes are mainly located in the unique regions. On the contrary, genes, miRNAs, and circular RNAs involved in MDV pathogenesis, latency, and tumor formation are located in the repeat regions and thus each of them is represented twice in the genome (Chasseur et al., 2022). Manipulation with these virulence factors was shown to be quite delicate as any alterations in one segment are repaired by homologous recombination (HR) during virus reconstitution, using the retained segment as a template. Therefore, in our study "Marek's disease virus requires both copies of the inverted repeat regions for efficient *in vivo* replication and pathogenesis" we generated a panel of BAC viruses which simplify the modification of diploid genes. By deleting the majority of one set of inverted repeats, only one round of en-

passant mutagenesis is required for the requested mutation which is then automatically duplicated into the second repeat region by HR (Tischer et al., 2010; Tischer et al., 2006). The recombinants were confirmed to rapidly reconstitute the deleted repeat region and both *in vitro* and *in vivo* experiments demonstrated that the viruses behave like wildtype. Moreover, these viruses were shown to be very useful and are frequently utilized not only in our lab to generate new MDV mutants (Vychodil et al., 2022; You et al., 2021a; You *et al.*, 2021b).

In addition, few studies also dealt with the question whether herpesviruses with repeat regions need the second set of diploid genes. Experiments done on HSV-1, HCMV, and EHV-1 describe that recombinant viruses with only one set of diploid genes are capable to grow and spread *in vitro* comparable to wildtype (Ahn et al., 2011; Jenkins et al., 1996; Sauer et al., 2010). On the other hand, quite different scenarios were observed in animals. When tested *in vivo*, the recombinant HSV-1 and EHV-1 viruses displayed significantly impaired pathogenicity with decreased viral titers in infected tissues (Ahn *et al.*, 2011; Jenkins *et al.*, 1996). These findings are consistent also with our results on MDV. However, it should be mentioned that none of these previous animal experiments were carried out in the natural host and thus might have not entirely reflected the species-specific adaptation capabilities of the viruses. To our best knowledge, our study was the first publication that investigated the behavior of a haploid E class genome herpesvirus in the natural virus-host settings.

It is also worth mentioning that herpesviruses with inverted repeat regions are capable to undergo genome isomerization. During DNA replication, both unique regions (the U_L and U_S fragments) can freely invert relative to each other, thereby generating four distinct genomic isomers that differ in the relative orientation of the unique segments (Delius and Clements, 1976). This process is induced by homologous recombination (Smiley et al., 1981; Weber et al., 1988). The construction of virus recombinants with haploid set of genes thus inevitably leads to a "frozen" genome arrangement. Therefore, it can be difficult to distinguish what is the effect of isomerization inability on the virus behavior and what is the impact of the suboptimal genome length. However, when we take into account that there are herpesviruses without any repeat regions in their genome, it is highly improbable isomerization would be an essential feature for herpesvirus pathogenesis. Moreover, a virus that naturally lacks repeat regions can gain the ability to generate isomers during replication just by inserting some artificial inverted segments in its genome (McVoy and Ramnarain, 2000). It thus appears that genome isomerization might be only a consequence of the acquisition of inverted repeats combined with the highly recombinogenic nature of the herpesvirus replication machinery.

Lastly, another study pointed out that even the size of the viral genome might play an important role in the virus pathogenicity (Cui et al., 2009). Herpesviruses are known to tolerate large-

scale genome rearrangements upon insertions or deletions. This feature makes them attractive to be used as gene therapy vectors or live-attenuated recombinant vaccine vectors (Mody et al., 2020; Sadigh et al., 2018; Williams et al., 2019). It has been speculated that longer non-essential repetitive sequences might provide herpesviruses with an evolutionary advantage of genetic adaptation with the ability to maintain the optimal genome length. In case a virus gains an advantageous gene or loses any sequence, it can easily adjust its genome size by undergoing alterations or modifications within repeat regions (Cui *et al.*, 2009). However, there are limits for the length of viral DNA. In previous studies, it was shown that trespassing the critical length inevitably leads to spontaneous deletions since the longer viral genome cannot fit in the capsid anymore. On the contrary, too short vDNA might interfere with virus replication by influencing the cleavage site spacing for virus packaging, as probably also seen in our study with ΔIR_{LS} mutant (Cui *et al.*, 2009; Oxford et al., 2008; Prichard et al., 2001). Although the ΔIR_{LS} virus has all genes and genomic sequences present and still functioning, deletion of almost 15 % of genomic DNA might have disrupted the integrity of viral genome leading to impaired replication properties.

4.3 Establishing a method for real-time optical detection of herpesvirus genomes in living cells

In this study, the well-established *tetO*/TetR system was utilized to visualize MDV DNA genome in real-time. By introducing a repetitive *tetO* sequence into ΔIR_{LS} mutant, we generated two MDV recombinant viruses which can be used for different purposes. One of the viruses, vTetO, needs to come into a cell that produces TetR protein which can directly bind to *tetO* sequence. This allows us to detect the very early processes like virus entry into the nucleus or the onset of VRCs, as well as the quiescent stage of MDV when the expression of the majority of viral genes is silenced. The second virus, vTetO-TetR, harbors the expression cassette for TetR-GFP in its genome and can thus be used in primary cells. The amount of protein and time point of expression is regulated by the virus itself depending on the position of TetR-GFP in vDNA. During my PhD, I generated various recombinant vTetO-TetR viruses with differently positioned TetR-GFP expression cassette (Figure 19). First, the TetR-GFP gene was inserted into Mini-F cassette under a strong pTK promoter leading to an excessive protein expression during lytic replication. This virus was the first one where we saw a specific dotted structure of VRCs within a nucleus which proved that the *tetO*/TetR system is working in MDV. However, since the pTK promoter is silenced during latency, such a virus does not produce TetR-GFP after genome integration. Therefore, I constructed another recombinant vTetO-TetR where the repressor was fused with the 5' end of LAT locus. LAT is abundant in MDV-transformed lymphoblastoid cells and the 10 kbp long RNA map antisense to the ICP4

gene (Cantello *et al.*, 1994). However, the RNA transcripts are not translated. We thus inserted an internal ribosomal entry site (IRES) sequence at the beginning of the locus to achieve translation of the repressor (Sachs et al., 1997). Although this virus was growing a little bit slower than wildtype, we detected nice VRCs without additional background of unbound TetR-GFP and used this virus for several live cell imaging experiments. Unfortunately, we observed after some time that the virus lytic replication was affected. We assumed that the TetR expression altered LAT miRNAs transcription which probably interfered with antisense ICP4 transcripts. Therefore, to avoid any further detriments of virus propagation, we decided to fuse the TetR-GFP expression cassette through a self-cleaving P2A peptide (Kim et al., 2011). In this case, the certain viral gene and TetR-GFP should be produced as a one linked transcript which is later during translation separated into two independent proteins. In the next vTetO-TetR, TetR-GFP was fused either with the 3' end of meq or with the 3' end of exon 3 of vIL8/vCXCL13 gene. Both proteins are known to be expressed during lytic and latent stages of infection. In transfected fibroblasts, however, the meq virus did not produce any fluorescent signal. Therefore, I decided to continue with vTetO-TetR in vIL8/CXCL13. This virus was finally used in the experiments which were published in "Visualization of Marek's disease virus genomes in living cells during lytic replication and latency".
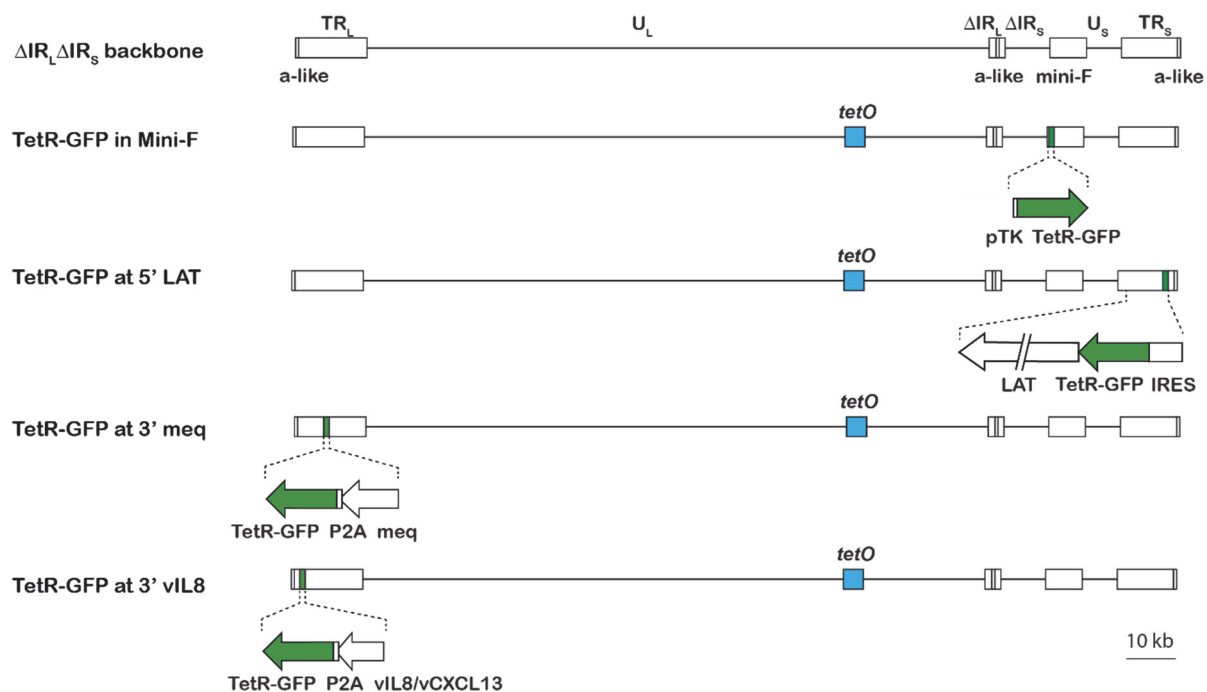

Figure 19*. Overview of various vTetO-TetR recombinant BAC clones. The recombinant viruses were generated using the RB-1B $\Delta IR_L\Delta IR_S$ BAC which lacks most of the IR_L and IR_S region. The unique long and short regions (U_L and U_S) and the a–like sequences are indicated. To achieve optimal protein expression, the TetR-GFP cassette was inserted and characterized at several different positions within the mini-F locus or the terminal repeats long and short (TR_L, TR_S). Finally, the fusion of TetR-GFP with the 3' end of vIL8/vCXCL13 through a self-

cleaving p2a peptide resulted in balanced protein expression. TetR-GFP is depicted in dark green, the *tetO* sequence in blue.

Recently, similar studies using the ANCHOR™ labelling technology visualized herpesvirus genomes of HCMV and EHV-1 during lytic phase of infection (Mariame *et al.*, 2018; Quentin-Froignant et al., 2021). Intriguingly, using correlative fluorescence/electron microscopy, it was shown that HCMV drags fluorescently labeled OR proteins along into the capsid and thus even enveloped particles can be visualized outside the nucleus (Mariame *et al.*, 2018). Nonetheless, the precise mechanism how the proteins get inside a capsid is still unknown. It is assumed, that all fluorescent proteins are presumably stripped from herpesvirus genomes during translocation through the narrow portal. The capsid portal of HCMV, the largest herpesvirus, has diameter of 26 to 30 Ångström (Å) (Li et al., 2021) and the DNA helix itself has already a diameter of 20 Å. Therefore, it seems that the fluorescent OR proteins, which are in excess and diffusely distributed in the whole cell, might get packaged during assembly of procapsids. Although we did not focus on detection of MDV genomes outside the nucleus in our publication, we cannot rule out that even in our system TetR-mCherry might get packaged in procapsids as well. Moreover, due to an NLS on the TetR, the cytoplasm remains free without any fluorescent background to easily distinguish fluorescent signals which might correspond to virions.

To our best knowledge, we were first who reported about optical detection of latent virus in a living host cell. In our study, we visualized latent vTetO in T cells which are stably expressing TetR-mCherry protein. The fluorescence intensity of TetR that is bound to *tetO* sequence was several times higher than the one of the unbound TetR floating in the nucleus, making the detection of latent virus trustworthy. Unfortunately, only a small fraction of T cells that got infected is harboring a latent virus. In our publication "A Cell Culture System to Investigate Marek's Disease Virus Integration into Host Chromosomes", we optimized MDV infection of T cells and calculated viral genome copies per cell 14 dpi (You et al., 2021c). According to these calculations using RB-1B wildtype, we detect on average one copy of vDNA per ten cells by qPCR. However, both vTetO and vTetO-TetR virus stocks did not have high virus titer because they were frozen during low virus passage. Titrated stocks were approximately ten times lower than of RB-1B used in our *in vitro* assay. We therefore count with approximately one virus genome per 100 cells. Such a low virus presence makes the screening of cells by microscope quite time consuming. Therefore, it was important for us to further improve the identification of infected cells. During lytic infection, both vTetO and vTetO-TetR are expressing a large amount of GFP or E2-Crimson proteins, respectively. This approach allows us to identify infected cells which can be fluorescently sorted using fluorescence-activated cell sorting (FACS). Although FACS sorting is associated with cellular stress, we managed to

separate fluorescently positive cells and maintained them in the culture. Unfortunately, the majority of the sorted cells died and 14 dpi only few copies of vDNA were detected by qPCR. Therefore, to avoid cell sorting, we tried to increase the number of latently infected cells by hindering viruses to lytically replicate and pushing it towards quiescent stage. To achieve this, T cells were treated directly after overlay infection with interferon alpha (IFNα) and gamma (IFNγ) which were shown to efficiently reduce MDV replication both *in vitro* and *in vivo* (Bertzbach et al., 2019a; Jarosinski et al., 2001; Xing and Schat, 2000). After several days post infection, when the cells restored their proliferation, individual cells were isolated by limiting dilution to make monoclonal cell lines harboring latent virus. Although I repeated this experiment several times and did lot of optimization steps, I was unable to detect any vDNA in those growing monoclonal cell lines. Therefore, we came up with another strategy. I generated recombinant viruses which should help to increase the number of infected cells by getting rid of uninfected ones. In this approach, puromycin or hygromycin resistance gene cassettes were inserted at the 3' end of exon 3 of vIL8/CXCL13 in vTetO virus to survive antibiotics treatment. Unfortunately, this plan was not quite successful. Although the virus constructs were viable and growing in fibroblasts, all cells died during the antibiotics selection without any difference. Therefore, we were obliged to use microscope software and look for distinct signal intensities to find latent cells among uninfected ones at the end.

Nevertheless, there might be another way of getting a monoclonal cell population with integrated vTetO MDV. As MD is characterized by tumor clonality (Delecluse et al., 1993; Mwangi *et al.*, 2011), we might utilize this feature to our advantage. Several MDV-transformed T cell lines has been established *ex vivo* from tumor biopsies of experimentally infected chickens (Akiyama and Kato, 1974). Infecting chickens with the vTetO and/or vTetO-TetR virus would lead to formation of lymphomas from which transformed lymphoblastoid cells could be cultured *in vitro*. To visualize the integrated vTetO, TetR-mCherry needs to be subsequently introduced to the transformed cells. Previously it was shown that recombinant MDVs expressing fluorescent proteins behave similar to wildtype *in vivo* (Jarosinski et al., 2015). I would therefore assume that also vTetO-TetR is able to produce TetR-GFP in infected chickens. Such cell lines would significantly aid in further studies of the fate of vDNA during different stages.

In the context of MDV integration, an immense advantage of the live-cell imaging system is the possibility to track establishment and timing of virus latency, kinetics of telomere association and reactivation, and colocalization of different viral or cellular proteins with vDNA in real-time. At the end of my PhD, I started to work on generation of chicken T cell line stably expressing both TetR-mCherry and fluorescently labeled TRF2 protein which would enable us to colocalize integrated vDNA with host telomeres. Unfortunately, due to some unforeseen

complications with the plasmid, this work wasn't completely finished yet and would require further elaborations.

Besides MDV, our lab is dealing also with HHV-6A and its integration into human telomeres. As HHV-6A reconstitution from BAC was proved to be challenging, we utilized the SunTag system to avoid this lengthy and complicated process. The advantage of this system compared to *tetO*/TetR system is that no DNA sequence has to be inserted into virus genome and thus any previously reconstituted HHV-6A can be used. All three components necessary for virus genome visualization (dCas9-24xGCN4, scFv-sfGFP, and sgRNAs) are expressed directly from cells. However, also here we faced some difficulties. First of all, the stability of dCas9-24xGCN4 which was delivered in cells by lentivirus is rather low and requires constant antibiotics selection. Moreover, another problem posed the high GFP background of unbound scFv-sfGFP. As previously shown, this could be overcome by using dCas9 tagged with tandem fluorophores (3xGFP or 3xmCherry) (Ma et al., 2015). Last but not least, neither HHV-6A nor MDV possess long stretches of repetitive DNA which could be used for binding of multiple sgRNAs. In direct repeats, there is ca 3 kbp long repetitive element composed of 28 copies of 104 bp and with 90% identity between repeats. These tandem repeats were used as sgRNA target. Unfortunately, using only 28 copies of sgRNA failed to detect the vDNA. By testing the sensitivity of our system, we revealed that at least 170 copies of sgRNA are required for reliable detection. Since HHV-6A does not possess that many repetitive DNA elements in its genome, multiple sgRNAs targets have to be expressed. Thus, a small pooled library of 20 different sgRNAs against non-essential HHV-6A genes was generated employing a gRNA multiplexing delivery platform (Shao et al., 2018). Unfortunately, despite all efforts to adapt the SunTag system to HHV-6A, the gathered results affirmed that this approach proved to be inadequate for this virus. Therefore, we were working on application of the *tetO*/TetR system into HHV-6A in the end. During my PhD, I generated 293T (derivate of human embryonic kidney cells containing the SV40 large T antigen), U2OS (human bone osteosarcoma epithelial cells), and JJHan (human lymphoblastic leukemia T cells) cell lines stably expressing fluorescently labeled TetR protein. These cells can be transfected or infected by HHV-6A containing *tetO* arrays enabling straightforward visualization using a fluorescent spinning-disk confocal microscopy. Lastly, I also collaborated with Dr. Alex Evilevitch's lab (Lund University, Sweden), consulted the adaptation of *tetO*/TetR system for HSV-1, and provided them our TetR-GFP plasmid and cell lines stably expressing TetR-mCherry.

Taken together, we established a visualization system to detect MDV genomes in living cells and proved that this system (i) is working accurately, (ii) is sensitive enough to detect latent

virus in infected T cells, (iii) and enables identification and/or verification of other potential cellular and/or viral key players that might facilitate virus integration.

4.4 Final remarks and outlook

In our group *Viral Integration, Tumorigenesis, and Virus Evolution* led by Prof. Dr. Kaufer, herpesviruses are the main source of our research. We are working predominantly with MDV and HHV-6A viruses as both are integrating into host telomeres using TMR sequences. Until now, the role of integrated vDNA in virus pathogenesis and the molecular mechanism of herpesvirus genome integration and reactivation are still poorly understood. Therefore, the lab aims (i) to explore the fate of virus genomes during integration and reactivation, (ii) to identify host and virus factors involved in both processes, and (iii) to develop a system for excision of integrated herpesvirus from host telomeres to prevent virus reactivation and its biological consequences. During my PhD, I aid in some of the above mentioned aims as some experiments and procedures were partially overlapping with my main project. Besides developing a system for tracking virus genomes during integration and reactivation, I was also assisting in adaptation and validation of the integration assay to MDV which was previously used for HHV-6A (Gravel et al., 2017). Since investigation of MDV integration has been dependent on animal experiments, we optimized cell culture-based infection conditions and set up a system where MDV could latently infect immortalized chicken T cells. The maintenance and integration of viral DNA is evaluated using qPCR and FISH methods. This quantitative assay allows us to assess MDV genome maintenance and integration *in vitro* within only two weeks. Although it cannot completely substitute *in vivo* experiments, it could serve as a bottleneck when testing many different recombinant viruses to filter out which viral factors are involved in MDV integration. The induction of deadly lymphomas can be further investigated *in vivo* which would greatly reduce the number of animals used in animal experiments.

Moreover, the establishment and maintenance of latency, as well as reactivation, are associated with epigenetic modifications. In collaboration with other institutes, our lab provided the first chromatin landscape of integrated HHV-6A. Results revealed that the latent HHV-6A genome lies in highly condensed heterochromatin and is associated with H3K9me and H3K27me3 histone modifications. Surprisingly, the viral genome was completely transcriptionally silent and even viral associated transcripts and miRNAs could not be detected (Saviola et al., 2019). These findings suggest that histone modifications and chromatin condensation can play an important role in regulation of integrated herpesviruses.

Lastly, *in vitro* and *in vivo* targeted excision of integrated virus is the only way how to permanently remove herpesvirus genome from the host cell. It has been shown that

CRISPR/Cas9 system can efficiently disrupt HIV-1 expression machinery and excise latent proviral DNA from host chromosomes (Ebina et al., 2013). In the context of herpesviruses, our lab showed that combination of multiple gRNAs targeting essential viral genes completely abrogates virus replication *in vitro* (Hagag et al., 2020) and is able to excise HHV-6A from majority of cells harboring integrated virus (data not published).

5   Summary

Marek's disease virus genome replication, telomere integration, and live-cell visualization

Herpesviruses maintain their genome lifelong in its host by establishing a latent phase of infection. Marek's disease virus (MDV) is a chicken herpesvirus causing fatal lymphomas and the vaccination against MD is considered to be the first example for vaccination against an agent causing cancer. MDV, as well as some other herpesviruses, achieves latency by incorporating its genome into host telomeres. However, many steps and factors involved in genome integration and reactivation process remain unclear. Our current knowledge about herpesvirus integration is mainly based on results from animal experiments and fluorescence *in situ* hybridization (FISH). However, FISH cannot be used for a real-time detection of integrated MDV. In this thesis, I established a visualization system utilizing the tetracycline operator/repressor (*tetO*/TetR) system to optically detect and track MDV genomes without any other additional staining in living cells during different stages of infection.

MDV genome consists of two unique regions both flanked by two inverted repeat regions. Genes found in repeat regions are present twice in the genome, several of which are involved in MDV pathogenesis, tumorigenesis, and latency. Therefore, I generated a platform virus lacking the majority of internal repeats (ΔIR_{LS-HR}) to facilitate a straightforward mutation of the virus genome in the repeat region. I demonstrated that such a virus can rapidly restore the deleted repeat region when short terminal sequences are left for homologous recombination. Conversely, viruses unable to restore the internal repeats (ΔIR_{LS}) showed impaired replication and pathogenesis in infected chickens corroborating previous findings in related herpesviruses where deletion of inverted repeat region affected virus pathogenicity.

To generate MDV mutants whose genome can be directly detected by microscopy, the *tetO* sequence was inserted into the ΔIR_{LS-HR} backbone. Fluorescently labeled TetR proteins that specifically bind to *tetO* sequence were expressed either from cells or from the virus itself. Using this visualization technique, replicating virus genomes, genesis and mobility of viral replication compartments and latent virus were detected. Moreover, these viruses also express another fluorescent protein with a different color for unambiguous identification of infected cells during the lytic stage of virus infection. The combination of both fluorescent proteins revealed not only that MDV can induce syncytia in primary chicken embryo cells, but also that the virus does not replicate in all nuclei of a syncytium. Taken together, ΔIR_{LS-HR} serves as an excellent platform to generate recombinant viruses and in combination with

tetO/TetR system we established a powerful tool to visualize virus genomes and to trace the impact of different mutations or gene deletions on the behavior of MDV during lytic replication, latency, and reactivation.

6 Zusammenfassung

Marek's Disease Virus Genomreplikation, Telomer-Integration und Genomvisualisierung in lebenden Zellen

Herpesviren bewahren ihr Genom lebenslang in ihrem Wirt, indem sie während der Infektion eine latente Phase etablieren. Das Alphaherpesvirus der Marek'schen Krankheit (*Marek's disease virus*, MDV) ist ein weitverbreitetes Hühnerherpesvirus, welches tödliche Lymphome verursacht. Die Impfung gegen die Marek'sche Krankheit gilt als erstes Beispiel für eine Impfung gegen einen Krebserreger. MDV, wie auch einige andere Herpesviren, erreicht seine Latenz, indem es sein Genom in die Wirts-Telomere einbaut. Viele Schritte und Faktoren, die bei der Genomintegration und Reaktivierung eine Rolle spielen, sind jedoch noch ungeklärt. Unser derzeitiges Wissen über die Integration von Herpesviren basiert hauptsächlich auf Ergebnissen aus Tierversuchen und der Fluoreszenz-*in-situ*-Hybridisierung (FISH). FISH kann jedoch nicht als Echtzeit-Nachweis eines integrierten MDV verwendet werden. In dieser Arbeit wurde ein Visualisierungssystem unter Verwendung des Tetracyclin-Operator/Repressor-Systems (*tetO*/TetR) entwickelt. Mit dem System lassen sich MDV-Genome in lebenden Zellen während der verschiedenen Infektionsstadien optisch nachweisen und verfolgen, ohne dass eine zusätzliche Färbung erforderlich ist.

Das MDV-Genom besteht aus zwei einzigartigen Regionen, die beide von zwei invertierten Repeat-Regionen umrandet werden. Der Aufbau der Repeat-Regionen ist zweifach ausgeführt. Die Genomgruppe enthält mehrere Gene welche an der Pathogenese, Tumorgenese und Latenz von MDV beteiligt sind. Daher wurde ein Plattformvirus entwickelt, dem der Großteil der internen Repeats fehlt (ΔIR_{LS-HR}), um eine unkomplizierte Mutation des Virusgenoms in der Repeat-Region zu ermöglichen. Es konnte nachgewiesen werden, dass ein solches Virus die gelöschte Repeat-Region schnell wiederherstellen kann, wenn kurze terminale Sequenzen für die homologe Rekombination übrigbleiben. Umgekehrt zeigte ein Virus, das nicht in der Lage war, die internen Repeats wiederherzustellen (ΔIR_{LS}), eine beeinträchtigte Virusreplikation und Pathogenese in infizierten Hühnern. Dies stimmt mit früheren Ergebnissen zu verwandten Herpesviren, bei denen die Deletion der invertierten Repeat-Region die Pathogenität des Virus beeinträchtigte, überein.

Um MDV Mutanten zu erzeugen, deren Genome direkt unter dem Mikroskop nachgewiesen werden können, wurde die *tetO*-Sequenz in das ΔIR_{LS-HR} eingefügt. Fluoreszenzmarkierte TetR-Proteine, die spezifisch an die *tetO*-Sequenz binden, werden dadurch entweder von Zellen oder von dem Virus eigenständig produziert. Mit dieser Visualisierungstechnik konnten

replizierende Virusgenome, die Entstehung und Mobilität von viralen Replikationskompartimenten und latente Viren nachgewiesen werden. Darüber hinaus produzieren diese Viren während des lytischen Infektionsstadiums noch ein weiteres fluoreszierendes Protein von unterschiedlicher Farbe zur eindeutigen Identifizierung der infizierten Zellen. Die Kombination beider fluoreszierender Proteine zeigte nicht nur, dass MDV Synzytien in primären Hühnerembryozellen induzieren kann, sondern auch, dass das Virus nicht in allen Kernen eines Synzytiums repliziert. Alles in Allem dient ΔIR_{LS-HR} als hervorragendes Werkzeug zur Erzeugung rekombinanter Viren, und in Kombination mit dem *tetO*/TetR-System konnte eine leistungsfähige Herangehensweise zur Visualisierung von Virusgenomen und zur Verfolgung der Auswirkungen verschiedener Mutationen oder Gendeletionen auf das Verhalten von MDV während der lytischen Replikation, Latenz und Reaktivierung geschaffen werden.

7 References

Ahn, B., Zhang, Y., Osterrieder, N., and O'Callaghan, D.J. (2011). Properties of an equine herpesvirus 1 mutant devoid of the internal inverted repeat sequence of the genomic short region. Virology *410*, 327-335. 10.1016/j.virol.2010.11.020.

Akiyama, Y., and Kato, S. (1974). Two cell lines from lymphomas of Marek's disease. Biken J *17*, 105-116.

Arbuckle, J.H., Medveczky, M.M., Luka, J., Hadley, S.H., Luegmayr, A., Ablashi, D., Lund, T.C., Tolar, J., De Meirleir, K., Montoya, J.G., et al. (2010). The latent human herpesvirus-6A genome specifically integrates in telomeres of human chromosomes in vivo and in vitro. Proc Natl Acad Sci U S A *107*, 5563-5568. 10.1073/pnas.0913586107.

Arnaudeau, C., Helleday, T., and Jenssen, D. (1999). The RAD51 protein supports homologous recombination by an exchange mechanism in mammalian cells. J Mol Biol *289*, 1231-1238. 10.1006/jmbi.1999.2856.

Baaten, B.J., Staines, K.A., Smith, L.P., Skinner, H., Davison, T.F., and Butter, C. (2009). Early replication in pulmonary B cells after infection with Marek's disease herpesvirus by the respiratory route. Viral Immunol *22*, 431-444. 10.1089/vim.2009.0047.

Balasubramanian, N., Bai, P., Buchek, G., Korza, G., and Weller, S.K. (2010). Physical interaction between the herpes simplex virus type 1 exonuclease, UL12, and the DNA double-strand break-sensing MRN complex. J Virol *84*, 12504-12514. 10.1128/JVI.01506-10.

Barrow, A.D., Burgess, S.C., Baigent, S.J., Howes, K., and Nair, V.K. (2003). Infection of macrophages by a lymphotropic herpesvirus: a new tropism for Marek's disease virus. Journal of General Virology *84*, 2635-2645. 10.1099/vir.0.19206-0.

Bediaga, N.G., Coughlan, H.D., Johanson, T.M., Garnham, A.L., Naselli, G., Schroder, J., Fearnley, L.G., Bandala-Sanchez, E., Allan, R.S., Smyth, G.K., and Harrison, L.C. (2021). Multi-level remodelling of chromatin underlying activation of human T cells. Sci Rep *11*, 528. 10.1038/s41598-020-80165-9.

Berthault, C., Larcher, T., Hartle, S., Vautherot, J.F., Trapp-Fragnet, L., and Denesvre, C. (2018). Atrophy of primary lymphoid organs induced by Marek's disease virus during early infection is associated with increased apoptosis, inhibition of cell proliferation and a severe B-lymphopenia. Vet Res *49*, 31. 10.1186/s13567-018-0526-x.

Bertzbach, L.D., Conradie, A.M., You, Y., and Kaufer, B.B. (2020). Latest Insights into Marek's Disease Virus Pathogenesis and Tumorigenesis. Cancers (Basel) *12*. 10.3390/cancers12030647.

Bertzbach, L.D., Harlin, O., Hartle, S., Fehler, F., Vychodil, T., Kaufer, B.B., and Kaspers, B. (2019a). IFNalpha and IFNgamma Impede Marek's Disease Progression. Viruses *11*. 10.3390/v11121103.

Bertzbach, L.D., Kheimar, A., Ali, F.A.Z., and Kaufer, B.B. (2018). Viral Factors Involved in Marek's Disease Virus (MDV) Pathogenesis. Current Clinical Microbiology Reports *5*, 238-244. 10.1007/s40588-018-0104-z.

Bertzbach, L.D., van Haarlem, D.A., Hartle, S., Kaufer, B.B., and Jansen, C.A. (2019b). Marek's Disease Virus Infection of Natural Killer Cells. Microorganisms *7*. 10.3390/microorganisms7120588.

Boersma, S., Rabouw, H.H., Bruurs, L.J.M., Pavlovic, T., van Vliet, A.L.W., Beumer, J., Clevers, H., van Kuppeveld, F.J.M., and Tanenbaum, M.E. (2020). Translation and Replication Dynamics of Single RNA Viruses. Cell *183*, 1930-1945 e1923. 10.1016/j.cell.2020.10.019.

Brown, J.C., and Newcomb, W.W. (2011). Herpesvirus capsid assembly: insights from structural analysis. Curr Opin Virol *1*, 142-149. 10.1016/j.coviro.2011.06.003.

Burnside, J., Bernberg, E., Anderson, A., Lu, C., Meyers, B.C., Green, P.J., Jain, N., Isaacs, G., and Morgan, R.W. (2006). Marek's disease virus encodes MicroRNAs that map to meq and the latency-associated transcript. J Virol *80*, 8778-8786. 10.1128/JVI.00831-06.

Bystricky, K., Gallardo, F., Lane, D., and Dubarry, N. (2012). Constructs and method for regulating gene expression or for detecting and controlling a DNA locus in eukaryotes. FR patent WO/2012/127047, patent application PCT/EP2012/055258, and granted 2012.

Bystricky, K., Heun, P., Gehlen, L., Langowski, J., and Gasser, S.M. (2004). Long-range compaction and flexibility of interphase chromatin in budding yeast analyzed by high-resolution imaging techniques. Proc Natl Acad Sci U S A *101*, 16495-16500. 10.1073/pnas.0402766101.

Calnek, B.W. (2001). Pathogenesis of Marek's disease virus infection. Curr Top Microbiol Immunol *255*, 25-55. 10.1007/978-3-642-56863-3_2.

Cantello, J.L., Anderson, A.S., and Morgan, R.W. (1994). Identification of latency-associated transcripts that map antisense to the ICP4 homolog gene of Marek's disease virus. J Virol *68*, 6280-6290. 10.1128/JVI.68.10.6280-6290.1994.

Chakraborty, P., Vervelde, L., Dalziel, R.G., Wasson, P.S., Nair, V., Dutia, B.M., and Kaiser, P. (2017). Marek's disease virus infection of phagocytes: a de novo in vitro infection model. J Gen Virol *98*, 1080-1088. 10.1099/jgv.0.000763.

Chan, P.K., Ng, H.K., Hui, M., and Cheng, A.F. (2001). Prevalence and distribution of human herpesvirus 6 variants A and B in adult human brain. J Med Virol *64*, 42-46. 10.1002/jmv.1015.

Chasseur, A.S., Trozzi, G., Istasse, C., Petit, A., Rasschaert, P., Denesvre, C., Kaufer, B.B., Bertzbach, L.D., Muylkens, B., and Coupeau, D. (2022). Marek's Disease Virus Virulence Genes Encode Circular RNAs. J Virol, e0032122. 10.1128/jvi.00321-22.

Chbab, N., Egerer, A., Veiga, I., Jarosinski, K.W., and Osterrieder, N. (2010). Viral control of vTR expression is critical for efficient formation and dissemination of lymphoma induced by Marek's disease virus (MDV). Vet Res *41*, 56. 10.1051/vetres/2010026.

Cohen, E.M., and Kobiler, O. (2016). Gene Expression Correlates with the Number of Herpes Viral Genomes Initiating Infection in Single Cells. PLoS Pathog *12*, e1006082. 10.1371/journal.ppat.1006082.

Cohen, J.I. (2020). Herpesvirus latency. J Clin Invest *130*, 3361-3369. 10.1172/JCI136225.

Coleman, H.M., Connor, V., Cheng, Z.S.C., Grey, F., Preston, C.M., and Efstathiou, S. (2008). Histone modifications associated with herpes simplex virus type 1 genomes during quiescence and following ICP0-mediated de-repression. J Gen Virol *89*, 68-77. 10.1099/vir.0.83272-0.

Conradie, A.M., Bertzbach, L.D., Bhandari, N., Parcells, M., and Kaufer, B.B. (2019). A Common Live-Attenuated Avian Herpesvirus Vaccine Expresses a Very Potent Oncogene. mSphere *4*. 10.1128/mSphere.00658-19.

Conradie, A.M., Bertzbach, L.D., Trimpert, J., Patria, J.N., Murata, S., Parcells, M.S., and Kaufer, B.B. (2020). Distinct polymorphisms in a single herpesvirus gene are capable of enhancing virulence and mediating vaccinal resistance. PLoS Pathog *16*, e1009104. 10.1371/journal.ppat.1009104.

References

Cui, X., Lee, L.F., Reed, W.M., Kung, H.J., and Reddy, S.M. (2004). Marek's disease virus-encoded vIL-8 gene is involved in early cytolytic infection but dispensable for establishment of latency. J Virol *78*, 4753-4760. 10.1128/jvi.78.9.4753-4760.2004.

Cui, X., McGregor, A., Schleiss, M.R., and McVoy, M.A. (2009). The impact of genome length on replication and genome stability of the herpesvirus guinea pig cytomegalovirus. Virology *386*, 132-138. 10.1016/j.virol.2008.12.030.

Cui, Z.Q., Zhang, Z.P., Zhang, X.E., Wen, J.K., Zhou, Y.F., and Xie, W.H. (2005). Visualizing the dynamic behavior of poliovirus plus-strand RNA in living host cells. Nucleic Acids Res *33*, 3245-3252. 10.1093/nar/gki629.

Davison, F., and Nair, V. (2004). Marek's Disease: An Evolving Problem (Elsevier Academic Press).

de Bruyn Kops, A., and Knipe, D.M. (1994). Preexisting nuclear architecture defines the intranuclear location of herpesvirus DNA replication structures. J Virol *68*, 3512-3526. 10.1128/JVI.68.6.3512-3526.1994.

Delecluse, H.J., and Hammerschmidt, W. (1993). Status of Marek's disease virus in established lymphoma cell lines: herpesvirus integration is common. J Virol *67*, 82-92. 10.1128/JVI.67.1.82-92.1993.

Delecluse, H.J., Schüller, S., and Hammerschmidt, W. (1993). Latent Marek's disease virus can be activated from its chromosomally integrated state in herpesvirus-transformed lymphoma cells. EMBO J *12*, 3277-3286.

Delius, H., and Clements, J.B. (1976). A partial denaturation map of herpes simplex virus type 1 DNA: evidence for inversions of the unique DNA regions. J Gen Virol *33*, 125-133. 10.1099/0022-1317-33-1-125.

Dembowski, J.A., and DeLuca, N.A. (2018). Temporal Viral Genome-Protein Interactions Define Distinct Stages of Productive Herpesviral Infection. mBio *9*. 10.1128/mBio.01182-18.

Denesvre, C., Blondeau, C., Lemesle, M., Le Vern, Y., Vautherot, D., Roingeard, P., and Vautherot, J.F. (2007). Morphogenesis of a highly replicative EGFPVP22 recombinant Marek's disease virus in cell culture. J Virol *81*, 12348-12359. 10.1128/JVI.01177-07.

Ebina, H., Misawa, N., Kanemura, Y., and Koyanagi, Y. (2013). Harnessing the CRISPR/Cas9 system to disrupt latent HIV-1 provirus. Sci Rep *3*, 2510. 10.1038/srep02510.

Engel, A.T., Selvaraj, R.K., Kamil, J.P., Osterrieder, N., and Kaufer, B.B. (2012). Marek's disease viral interleukin-8 promotes lymphoma formation through targeted recruitment of B cells and CD4+ CD25+ T cells. J Virol *86*, 8536-8545. 10.1128/JVI.00556-12.

Epstein, A.L. (2005). HSV-1-based amplicon vectors: design and applications. Gene Ther *12 Suppl 1*, S154-158. 10.1038/sj.gt.3302617.

Fakhrul Islam, A.F., Walkden-Brown, S.W., Groves, P.J., and Underwood, G.J. (2008). Kinetics of Marek's disease virus (MDV) infection in broiler chickens 1: effect of varying vaccination to challenge interval on vaccinal protection and load of MDV and herpesvirus of turkey in the spleen and feather dander over time. Avian Pathol *37*, 225-235. 10.1080/03079450701802230.

FAO (2021a). FAOSTAT - free access to food and agriculture data. http://www.fao.org/faostat/en/#compare. (Accessed on 16 June 2021)

FAO (2021b). Meat market review: Overview of global meat market developments in 2020. March 2021. http://www.fao.org/3/cb3700en/cb3700en.pdf. (Accessed on 16 June 2021)

Fields, B.N., Knipe, D.M., and Howley, P.M. (2007). Fields Virology, 5th Edition (Wolters Kluwer Health).

Flint, S.J., Racaniello, V.R., Rall, G.F., Skalka, A.M., and Enquist, L.W. (2015). Principles of Virology, 4th Edition (American Society for Microbiology). 10.1128/9781555818951.

Fraefel, C., Bittermann, A.G., Büeler, H., Heid, I., Bächi, T., and Ackermann, M. (2004). Spatial and Temporal Organization of Adeno-Associated Virus DNA Replication in Live Cells. Journal of Virology *78*, 389-398. 10.1128/jvi.78.1.389-398.2004.

Full, F., and Ensser, A. (2019). Early Nuclear Events after Herpesviral Infection. J Clin Med *8*. 10.3390/jcm8091408.

Gallardo, F., Schmitt, D., Brandely, R., Brua, C., Silvestre, N., Findeli, A., Foloppe, J., Top, S., Kappler-Gratias, S., Quentin-Froignant, C., et al. (2020). Fluorescent Tagged Vaccinia Virus Genome Allows Rapid and Efficient Measurement of Oncolytic Potential and Discovery of Oncolytic Modulators. Biomedicines *8*. 10.3390/biomedicines8120543.

Gilbert-Girard, S., Gravel, A., Collin, V., Wight, D.J., Kaufer, B.B., Lazzerini-Denchi, E., and Flamand, L. (2020). Role for the shelterin protein TRF2 in human herpesvirus 6A/B chromosomal integration. PLoS Pathog *16*, e1008496. 10.1371/journal.ppat.1008496.

Glauser, D.L., Strasser, R., Laimbacher, A.S., Saydam, O., Clement, N., Linden, R.M., Ackermann, M., and Fraefel, C. (2007). Live covisualization of competing adeno-associated virus and herpes simplex virus type 1 DNA replication: molecular mechanisms of interaction. J Virol *81*, 4732-4743. 10.1128/JVI.02476-06.

Gonzalez-Serricchio, A.S., and Sternberg, P.W. (2006). Visualization of C. elegans transgenic arrays by GFP. BMC Genet *7*, 36. 10.1186/1471-2156-7-36.

Gossen, M., and Bujard, H. (1992). Tight control of gene expression in mammalian cells by tetracycline-responsive promoters. Proc Natl Acad Sci U S A *89*, 5547-5551. 10.1073/pnas.89.12.5547.

Gravel, A., Dubuc, I., Wallaschek, N., Gilbert-Girard, S., Collin, V., Hall-Sedlak, R., Jerome, K.R., Mori, Y., Carbonneau, J., Boivin, G., et al. (2017). Cell Culture Systems To Study Human Herpesvirus 6A/B Chromosomal Integration. J Virol *91*. 10.1128/JVI.00437-17.

Greco, A., Fester, N., Engel, A.T., and Kaufer, B.B. (2014). Role of the short telomeric repeat region in Marek's disease virus replication, genomic integration, and lymphomagenesis. J Virol *88*, 14138-14147. 10.1128/JVI.02437-14.

Grunewald, K., Desai, P., Winkler, D.C., Heymann, J.B., Belnap, D.M., Baumeister, W., and Steven, A.C. (2003). Three-dimensional structure of herpes simplex virus from cryo-electron tomography. Science *302*, 1396-1398. 10.1126/science.1090284.

Haertle, S., Alzuheir, I., Busalt, F., Waters, V., Kaiser, P., and Kaufer, B.B. (2017). Identification of the Receptor and Cellular Ortholog of the Marek's Disease Virus (MDV) CXC Chemokine. Front Microbiol *8*, 2543. 10.3389/fmicb.2017.02543.

Hagag, I.T., Wight, D.J., Bartsch, D., Sid, H., Jordan, I., Bertzbach, L.D., Schusser, B., and Kaufer, B.B. (2020). Abrogation of Marek's disease virus replication using CRISPR/Cas9. Sci Rep *10*, 10919. 10.1038/s41598-020-67951-1.

Haq, K., Schat, K.A., and Sharif, S. (2013). Immunity to Marek's disease: where are we now? Dev Comp Immunol *41*, 439-446. 10.1016/j.dci.2013.04.001.

Harmache, A. (2014). A virulent bioluminescent and fluorescent dual-reporter Marek's disease virus unveils an alternative spreading pathway in addition to cell-to-cell contact. J Virol *88*, 11617-11623. 10.1128/JVI.01482-14.

Heidari, M., Huebner, M., Kireev, D., and Silva, R.F. (2008). Transcriptional profiling of Marek's disease virus genes during cytolytic and latent infection. Virus Genes *36*, 383-392. 10.1007/s11262-008-0203-7.

Hinsberger, A., Graillot, B., Blachere Lopez, C., Juliant, S., Cerutti, M., King, L.A., Possee, R.D., Gallardo, F., and Lopez Ferber, M. (2020). Tracing Baculovirus AcMNPV Infection Using a Real-Time Method Based on ANCHOR(TM) DNA Labeling Technology. Viruses *12*. 10.3390/v12010050.

ICTV Reports (2021). Virus Taxonomy: 2021 Release https://talk.ictvonline.org/ictv-reports/ictv_9th_report/dsdna-viruses-2011/w/dsdna_viruses/89/herpesvirales. (Accessed on 11 June 2021)

Imakawa, K., Nakagawa, S., and Miyazawa, T. (2015). Baton pass hypothesis: successive incorporation of unconserved endogenous retroviral genes for placentation during mammalian evolution. Genes Cells *20*, 771-788. 10.1111/gtc.12278.

Jarosinski, K.W., Donovan, K.M., and Du, G. (2015). Expression of fluorescent proteins within the repeat long region of the Marek's disease virus genome allows direct identification of infected cells while retaining full pathogenicity. Virus Res *201*, 50-60. 10.1016/j.virusres.2015.02.012.

Jarosinski, K.W., Jia, W., Sekellick, M.J., Marcus, P.I., and Schat, K.A. (2001). Cellular responses in chickens treated with IFN-alpha orally or inoculated with recombinant Marek's disease virus expressing IFN-alpha. J Interferon Cytokine Res *21*, 287-296. 10.1089/107999001300177475.

Jarosinski, K.W., and Schat, K.A. (2007). Multiple alternative splicing to exons II and III of viral interleukin-8 (vIL-8) in the Marek's disease virus genome: the importance of vIL-8 exon I. Virus Genes *34*, 9-22. 10.1007/s11262-006-0004-9.

Jarosinski, K.W., Tischer, B.K., Trapp, S., and Osterrieder, N. (2006). Marek's disease virus: lytic replication, oncogenesis and control. Expert Rev Vaccines *5*, 761-772. 10.1586/14760584.5.6.761.

Jenkins, F.J., Donoghue, A.M., and Martin, J.R. (1996). Deletion of the Herpes simplex 1 internal repeat sequences affects pathogenicity in the mouse. Front Biosci *1*, a59-68. 10.2741/a106.

Kaufer, B.B., Jarosinski, K.W., and Osterrieder, N. (2011). Herpesvirus telomeric repeats facilitate genomic integration into host telomeres and mobilization of viral DNA during reactivation. J Exp Med *208*, 605-615. 10.1084/jem.20101402.

Kaufer, B.B., Trapp, S., Jarosinski, K.W., and Osterrieder, N. (2010). Herpesvirus telomerase RNA(vTR)-dependent lymphoma formation does not require interaction of vTR with telomerase reverse transcriptase (TERT). PLoS Pathog *6*, e1001073. 10.1371/journal.ppat.1001073.

Kennedy, P.G., Rovnak, J., Badani, H., and Cohrs, R.J. (2015). A comparison of herpes simplex virus type 1 and varicella-zoster virus latency and reactivation. J Gen Virol *96*, 1581-1602. 10.1099/vir.0.000128.

Kieser, Q., Paszkowski, P., Lin, J., Evans, D., and Noyce, R. (2019). Visualizing Poxvirus Replication and Recombination Using Live-Cell Imaging. Methods Mol Biol *2023*, 221-235. 10.1007/978-1-4939-9593-6_14.

Kim, J.H., Lee, S.R., Li, L.H., Park, H.J., Park, J.H., Lee, K.Y., Kim, M.K., Shin, B.A., and Choi, S.Y. (2011). High cleavage efficiency of a 2A peptide derived from porcine teschovirus-1 in human cell lines, zebrafish and mice. PLoS One *6*, e18556. 10.1371/journal.pone.0018556.

Kobiler, O., and Weitzman, M.D. (2019). Herpes simplex virus replication compartments: From naked release to recombining together. PLoS Pathog *15*, e1007714. 10.1371/journal.ppat.1007714.

Komatsu, T., Quentin-Froignant, C., Carlon-Andres, I., Lagadec, F., Rayne, F., Ragues, J., Kehlenbach, R.H., Zhang, W., Ehrhardt, A., Bystricky, K., et al. (2018). In Vivo Labelling of Adenovirus DNA Identifies Chromatin Anchoring and Biphasic Genome Replication. J Virol *92*. 10.1128/JVI.00795-18.

Lander, E.S., Linton, L.M., Birren, B., Nusbaum, C., Zody, M.C., Baldwin, J., Devon, K., Dewar, K., Doyle, M., FitzHugh, W., et al. (2001). Initial sequencing and analysis of the human genome. Nature *409*, 860-921. 10.1038/35057062.

Lee, L.F., Wu, P., Sui, D., Ren, D., Kamil, J., Kung, H.J., and Witter, R.L. (2000). The complete unique long sequence and the overall genomic organization of the GA strain of Marek's disease virus. Proc Natl Acad Sci U S A *97*, 6091-6096. 10.1073/pnas.97.11.6091.

Levy, J.A., Ferro, F., Greenspan, D., and Lennette, E.T. (1990). Frequent isolation of HHV-6 from saliva and high seroprevalence of the virus in the population. The Lancet *335*, 1047-1050. 10.1016/0140-6736(90)92628-u.

Li, X., and Heyer, W.D. (2008). Homologous recombination in DNA repair and DNA damage tolerance. Cell Res *18*, 99-113. 10.1038/cr.2008.1.

Li, Z., Pang, J., Dong, L., and Yu, X. (2021). Structural basis for genome packaging, retention, and ejection in human cytomegalovirus. Nat Commun *12*, 4538. 10.1038/s41467-021-24820-3.

Liao, Y., Lupiani, B., Izumiya, Y., and Reddy, S.M. (2021). Marek's disease virus Meq oncoprotein interacts with chicken HDAC 1 and 2 and mediates their degradation via proteasome dependent pathway. Sci Rep *11*, 637. 10.1038/s41598-020-80792-2.

Lisby, M., Mortensen, U.H., and Rothstein, R. (2003). Colocalization of multiple DNA double-strand breaks at a single Rad52 repair centre. Nat Cell Biol *5*, 572-577. 10.1038/ncb997.

Liu, F., and Zhou, Z.H. (2007). Comparative virion structures of human herpesviruses. In Human Herpesviruses: Biology, Therapy, and Immunoprophylaxis, (Cambridge University Press).

Liu, Y.T., Jih, J., Dai, X., Bi, G.Q., and Zhou, Z.H. (2019). Cryo-EM structures of herpes simplex virus type 1 portal vertex and packaged genome. Nature *570*, 257-261. 10.1038/s41586-019-1248-6.

Luo, J., Mitra, A., Tian, F., Chang, S., Zhang, H., Cui, K., Yu, Y., Zhao, K., and Song, J. (2012). Histone methylation analysis and pathway predictions in chickens after MDV infection. PLoS One *7*, e41849. 10.1371/journal.pone.0041849.

Luo, X., Xue, B., Feng, G., Zhang, J., Lin, B., Zeng, P., Li, H., Yi, H., Zhang, X.L., Zhu, H., and Nie, Z. (2019). Lighting up the Native Viral RNA Genome with a Fluorogenic Probe for the Live-Cell Visualization of Virus Infection. J Am Chem Soc *141*, 5182-5191. 10.1021/jacs.8b10265.

Lupiani, B., Lee, L.F., Cui, X., Gimeno, I., Anderson, A., Morgan, R.W., Silva, R.F., Witter, R.L., Kung, H.J., and Reddy, S.M. (2004). Marek's disease virus-encoded Meq gene is involved in transformation of lymphocytes but is dispensable for replication. Proc Natl Acad Sci U S A *101*, 11815-11820. 10.1073/pnas.0404508101.

References

Ma, H., Naseri, A., Reyes-Gutierrez, P., Wolfe, S.A., Zhang, S., and Pederson, T. (2015). Multicolor CRISPR labeling of chromosomal loci in human cells. Proc Natl Acad Sci U S A *112*, 3002-3007. 10.1073/pnas.1420024112.

Ma, Y., Mao, G., Huang, W., Wu, G., Yin, W., Ji, X., Deng, Z., Cai, Z., Zhang, X.E., He, Z., and Cui, Z. (2019). Quantum Dot Nanobeacons for Single RNA Labeling and Imaging. J Am Chem Soc *141*, 13454-13458. 10.1021/jacs.9b04659.

Makhov, A.M., and Griffith, J.D. (2006). Visualization of the annealing of complementary single-stranded DNA catalyzed by the herpes simplex virus type 1 ICP8 SSB/recombinase. J Mol Biol *355*, 911-922. 10.1016/j.jmb.2005.11.022.

Mao, Z., Seluanov, A., Jiang, Y., and Gorbunova, V. (2007). TRF2 is required for repair of nontelomeric DNA double-strand breaks by homologous recombination. Proc Natl Acad Sci U S A *104*, 13068-13073. 10.1073/pnas.0702410104.

Mariame, B., Kappler-Gratias, S., Kappler, M., Balor, S., Gallardo, F., and Bystricky, K. (2018). Real-time visualization and quantification of human Cytomegalovirus replication in living cells using the ANCHOR DNA labeling technology. J Virol. 10.1128/JVI.00571-18.

McPherson, M.C., Cheng, H.H., and Delany, M.E. (2016). Marek's disease herpesvirus vaccines integrate into chicken host chromosomes yet lack a virus-host phenotype associated with oncogenic transformation. Vaccine *34*, 5554-5561. 10.1016/j.vaccine.2016.09.051.

McSwiggen, D.T., Hansen, A.S., Teves, S.S., Marie-Nelly, H., Hao, Y., Heckert, A.B., Umemoto, K.K., Dugast-Darzacq, C., Tjian, R., and Darzacq, X. (2019). Evidence for DNA-mediated nuclear compartmentalization distinct from phase separation. Elife *8*. 10.7554/eLife.47098.

McVoy, M.A., and Ramnarain, D. (2000). Machinery to support genome segment inversion exists in a herpesvirus which does not naturally contain invertible elements. J Virol *74*, 4882-4887. 10.1128/jvi.74.10.4882-4887.2000.

Mi, S., Lee, X., Li, X., Veldman, G.M., Finnerty, H., Racie, L., LaVallie, E., Tang, X.Y., Edouard, P., Howes, S., et al. (2000). Syncytin is a captive retroviral envelope protein involved in human placental morphogenesis. Nature *403*, 785-789. 10.1038/35001608.

Michaelis, C., Ciosk, R., and Nasmyth, K. (1997). Cohesins: Chromosomal Proteins that Prevent Premature Separation of Sister Chromatids. Cell *91*, 35-45. 10.1016/s0092-8674(01)80007-6.

Mitra, A., Luo, J., He, Y., Gu, Y., Zhang, H., Zhao, K., Cui, K., and Song, J. (2015). Histone modifications induced by MDV infection at early cytolytic and latency phases. BMC Genomics *16*, 311. 10.1186/s12864-015-1492-6.

Mody, P.H., Pathak, S., Hanson, L.K., and Spencer, J.V. (2020). Herpes Simplex Virus: A Versatile Tool for Insights Into Evolution, Gene Delivery, and Tumor Immunotherapy. Virology (Auckl) *11*, 1178122X20913274. 10.1177/1178122X20913274.

Mok, H., and Yakimovich, A. (2019). Click Chemistry-Based Labeling of Poxvirus Genomes. Methods Mol Biol *2023*, 209-220. 10.1007/978-1-4939-9593-6_13.

Mukherjee, A.K., Sharma, S., Sengupta, S., Saha, D., Kumar, P., Hussain, T., Srivastava, V., Roy, S.D., Shay, J.W., and Chowdhury, S. (2018). Telomere length-dependent transcription and epigenetic modifications in promoters remote from telomere ends. PLoS Genet *14*, e1007782. 10.1371/journal.pgen.1007782.

Muller, T.G., Sakin, V., and Muller, B. (2019). A Spotlight on Viruses-Application of Click Chemistry to Visualize Virus-Cell Interactions. Molecules *24*. 10.3390/molecules24030481.

Mwangi, W.N., Smith, L.P., Baigent, S.J., Beal, R.K., Nair, V., and Smith, A.L. (2011). Clonal structure of rapid-onset MDV-driven CD4+ lymphomas and responding CD8+ T cells. PLoS Pathog *7*, e1001337. 10.1371/journal.ppat.1001337.

Nicoll, M.P., Hann, W., Shivkumar, M., Harman, L.E., Connor, V., Coleman, H.M., Proenca, J.T., and Efstathiou, S. (2016). The HSV-1 Latency-Associated Transcript Functions to Repress Latent Phase Lytic Gene Expression and Suppress Virus Reactivation from Latently Infected Neurons. PLoS Pathog *12*, e1005539. 10.1371/journal.ppat.1005539.

Nilaratanakul, V., Hauer, D.A., and Griffin, D.E. (2017). Development and characterization of Sindbis virus with encoded fluorescent RNA aptamer Spinach2 for imaging of replication and immune-mediated changes in intracellular viral RNA. J Gen Virol *98*, 992-1003. 10.1099/jgv.0.000755.

Nilaratanakul, V., Hauer, D.A., and Griffin, D.E. (2020). Development of encoded Broccoli RNA aptamers for live cell imaging of alphavirus genomic and subgenomic RNAs. Sci Rep *10*, 5233. 10.1038/s41598-020-61573-3.

Nogueira, A., Fernandes, M., Catarino, R., and Medeiros, R. (2019). RAD52 Functions in Homologous Recombination and Its Importance on Genomic Integrity Maintenance and Cancer Therapy. Cancers (Basel) *11*. 10.3390/cancers11111622.

Oh, J., and Fraser, N.W. (2008). Temporal association of the herpes simplex virus genome with histone proteins during a lytic infection. J Virol *82*, 3530-3537. 10.1128/JVI.00586-07.

Orth, P., Cordes, F., Schnappinger, D., Hillen, W., Saenger, W., and Hinrichs, W. (1998). Conformational changes of the Tet repressor induced by tetracycline trapping. J Mol Biol *279*, 439-447. 10.1006/jmbi.1998.1775.

Osterrieder, N., Kamil, J.P., Schumacher, D., Tischer, B.K., and Trapp, S. (2006). Marek's disease virus: from miasma to model. Nat Rev Microbiol *4*, 283-294. 10.1038/nrmicro1382.

Oxford, K.L., Eberhardt, M.K., Yang, K.W., Strelow, L., Kelly, S., Zhou, S.S., and Barry, P.A. (2008). Protein coding content of the UL)b' region of wild-type rhesus cytomegalovirus. Virology *373*, 181-188. 10.1016/j.virol.2007.10.040.

Padhi, A., and Parcells, M.S. (2016). Positive Selection Drives Rapid Evolution of the meq Oncogene of Marek's Disease Virus. PLoS One *11*, e0162180. 10.1371/journal.pone.0162180.

Parcells, M.S., Lin, S.F., Dienglewicz, R.L., Majerciak, V., Robinson, D.R., Chen, H.C., Wu, Z., Dubyak, G.R., Brunovskis, P., Hunt, H.D., et al. (2001). Marek's disease virus (MDV) encodes an interleukin-8 homolog (vIL-8): characterization of the vIL-8 protein and a vIL-8 deletion mutant MDV. J Virol *75*, 5159-5173. 10.1128/JVI.75.11.5159-5173.2001.

Perez-Losada, M., Arenas, M., Galan, J.C., Palero, F., and Gonzalez-Candelas, F. (2015). Recombination in viruses: mechanisms, methods of study, and evolutionary consequences. Infect Genet Evol *30*, 296-307. 10.1016/j.meegid.2014.12.022.

Previdelli, R.L., Bertzbach, L.D., Wight, D.J., Vychodil, T., You, Y., Arndt, S., and Kaufer, B.B. (2019). The Role of Marek's Disease Virus UL12 and UL29 in DNA Recombination and the Virus Lifecycle. Viruses *11*. 10.3390/v11020111.

Prichard, M.N., Penfold, M.E., Duke, G.M., Spaete, R.R., and Kemble, G.W. (2001). A review of genetic differences between limited and extensively passaged human cytomegalovirus strains. Rev Med Virol *11*, 191-200. 10.1002/rmv.315.

Prusty, B.K., Gulve, N., Rasa, S., Murovska, M., Hernandez, P.C., and Ablashi, D.V. (2017). Possible chromosomal and germline integration of human herpesvirus 7. J Gen Virol *98*, 266-274. 10.1099/jgv.0.000692.

Quentin-Froignant, C., Kappler-Gratias, S., Top, S., Bertagnoli, S., and Gallardo, F. (2021). ANCHOR-tagged equine herpesvirus 1: A new tool for monitoring viral infection and discovering new antiviral compounds. J Virol Methods *294*, 114194. 10.1016/j.jviromet.2021.114194.

Robinett, C.C., Straight, A., Li, G., Willhelm, C., Sudlow, G., Murray, A., and Belmont, A.S. (1996). In vivo localization of DNA sequences and visualization of large-scale chromatin organization using lac operator/repressor recognition. J Cell Biol *135*, 1685-1700. 10.1083/jcb.135.6.1685.

Robinson, C.M., Cheng, H.H., and Delany, M.E. (2014). Temporal kinetics of Marek's disease herpesvirus: integration occurs early after infection in both B and T cells. Cytogenet Genome Res *144*, 142-154. 10.1159/000368379.

Robinson, C.M., Hunt, H.D., Cheng, H.H., and Delany, M.E. (2010). Chromosomal integration of an avian oncogenic herpesvirus reveals telomeric preferences and evidence for lymphoma clonality. Herpesviridae *1*, 5. 10.1186/2042-4280-1-5.

Roukos, V., Burgess, R.C., and Misteli, T. (2014). Generation of cell-based systems to visualize chromosome damage and translocations in living cells. Nat Protoc *9*, 2476-2492. 10.1038/nprot.2014.167.

Roukos, V., Voss, T.C., Schmidt, C.K., Lee, S., Wangsa, D., and Misteli, T. (2013). Spatial dynamics of chromosome translocations in living cells. Science *341*, 660-664. 10.1126/science.1237150.

Sachs, A.B., Sarnow, P., and Hentze, M.W. (1997). Starting at the Beginning, Middle, and End: Translation Initiation in Eukaryotes. Cell *89*, 831-838. 10.1016/s0092-8674(00)80268-8.

Sadigh, Y., Powers, C., Spiro, S., Pedrera, M., Broadbent, A., and Nair, V. (2018). Gallid herpesvirus 3 SB-1 strain as a recombinant viral vector for poultry vaccination. NPJ Vaccines *3*, 21. 10.1038/s41541-018-0056-6.

Santangelo, P., Nitin, N., LaConte, L., Woolums, A., and Bao, G. (2006). Live-cell characterization and analysis of a clinical isolate of bovine respiratory syncytial virus, using molecular beacons. J Virol *80*, 682-688. 10.1128/JVI.80.2.682-688.2006.

Sauer, A., Wang, J.B., Hahn, G., and McVoy, M.A. (2010). A human cytomegalovirus deleted of internal repeats replicates with near wild type efficiency but fails to undergo genome isomerization. Virology *401*, 90-95. 10.1016/j.virol.2010.02.016.

Saviola, A.J., Zimmermann, C., Mariani, M.P., Signorelli, S.A., Gerrard, D.L., Boyd, J.R., Wight, D.J., Morissette, G., Gravel, A., Dubuc, I., et al. (2019). Chromatin Profiles of Chromosomally Integrated Human Herpesvirus-6A. Front Microbiol *10*, 1408. 10.3389/fmicb.2019.01408.

Schat, K.A., Piepenbrink, M.S., Buckles, E.L., Schukken, Y.H., and Jarosinski, K.W. (2013). Importance of differential expression of Marek's disease virus gene pp38 for the pathogenesis of Marek's disease. Avian Dis *57*, 503-508. 10.1637/10414-100612-Reg.1.

Schumacher, A.J., Mohni, K.N., Kan, Y., Hendrickson, E.A., Stark, J.M., and Weller, S.K. (2012). The HSV-1 exonuclease, UL12, stimulates recombination by a single strand annealing mechanism. PLoS Pathog *8*, e1002862. 10.1371/journal.ppat.1002862.

Sekine, E., Schmidt, N., Gaboriau, D., and O'Hare, P. (2017). Spatiotemporal dynamics of HSV genome nuclear entry and compaction state transitions using bioorthogonal chemistry and super-resolution microscopy. PLoS Pathog *13*, e1006721. 10.1371/journal.ppat.1006721.

Severini, A., Scraba, D.G., and Tyrrell, D.L. (1996). Branched structures in the intracellular DNA of herpes simplex virus type 1. J Virol *70*, 3169-3175. 10.1128/JVI.70.5.3169-3175.1996.

Seyffert, M., Georgi, F., Tobler, K., Bourqui, L., Anfossi, M., Michaelsen, K., Vogt, B., Greber, U.F., and Fraefel, C. (2021). The HSV-1 Transcription Factor ICP4 Confers Liquid-Like Properties to Viral Replication Compartments. Int J Mol Sci *22*. 10.3390/ijms22094447.

Shao, S., Chang, L., Sun, Y., Hou, Y., Fan, X., and Sun, Y. (2018). Multiplexed sgRNA Expression Allows Versatile Single Nonrepetitive DNA Labeling and Endogenous Gene Regulation. ACS Synth Biol *7*, 176-186. 10.1021/acssynbio.7b00268.

Sikorski, R.S., and Hieter, P. (1989). A system of shuttle vectors and yeast host strains designed for efficient manipulation of DNA in Saccharomyces cerevisiae. Genetics *122*, 19-27.

Smiley, J.R., Fong, B.S., and Leung, W.-C. (1981). Construction of a double-jointed herpes simplex viral DNA molecule: Inverted repeats are required for segment inversion, and direct repeats promote deletions. Virology *113*, 345-362. 10.1016/0042-6822(81)90161-6.

Song, S., and Johnson, F.B. (2018). Epigenetic Mechanisms Impacting Aging: A Focus on Histone Levels and Telomeres. Genes (Basel) *9*. 10.3390/genes9040201.

Sourvinos, G., and Everett, R.D. (2002). Visualization of parental HSV-1 genomes and replication compartments in association with ND10 in live infected cells. EMBO J *21*, 4989-4997. 10.1093/emboj/cdf458.

Spaete, R., and Frenkel, N. (1982). The herpes simplex virus amplicon: A new eucaryotic defective-virus cloning-amplifying vector. Cell *30*, 295-304. 10.1016/0092-8674(82)90035-6.

Straight, A.F., Belmont, A.S., Robinett, C.C., and Murray, A.W. (1996). GFP tagging of budding yeast chromosomes reveals that protein–protein interactions can mediate sister chromatid cohesion. Current Biology *6*, 1599-1608. 10.1016/s0960-9822(02)70783-5.

Strassheim, S., Stik, G., Rasschaert, D., and Laurent, S. (2012). mdv1-miR-M7-5p, located in the newly identified first intron of the latency-associated transcript of Marek's disease virus, targets the immediate-early genes ICP4 and ICP27. J Gen Virol *93*, 1731-1742. 10.1099/vir.0.043109-0.

Strukov, Y.G., and Belmont, A.S. (2008). Development of Mammalian Cell Lines with lac Operator-Tagged Chromosomes. CSH Protoc *2008*, pdb prot4903. 10.1101/pdb.prot4903.

Subramaniam, S., Johnston, J., Preeyanon, L., Brown, C.T., Kung, H.J., and Cheng, H.H. (2013). Integrated analyses of genome-wide DNA occupancy and expression profiling identify key genes and pathways involved in cellular transformation by a Marek's disease virus oncoprotein, Meq. J Virol *87*, 9016-9029. 10.1128/JVI.01163-13.

Tanenbaum, M.E., Gilbert, L.A., Qi, L.S., Weissman, J.S., and Vale, R.D. (2014). A protein-tagging system for signal amplification in gene expression and fluorescence imaging. Cell *159*, 635-646. 10.1016/j.cell.2014.09.039.

Taylor, T.J., McNamee, E.E., Day, C., and Knipe, D.M. (2003). Herpes simplex virus replication compartments can form by coalescence of smaller compartments. Virology *309*, 232-247. 10.1016/s0042-6822(03)00107-7.

Tischer, B.K., Smith, G.A., and Osterrieder, N. (2010). En passant mutagenesis: a two step markerless red recombination system. Methods Mol Biol *634*, 421-430. 10.1007/978-1-60761-652-8_30.

Tischer, B.K., von Einem, J., Kaufer, B., and Osterrieder, N. (2006). Two-step red-mediated recombination for versatile high-efficiency markerless DNA manipulation in Escherichia coli. Biotechniques *40*, 191-197. 10.2144/000112096.

Tomer, E., Cohen, E.M., Drayman, N., Afriat, A., Weitzman, M.D., Zaritsky, A., and Kobiler, O. (2019). Coalescing replication compartments provide the opportunity for recombination between coinfecting herpesviruses. FASEB J *33*, 9388-9403. 10.1096/fj.201900032R.

Trapp, S., Parcells, M.S., Kamil, J.P., Schumacher, D., Tischer, B.K., Kumar, P.M., Nair, V.K., and Osterrieder, N. (2006). A virus-encoded telomerase RNA promotes malignant T cell lymphomagenesis. J Exp Med *203*, 1307-1317. 10.1084/jem.20052240.

Tulman, E.R., Afonso, C.L., Lu, Z., Zsak, L., Rock, D.L., and Kutish, G.F. (2000). The genome of a very virulent Marek's disease virus. J Virol *74*, 7980-7988. 10.1128/jvi.74.17.7980-7988.2000.

Vazquez, J., Belmont, A.S., and Sedat, J.W. (2002). The Dynamics of Homologous Chromosome Pairing during Male Drosophila Meiosis. Current Biology *12*, 1473-1483. 10.1016/s0960-9822(02)01090-4.

Vinayagamurthy, S., Ganguly, A., and Chowdhury, S. (2020). Extra-telomeric impact of telomeres: Emerging molecular connections in pluripotency or stemness. J Biol Chem *295*, 10245-10254. 10.1074/jbc.REV119.009710.

Vychodil, T., Wight, D.J., Nascimento, M., Jolmes, F., Korte, T., Herrmann, A., and Kaufer, B.B. (2022). Visualization of Marek's Disease Virus Genomes in Living Cells during Lytic Replication and Latency. Viruses *14*. 10.3390/v14020287.

Wallaschek, N., Sanyal, A., Pirzer, F., Gravel, A., Mori, Y., Flamand, L., and Kaufer, B.B. (2016). The Telomeric Repeats of Human Herpesvirus 6A (HHV-6A) Are Required for Efficient Virus Integration. PLoS Pathog *12*, e1005666. 10.1371/journal.ppat.1005666.

Wang, I.H., Suomalainen, M., Andriasyan, V., Kilcher, S., Mercer, J., Neef, A., Luedtke, N.W., and Greber, U.F. (2013). Tracking viral genomes in host cells at single-molecule resolution. Cell Host Microbe *14*, 468-480. 10.1016/j.chom.2013.09.004.

Weber, P.C., Challberg, M.D., Nelson, N.J., Levine, M., and Glorioso, J.C. (1988). Inversion events in the HSV-1 genome are directly mediated by the viral DNA replication machinery and lack sequence specificity. Cell *54*, 369-381. 10.1016/0092-8674(88)90200-0.

Weller, S.K., and Sawitzke, J.A. (2014). Recombination promoted by DNA viruses: phage lambda to herpes simplex virus. Annu Rev Microbiol *68*, 237-258. 10.1146/annurev-micro-091313-103424.

Williams, L.B.A., Fry, L.M., Herndon, D.R., Franceschi, V., Schneider, D.A., Donofrio, G., and Knowles, D.P. (2019). A recombinant bovine herpesvirus-4 vectored vaccine delivered via intranasal nebulization elicits viral neutralizing antibody titers in cattle. PLoS One *14*, e0215605. 10.1371/journal.pone.0215605.

Xing, Z., and Schat, K.A. (2000). Inhibitory effects of nitric oxide and gamma interferon on in vitro and in vivo replication of Marek's disease virus. J Virol *74*, 3605-3612. 10.1128/jvi.74.8.3605-3612.2000.

Ye, J., Renault, V.M., Jamet, K., and Gilson, E. (2014). Transcriptional outcome of telomere signalling. Nat Rev Genet *15*, 491-503. 10.1038/nrg3743.

Yeh, H.Y., Yates, M.V., Mulchandani, A., and Chen, W. (2010). Molecular beacon-quantum dot-Au nanoparticle hybrid nanoprobes for visualizing virus replication in living cells. Chem Commun (Camb) *46*, 3914-3916. 10.1039/c001553a.

You, Y., Conradie, A.M., Kheimar, A., Bertzbach, L.D., and Kaufer, B.B. (2021a). The Marek's Disease Virus Unique Gene MDV082 Is Dispensable for Virus Replication but Contributes to a Rapid Disease Onset. J Virol *95*, e0013121. 10.1128/JVI.00131-21.

You, Y., Hagag, I.T., Kheimar, A., Bertzbach, L.D., and Kaufer, B.B. (2021b). Characterization of a Novel Viral Interleukin 8 (vIL-8) Splice Variant Encoded by Marek's Disease Virus. Microorganisms *9*. 10.3390/microorganisms9071475.

You, Y., Vychodil, T., Aimola, G., Previdelli, R.L., Göbel, T.W., Bertzbach, L.D., and Kaufer, B.B. (2021c). A Cell Culture System to Investigate Marek's Disease Virus Integration into Host Chromosomes. Microorganisms *9*. 10.3390/microorganisms9122489.

8 List of publications

8.1 Scientific publications

Vychodil T, Wight DJ, Nascimento M, Jolmes F, Korte T, Herrmann A, Kaufer BB. 2022. Visualization of Marek's disease virus genomes in living cells during lytic replication and latency. Viruses *14*(2):287. https://doi.org/10.3390/v14020287

You Y#, **Vychodil T#**, Aimola G, Previdelli RL, Göbel TW, Bertzbach LD, Kaufer BB. 2021. A Cell Culture System to Investigate Marek's Disease Virus Integration into Host Chromosomes. Microorganisms 9(12):2489. https://doi.org/10.3390/microorganisms9122489

Vychodil T#, Conradie AM#, Trimpert J, Aswad A, Bertzbach LD, Kaufer BB. 2021. Marek's Disease Virus Requires Both Copies of the Inverted Repeat Regions for Efficient *In Vivo* Replication and Pathogenesis. Journal of Virology 95(3):e01256-20. https://journals.asm.org/doi/10.1128/JVI.01256-20

Bertzbach LD, Harlin O, Härtle S, Fehler F, **Vychodil T**, Kaufer BB, Kaspers B. 2019. IFNα and IFNγ Impede Marek's Disease Progression. Viruses 11(12):1103. https://doi.org/10.3390/v11121103

Previdelli RL, Bertzbach LD, Wight DJ, **Vychodil T**, You Y, Arndt S, Kaufer BB. 2019. The Role of Marek's Disease Virus UL12 and UL29 in DNA Recombination and the Virus Lifecycle. Viruses 11(2):111. https://doi.org/10.3390/v11020111

Bencherit D, Remy S, Le Vern Y, **Vychodil T**, Bertzbach LD, Kaufer BB, Denesvre C, Trapp-Fragnet L. 2017. Induction of DNA Damages upon Marek's Disease Virus Infection: Implication in Viral Replication and Pathogenesis. Journal of Virology 91(24):e01658-17. https://journals.asm.org/doi/10.1128/JVI.01658-17

\# shared co-first authorship

8.2 Talks and poster presentations

<u>Vychodil T</u> and Kaufer BB. Talk (10/2018): Visualization of the herpesvirus genomes in living cells. 13th Mini-Herpesvirus workshop, Hamburg, Germany

<u>Vychodil T</u>, Bertzbach LD, Kaufer BB. Talk (08/2018): A quantitative assay to assess Marek's disease virus genome integration *in vitro*. 12th International Symposium on Marek's Disease and Avian Herpesviruses, Yangzhou, China

<u>Vychodil T</u>, Bertzbach LD, Kaufer BB. Poster (04/2018): A quantitative assay to assess Marek's disease virus genome integration *in vitro*. ZIBI Graduate School Retreat, Rheinsberg, Germany

<u>Vychodil T</u> and Kaufer BB. Talk (03/2017): Visualization of the herpesvirus genomes in living cells. ZIBI Graduate School Retreat, Nauen, Germany

<u>Vychodil T</u> and Kaufer BB. Talk (07/2016): Visualization of the herpesvirus genomes in living cells. 11th International Symposium on Marek's Disease and Avian Herpesviruses, Tours, France

9 Acknowledgements

10 Funding Sources

11 Conflict of Interest

Within the scope of this work, the author declares no conflicts of interest.

12 Selbständigkeitserklärung

Hiermit bestätige ich, dass ich die vorliegende Arbeit selbständig angefertigt habe. Ich versichere, dass ich ausschließlich die angegebenen Quellen und Hilfen in Anspruch genommen habe.

Berlin, am 19.10.2022   Tereza Vychodil